FACULDADE DE ENGENHARIA DA UNIVERSIDADE DO PORTO



On-board Controller for Catenary Voltage Stabilization in Electrified Railway Systems

Pedro Alexandre Teixeira de Almeida

Mestrado Integrado em Engenharia Eletrotécnica e de Computadores

Supervisor: Professor Doutor António Pina Martins

July 25, 2023

© Pedro Almeida, 2023

Resumo

Nos últimos anos, a crescente atividade do transporte ferroviário exige avanços recorrentes nas tecnologias associadas. Apesar de ser um dos modos de transporte com menos emissões, os sistemas ferroviários eletrificados podem ainda melhorar em aspectos como eficiência energética e conforto dos passageiros. De facto, à medida que a sua procura cresce, é possível prever que o número de comboios a circular em cada linha ferroviária aumente também. Deste modo, para que se verifique uma alimentação estável das locomotivas, os atuais caminhos-de-ferro devem ser capazes de suportar esse aumento de tráfego sem manifestar quedas de tensão excessivas, que por sua vez poderão levar a um fornecimento insuficiente de energia para os comboios.

Este trabalho propõe uma estratégia ainda pouco explorada na literatura que visa a estabilização da tensão da linha catenária com recurso à compensação de potência reativa através do conversor monofásico de interface com a rede, presente no interior de cada comboio.

O estudo inicia com uma revisão abrangente das arquiteturas de alimentação e tração ferroviária, em conjunto com eventuais problemas identificados na qualidade da potência fornecida às locomotivas. Com especial foco no conversor do lado da rede, é feita uma revisão detalhada dos seus aspectos mais importantes, como a escolha do filtro, técnicas de modulação, e métodos de controlo passíveis de ser utilizados para mitigar os problemas em questão. São ainda discutidas algumas considerações de controlo digital que devem ser tidas em conta numa futura implementação prática.

Para validar os vários aspectos teóricos apresentados, é desenvolvido um modelo de simulação, no qual o conversor e os métodos de controlo propostos são testados numa perspetiva sistemática. Para além disso, a simulação serve também como uma ferramenta de previsão para futuras implementações práticas. Mais ainda, é desenvolvido um caso de estudo, no qual se simula um cenário realista, de forma a apoiar a estratégia proposta para estabilização da tensão na catenária. Desta forma, demonstrou-se uma diminuição na queda da tensão de alimentação de um comboio de 24.3%, através da injeção de potência reactiva na linha.

Finalmente, são também efetuados um conjunto de ensaios experimentais, correspondentes a várias etapas que validam tanto a metodologia proposta como os modelos de simulação.

Em suma, este trabalho proporciona uma validação detalhada e rigorosa da estratégia proposta, abordando tópicos de análise teórica, modelos de simulação com um caso de estudo de um cenário realista, e verificação experimental, tudo numa linha de trabalho contínua e sustentada.

Abstract

The ever increasing activity of railway transportation on the last years demands recurring advances in the associated technologies. Despite being one of the lowest emission modes of transportation, electrified railway systems can still improve in aspects such as energy efficiency and passenger comfort. In fact, as the demand grows, it is possible to foresee that the number of running trains on the same railway line will also rise. Consequently, for a stable supply operation, modern railroads should be capable of withstanding such traffic increase without manifesting a low voltage condition that leads to the incorrect power supply of the trains. This work proposes a less featured in the literature strategy to stabilize the catenary line voltage by means of reactive power compensation through the line-side single-phase converter placed inside of each train.

The study begins with a comprehensive review of the state-of-the-art railway supply and traction system architectures, along with identified issues on power supply quality. Special emphasis is placed on the interface converter between the train and the catenary, with a detailed overview of important aspects such as filter design, modulation techniques, and control methods employed to mitigate these power quality issues. Digital control considerations are also discussed to gain insights into practical implementation effects.

To validate the theoretical aspects presented, a simulation model is developed, where the proposed converter and control methods are tested, each subsystem at a time. Additionally, the simulation also serves as a prediction tool for future real-life implementations. Furthermore, a case study featuring a real-life scenario is also simulated to support the proposed strategy for catenary voltage stabilization. With this study case, a reduction of 24.3% in the train's supply voltage drop through reactive power injection was achieved.

Finally, a set of experimental procedures is also carried out, consisting of multiple stages that validate both the proposed methodology and the simulation models.

In summary, this research endeavor provides a comprehensive and rigorous validation of the proposed strategy, encompassing theoretical analysis, simulation modeling with a real-life scenario case study, and experimental verification in a sustained line of work.

Agradecimentos

Em primeiro lugar, gostaria de agradecer ao meu orientador, Prof. Doutor António Pina Martins, por todo auxílio, disponibilidade e conhecimento transmitido. Agradeço também a toda estrutura da *Nomad Tech* pelas condições proporcionadas para a realização desta Dissertação num ambiente descontraído, mas sempre de trabalho. Um agradecimento especial ao Doutor Vitor Morais pela atenção, apoio e motivação dadas ao longo deste trabalho. De igual forma, agradeço ao Pedro Moço e ao Rui Mendes por todas as dicas e por se mostrarem sempre prontos a ajudar.

Aos meus pais, Rui e Lurdes, e à minha irmã, Sofia, por toda a paciência e palavras de encorajamento, não só durante este trabalho como ao longo de todo o meu percurso académico, principalmente em finais de semestre (sei que não foi fácil). À minha namorada, Sara, por toda a compreensão, carinho e pequenos bons momentos proporcionados durante toda esta fase, essenciais para aliviar a cabeça.

Como não podia deixar de ser, um obrigado aos meus amigos, Albergaria, Capela, Filipe, Miguel, Paulo, Ricardo, Sengo, Veríssimo e Zé Pedro, pelos momentos de divertimento, descontração e 'estudo' em grupo, que se revelaram imprescindíveis. Mesmo não sendo da mesma área, obrigado também por todas as soluções e ideias 'engenhosas' que foram dando ao longo deste percurso, certamente deram jeito (algumas).

Sem vocês não era possível. A todos,
Muito Obrigado.

Pedro Almeida

"Ideas alone have little value.
An innovation's importance lies in its practical implementation."

Werner von Siemens

Contents

1 Introduction **1**
- 1.1 Context and Motivation . . . 2
  - 1.1.1 The Nomad Tech Challenge . . . 2
- 1.2 Main Goals . . . 3
- 1.3 Structure of this Document . . . 4

2 State of the Art **5**
- 2.1 Railway Electrification . . . 5
  - 2.1.1 Railway Power Supply Systems . . . 6
  - 2.1.2 Railway Traction Systems . . . 8
  - 2.1.3 The Portuguese Railway System and Rolling Stock . . . 9
  - 2.1.4 Power Quality Issues on Railway Traction . . . 10
- 2.2 Voltage-Oriented Control . . . 11
  - 2.2.1 Clarke and Park Transformations . . . 12
  - 2.2.2 Grid Synchronization . . . 13
  - 2.2.3 AC Current Control . . . 16
  - 2.2.4 DC Voltage Control . . . 18
- 2.3 Digital Control . . . 19
  - 2.3.1 The Digital PWM . . . 20
  - 2.3.2 Digital Filters . . . 21
  - 2.3.3 Controller Discretization Methods . . . 22
  - 2.3.4 Microcontroller Market . . . 26
- 2.4 Final Remarks . . . 27

3 Line-side Converters for Railway Traction **29**
- 3.1 Advances in Semiconductor Technology . . . 29
- 3.2 Common Converter Configurations . . . 30
  - 3.2.1 H-Bridge Converter . . . 30
  - 3.2.2 Multilevel Converter . . . 31
  - 3.2.3 Matrix Converter . . . 33
  - 3.2.4 Interleaved Configuration . . . 34
- 3.3 Filter Design . . . 35
- 3.4 Pulse Width Modulation . . . 36
- 3.5 Regenerative Braking . . . 38
- 3.6 Reactive Power Compensation . . . 39
  - 3.6.1 Strategies for Catenary Voltage Support . . . 40
  - 3.6.2 Standard EN 50388-1 . . . 45
- 3.7 Final Remarks . . . 45

4 Modelling and Simulation **47**
4.1 Introduction . . . 47
4.1.1 Supervision . . . 48
4.1.2 Workplan . . . 49
4.2 AC Current Control . . . 50
4.3 Grid Synchronization . . . 52
4.4 DC Voltage Control . . . 53
4.5 Reactive Power Control . . . 55
4.6 Discrete Implementation . . . 59
4.6.1 Controller Discretization . . . 59
4.6.2 Digital Filters . . . 60
4.6.3 General Code Structure . . . 61
4.6.4 Obtained Results . . . 62
4.7 Case Study . . . 64
4.8 Final Remarks . . . 67

5 Experimental Validation **69**
5.1 Introduction . . . 69
5.1.1 Experimental Setup . . . 70
5.1.2 Updated Code Structure . . . 70
5.1.3 Filtering . . . 71
5.2 Experiment A . . . 72
5.3 Experiment B . . . 73
5.4 Experiment C . . . 77
5.4.1 Reactive Power Controller . . . 80
5.5 Experiment D . . . 81
5.6 Final Remarks . . . 82

6 Main Conclusions and Future Work **83**
6.1 Summary and Contributions . . . 83
6.2 Future Work . . . 84

A Simulation Diagrams **85**
A.1 Complete Circuit Diagram . . . 85

B Experimentation Figures **87**
B.1 Experimental Setup . . . 87

C Utilized Software Tools **91**
C.1 *PSIM* . . . 91
C.2 *Dave IDE* . . . 92
C.3 *Micrium uC/Probe XMC* . . . 93
C.4 *PicoScope* . . . 94
C.5 *MATLAB* . . . 95

References **97**

List of Figures

2.1 Railway Power Supply Systems in Europe. From [7]. 6
2.2 DC Power Supply System. From [9]. 7
2.3 AC 15 kV 16.7 Hz Power Supply System. From [9]. 7
2.4 AC 25 kV 50Hz Power Supply System. From [9]. 8
2.5 Traction Converter for DC Power Supply. From [7]. 8
2.6 Traction Converter for AC Power Supply. Adapted from [7]. 9
2.7 Interleaved Traction System. From [10]. 9
2.8 Voltage oriented control basic block diagram. 12
2.9 Park Transformation Illustration. From [13]. 13
2.10 Subsystems of a PLL Block. Adapted from [14] 14
2.11 Modification for single-phase systems. From [15]. 14
2.12 E-PLL Diagram. From [14]. 15
2.13 SRF-PLL Diagram. From [16]. 15
2.14 SOGI-QSG Diagram. From [16]. 16
2.15 DSOGI-QSG Diagram. From [16]. 16
2.16 DSOGI-PLL Diagram. From [16]. 16
2.17 PI-based current control loop. 17
2.18 Diagram of an ideal PR controller with harmonic compensation. 18
2.19 PR-based current control loop. 18
2.20 PI-based DC voltage control loop in cascade with previous PR current controller. 19
2.21 Digital PWM scheme. From [18]. 20
2.22 Low-pass filter magnitude response. Adapted from [19]. 21
2.23 N order FIR filter block diagram. Adapted from [19]. 22
2.24 N order IIR filter block diagram. Adapted from [19]. 23
2.25 Trapezoidal (Tustin) approximation. From [18]. 24
2.26 Backward and forward Euler approximations. From [18]. 25

3.1 Converter Modes of Operations according to its waveforms. From [1]. 30
3.2 Circuit Diagram of a H-bridge single-phase converter. 31
3.3 Simplified MMC block diagram. SMx represents a specific sub module. From [28]. 32
3.4 Cascaded matrix converter (labeled as MVC). From [29]. 33
3.5 Output current waveforms from two interleaved converters. From [32]. 34
3.6 Bipolar PWM: modulating and carrier wave signals, (a) and resulting output wave at the AC side, (b). Adapted from [7]. 36
3.7 Unipolar PWM: modulating and carrier wave signals, (a), output in relation to the ground, (b), and resulting output wave on the AC side, (c). Adapted from [7]. . . 37
3.8 Phasor diagrams for the converter's operations with unitary power factor: rectifier operation (a) and inverter operation (b). 39

3.9 Phasor diagrams for the converter's operation with different power factor: lagging power factor (a) and leading power factor (b). . . . 40
3.10 Droop control strategy: droop characteristic curve (a) and basic display of this strategy (b). From [9]. . . . 44

4.1 Diagram of proposed power circuit. . . . 47
4.2 State Machine Diagrams: protection FSM (a) and operational FSM (b). . . . 49
4.3 *PSIM* Diagrams: power circuit (a) and control circuit (b). . . . 50
4.4 Resultant waveforms: I_s in blue, $I_{m,ref}$ in red and V_{conv} in lighter blue. . . . 51
4.5 FFSOGI-PLL diagram. . . . 52
4.6 Resultant waveforms: V_{grid}, V_{mag}, w on the graph above, and the estimated angle, $theta$, on the graph below. . . . 53
4.7 Resultant power circuit. . . . 53
4.8 Control circuit diagram with the DC voltage control loop. . . . 54
4.9 DC voltage (above), AC current (middle) and respective references, in red. Load power reference change (bottom). . . . 54
4.10 Reactive power response with leading power factor, in blue and reactive power reference, in red. . . . 56
4.11 AC current and voltage waveforms for both cases. With 0.95 (a) and 0.87 (adjusted) (b) leading power factors. . . . 57
4.12 Reactive power response with lagging power factor, in blue and reactive power reference, in red. . . . 57
4.13 AC current and voltage waveforms for both cases. With 0.95 (a) and 0.75 (b) lagging power factor. . . . 58
4.14 *PSIM s2z Converter* tool: PI (a) and PR (b) controllers discretization example. . . . 59
4.15 Noise and filtered signals: DC voltage (a) and AC current (b). . . . 61
4.16 General Code Structure. . . . 62
4.17 Pre-charge and control of the DC bus. . . . 63
4.18 Reactive power response with lagging power factor, in blue and reactive power reference, in red. . . . 63
4.19 AC current and voltage waveforms for a lagging power factor. . . . 63
4.20 Diagram of the modelled case study. . . . 64
4.21 Rms supply voltage of the two trains (top) and reactive power response (bottom) for each case: with zero (a) and 700 kVA capacitive (b) reactive power setpoints. 66

5.1 Diagram of the experimental setup. . . . 70
5.2 Updated Code Structure. . . . 71
5.3 100 Hz digital filter implemented for the DC bus voltage measurement. . . . 71
5.4 FFSOGI-PLL resultant waveforms: α and β components (a), phase angle θ_{PLL} (b), estimated frequency ω^*_{PLL} and voltage magnitude V^*_{mag} (c). . . . 73
5.5 Voltage drop at the terminals of an IGBT, in blue and corresponding AC current, in red. . . . 74
5.6 PR controller response with internally generated angle. . . . 75
5.7 PR Controller response with grid synchronization: from the starting point of operation (a) and after a reference change (b). . . . 76
5.8 System response with different negative reactive current references. . . . 78
5.9 System response with different positive reactive current references. . . . 79
5.10 Active and reactive power calculations for $i^*_d = 1$ A and $i^*_q = 7.5$A. . . . 80
5.11 System response for -500 VA (a) and +500 VA (b) reactive power references. . . . 81

5.12 DC voltage control. 81

B.1 Full experimental setup. 87
B.2 XMC and Acquisition Board. 88
B.3 Pre-charge circuit. 89

C.1 User interface of *PSIM* simulation software. 91
C.2 User interface of *Dave IDE*. 92
C.3 User interface of *Micrium*: code oscilloscope view. 93
C.4 User interface of *Micrium*: created HMI to introduce reference values and control the FSMs. 93
C.5 User interface of *PicoScope*, extracted during Experiment C. 94
C.6 User interface of *MATLAB*'s *filterDesigner* app 95

List of Tables

3.1 Switch commands in bipolar PWM. 36
3.2 Switch commands in unipolar PWM 37

4.1 Parameter values used in the simulation. 48
4.2 Case study parameters. 64
4.3 Obtained results for both simulation cases. 65

5.1 Conducted experiments and main goals. 69
5.2 Figure correspondence for different reactive reference currents. 77

Symbols and Abbreviations

AC	Alternating Current
DC	Direct Current
DSOGI-PLL	Double Second Order Generalized Integrator Phase-Locked Loop
E-PLL	Enhanced Phase-Locked Loop
FIR	Finite Impulse Response
IIR	Infinite Impulse Response
IGBT	Insulated-Gate Bipolar Transistor
PI	Proportional Integral
PLL	Phase-Locked Loop
PR	Proportional Resonant
PWM	Pulse-Width Modulation
SOGI-QSG	Second Order Generalized Integrator Quadrature Signal Generator
SRF-PLL	Synchronous Reference Frame Phase-Locked Loop
STATCOM	Static Synchronous Compensator
SVC	Static VAR Compensators

Chapter 1

Introduction

Railway transportation has been around since the early nineteenth century, but the electric railway concept was not implemented until the end of it. Werner von Siemens, a co-founder of the well-known company Siemens, was the first to demonstrate a fully electric train. This model was a direct current (DC) train with 2.2 kW of power and a 150 V supply [1]. Currently, there are numerous electrification systems that differ in supply voltage levels as well as in current form, DC or AC. The majority of motors in use are an alternating current (AC) motors, while the direct current (DC) motors are also a solution for some applications.

Over the last two decades, railway transportation activity has increased substantially. In fact, only on passenger activity, it has grown by 91%, now having an 8% share of the total motorised passenger transport activity [2]. Such an increase is always welcome since railway transportation is the least emission intensive mode of transportation in the European Union, with a global average of greenhouse gas emissions of 19 grams of carbon dioxide equivalent per passenger kilometer traveled. In comparison, two and three-wheelers emit 39 g CO2-eq/passenger-km globally, while small and medium-sized cars emit 148 g CO2-eq/passenger-km globally [3]. It becomes obvious that this is a strong solution to the mitigation of greenhouse gas emissions on transportation.

However, this increment also means that each railway line will sustain an also growing number of vehicles, augmenting the load supported by each one. Hence, it is of utmost importance that the line features enough capacity[1] to support a higher demand. In fact, the European Union has already recognized this issue and launched the multi annual program *Shift2Rail* which has the intent of developing groundbreaking railway technologies to improve the overall quality of the European railway infrastructure. In fact, this program presents "doubling the railway capacity" as one of its core objectives [4]. This serves as compelling evidence of the importance of considering the issue of limited railway line capacity and working on ways to improve it.

[1] In this context, line capacity is usually defined as the maximum number of trains running on the same supply line.

1.1 Context and Motivation

Another interesting observation is that the increased traffic but also the length also increases the voltage drops along certain supply line. Consequently, stabilizing the line voltage is also a solution to increase line capacity. However, there are more factors affecting the supply voltage level at the overhead line, which are related to the use of older trains. In fact, these type of rolling stock uses older traction technology, which presents poor power factor, drawing significant amounts of reactive power from the line. This also leads to significant drops in the supply voltage levels. Not only that, but the current injected into the line also has a great deal of harmonic content, affecting the line's power quality overall. In the ambit of this work, particular emphasis was placed on the study of the low voltage condition due to poor line capacity or heavy traffic on the same supply.

Power electronic equipment are one of the possible solutions to increase the line capacity. The modern tendencies in this matter aim to produce systems that can improve energy efficiency and passenger comfort all together [5]. The recent advances in this technology are due to enhancements in various sectors, such as in the power semiconductor devices, the cooling systems, drive systems and drive command methods. Several different systems are already in use to increase railway infrastructure capacity, in order to prevent low system voltage [6]. However, the mostly used methods are of static nature (SVCs, STATCOMs), which may lead to a less efficient operation when the train is far-off from the traction power substation (TPS).

Thanks to high-power semiconductor technology advances, railway traction units feature a PWM transistor based line-side converter, allowing bi-directional power flow. This characteristic enables the converter to perform in different operation modes such as traction, regenerative braking and reactive power control. Moreover, due to the adoption of IGBTs, this converter now provides a much 'cleaner' AC current, in comparison to the older ones. Indeed, the modern line-side converter, included in each train, is a useful piece of equipment not only to reduce the effects that heavy traffic and older trains have in the line's power quality, but also as possible and more efficient alternative. Hence, representing a two-way improvement for the railway traction system. This can be accomplished with careful design of the power converter's by precise selection of topology, passive and active components. Additionally, the traction control unit plays a pivotal role in this process as it continuously governs the converter's operation and effectively determines the best suitable response to the prevailing line conditions. The designed converter must operate withing the restrictions of the Standard EN 50388-1, as will later be addressed.

1.1.1 The Nomad Tech Challenge

This dissertation is to be conceived in a corporate setting with the assistance of *Nomad Tech*, a joint venture between *CP - Comboios de Portugal* and *Nomad Digital*. *Nomad Tech* is a Portuguese company devoted to modernizing and significantly improving the overall reliability of its customers' existing rolling stock. Its activities range from the control of on-board electrical

equipment and internal data acquisition, to customizable and remote conditions monitoring solutions, for example, of a complete train fleet, or even on-board power electronics solutions aimed at increasing energy savings, reducing equipment life cycle costs, or modernizing those already in play.

Concerning the modernization of on-board power electronics, some issues that railway operator face nowadays include the lack of certain components or the use of an older traction control unit that can be modernized. This is where this dissertation is framed in, presenting important contributions to support a modern control of the line-side power converter.

In the ambit of this work, several problems concerning the power quality in the railway supply lines are presented, along with potential approaches to mitigate them. Among those, particular emphasis was placed on the study of the low voltage condition due to poor line capacity or heavy traffic on the same supply. As such, the traction power converter of the CP Series 2300/2400 Electric Multiple Units is used as a case study in a simulation model, where this condition is observed and the proposed hypothesis of using the line-side converter to solve this issue is tested.

1.2 Main Goals

In view of the given context, the central objective of this dissertation is to develop a traction control unit for the line-side converter utilized in railway applications. The process to achieve this goal comprises an investigation of the current trends on railway traction converters, with emphasis on the circuit design, modulation and control techniques to improve its efficiency and power quality at the point of connection with the catenary. The further development, simulation and experimental work of the proposed controller and converter should serve as validation to the previously presented hypothesis.

With this intent and according to the conducted literature review, its possible to formulate four main questions that should be answered through the course of this document:

Q1. What are the main power quality issues associated with railway electrified systems?

Q2. How can the adoption of advanced control strategies of traction power converters contribute to the mitigation of those issues?

Q3. How to validate the effectiveness of these control strategies with simulation tools?

Q4. How to validate the simulations model with experimental demonstration in a real grid connected power converter?

To answer those questions this dissertation was divided in three main stages, representative of the evolution of the performed study. Starting with a literature review, followed by a presentation of simulation models and the respective results, and finalizing with an experimental demonstration with the aim of validating the proposed hypothesis.

1.3 Structure of this Document

The work developed throughout this dissertation resulted in six chapters, as described next.

Chapter 1 is the Introduction. It provides a historical and current background of electrified railway systems technology, how it serves as a context as well as a definition of the main goals proposed for this work.

Chapter 2 includes a review of the most important aspects of the railway fundamentals, such as the current power supply and traction system technologies used in electric railways, most observed power quality issues, review of control methods for line-side converters and digital control considerations.

Line-side converters, and all the related topics, such as converter typologies, filter design, modulation, and subsequent proposed applications is addressed in **Chapter 3**.

In **Chapter 4**, a simulation model of the proposed system is presented, along with the methodology employed, result analysis and a case study that intends to validate the proposed control methods in a real-life modeled scenario.

A physical implementation of the proposed control methodology, supported by the previously conducted simulation along with the achieved results is described in **Chapter 5**.

Finally, in **Chapter 6**, the main conclusion and answers to the proposed questions are given. Also, a small subsection is dedicated to discuss possible improvements and future lines of research.

Chapter 2

State of the Art

This chapter gives an overview of several important concepts needed to the understanding of this dissertation. Considering the relevancy of the railway transportation nowadays, an extended overview of different railway power supply configurations and concerning power quality issues that affect them is given. It is also addressed the on-board power electronics traction unit, that can be of different configurations, depending on the supply. Furthermore, an introduction to converter control methods and digital control is presented as a way to prepare a proposed solution and a future implementation.

2.1 Railway Electrification

As was previously mentioned, electrified railroads date back more than two centuries. Multiple types of electric railway systems emerged and are now widely used in Europe as a result of advancements in the technologies that cover them.
They can differ in the following aspects:

- Supply Voltage
- Type of current flow: AC or DC
- Frequency (in the case of AC systems)
- Disposition of the contact system

Because the local state of the art technologies were not the same for each region, the system adopted diverged from country to country. The variety of systems adopted in Europe is clearly displayed in Figure 2.1.

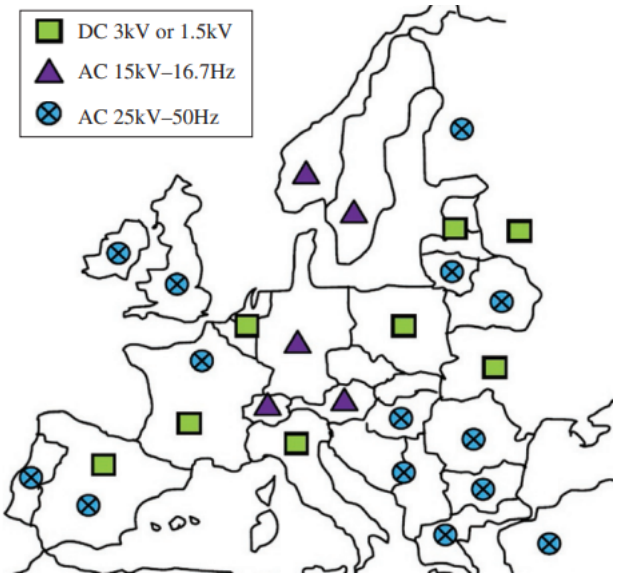


Figure 2.1: Railway Power Supply Systems in Europe. From [7].

2.1.1 Railway Power Supply Systems

Direct Current Railway Systems

Direct current systems were the first to be used in electrified railways. Nowadays, they're mostly used in subway and trams lines but also on trains on countries like Spain, Italy, the Netherlands, as is represented in Figure 2.1. In Portugal they are also used in the Cascais line.

This architecture allows current to be drawn directly from overhead lines with simpler on-board train electrification schemes, as there is no need for an on-board transformer and causing less voltage imbalances in the grid, in comparison to AC supply systems. However, in comparison to AC configurations, these systems are limited to relatively low voltages, which affects maximum train power. DC railway systems require wayside transformers and rectifier converters, present at traction substations, in order to adapt the 50 Hz voltage from the main grid [8]. The next figure depicts the usual configuration of these supply systems.

Concerning the contact configuration the use of a third rail instead of the catenary is also a widely used option on DC supply systems. The main advantage is the more compact disposition that allows for a less complex installation and thus, more economical. On the other hand, it can limit even further the maximum supply voltage in DC systems [1, 8]. In addition to the third rail, a fourth rail is also adopted in some systems, to a much lesser extent than the previously mentioned. The objective is to offer a pathway for the return current, thus, improving the energy efficiency and minimizing some effects such as corrosion of wayside metallic buried structures, for example.

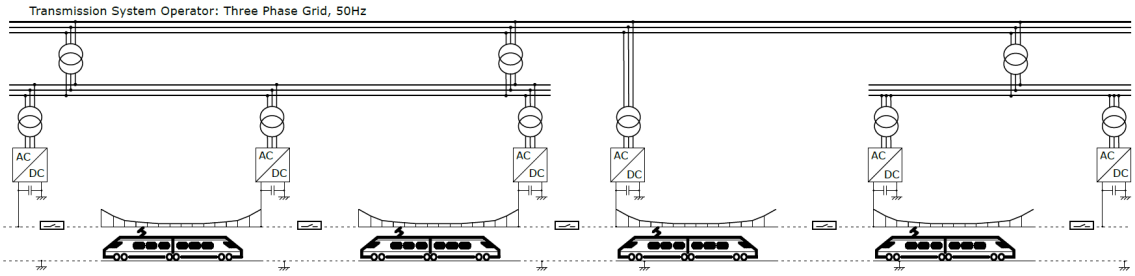


Figure 2.2: DC Power Supply System. From [9].

Alternating Current 15 kV 16.7 Hz Railway Systems

The most used architecture is the AC supply system. It allows for a high voltage at the line with suitable power while reducing the line currents to the trains [1].

Inside the AC supply systems there are two common configurations: 15 kV at 16.7 Hz (also known as railway frequency) and 25 kV at 50 Hz [1]. In the first, a rotary (mostly used in the past) or a static converter located at feeder substation are used to convert the electricity from the grid and after, a transformer lowers the mains voltage to 15 kV, usable by the train's power circuit [8, 7].

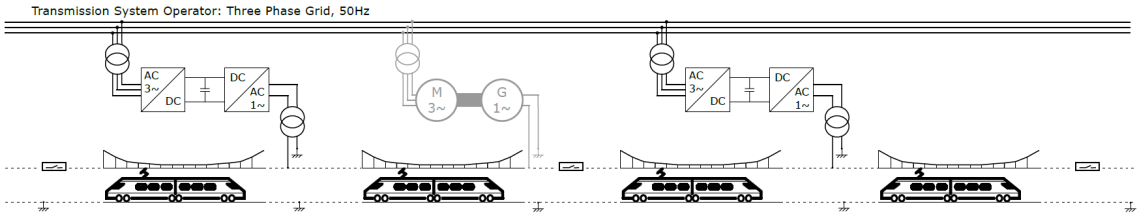


Figure 2.3: AC 15 kV 16.7 Hz Power Supply System. From [9].

Alternating Current 25 kV 50 Hz Railway Systems

The focus of this study is the Portuguese railway, which has a 25 kV supply system at the mains frequency of 50 Hz. On this type of systems, the power from the grid is transformed into the voltage level required in the catenary while maintaining its frequency, resulting in a less complex transformer solution, without the need of power electronics. The disadvantages of this architecture, on the other hand, are the unbalances injected on the line by the railway load (train). To reduce the effects of the moving railway load on supply lines, feeding substations are connected separately for each phase pair, dividing the catenary's continuous line into different sections, each fed by one substation. This implies that at certain points along the catenary, the train will not receive any form of supply, relying solely on its own inertia to move for a short period of time. These are known as Neutral Zones (NZ) and are depicted in the presented figures as a simple

[1] A 2x25 kV is also a commonly used configuration due to its ability to transmit higher power magnitudes while maintaining voltage levels within a practical range.

switch. It is also worth noting that this configuration reduces the amount of regenerative power that can be transferred back to the catenary, as will be later discussed in greater detail (see 3.5).

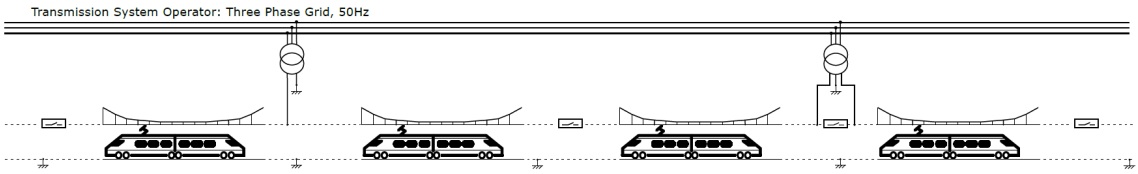


Figure 2.4: AC 25 kV 50Hz Power Supply System. From [9].

2.1.2 Railway Traction Systems

Concerning the railway on-board traction systems they naturally have different configurations depending on the supply architecture. Two different types of traction units are presented in this subsection.

Traction Systems with DC Power Supply

A simple power electronic converter is sufficient to drive the motor in systems with a DC power supply. This architecture is less expensive because there is no need for a transformer or a rectifier to be used, since the traction converter simply draws current from the catenary and then adjusts the voltage to drive the motors. The line filter functions as a resonance filter, reducing the amount of harmonics drawn from the grid. [5]. In the Fig. 2.5, a possible configuration for this system is presented.

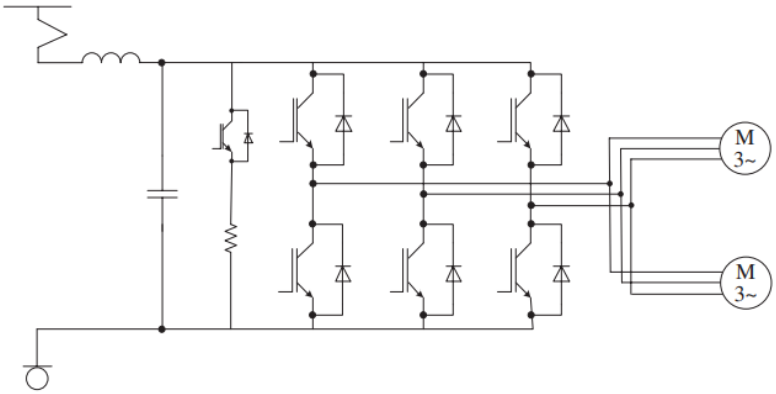


Figure 2.5: Traction Converter for DC Power Supply. From [7].

Traction Systems with AC Power Supply

In AC power supply systems, the rolling stock must include a more complex structure, when compared to the previously discussed configuration. In both, 16.7 or 50 Hz systems, a transformer

at the input of the traction converter is needed to lower the voltage originating from the catenary to a suitable value for the converter to operate. Moreover, a four quadrant single-phase converter is introduced at the catenary side, rectifying the AC voltage to a constant value on the DC-link. This converter provides control over the DC-link voltage level, possibility of bi-directional energy flow and the capability to regulate the power factor. A three-phase inverter, like the one shown before can then be connected at the DC bus, in order to drive the motor.

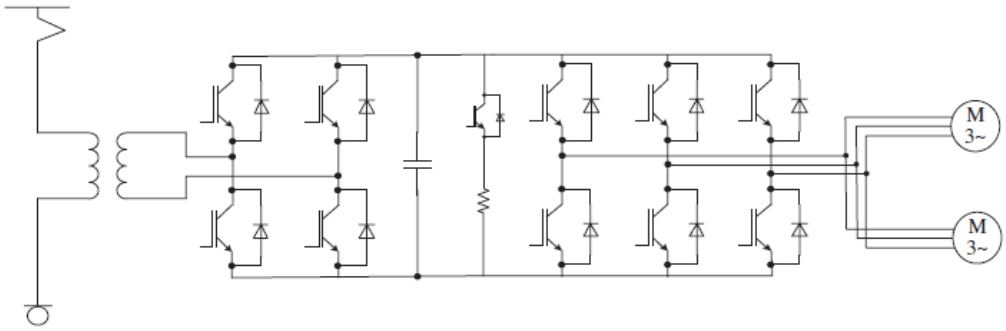


Figure 2.6: Traction Converter for AC Power Supply. Adapted from [7].

Another interesting and common configuration is the interleaving of two or more converters. For this case, the transformer must have two or more secondary windings, as the input power will be divided by each converter. The advantages of this configuration will be further developed in 3.2.4.

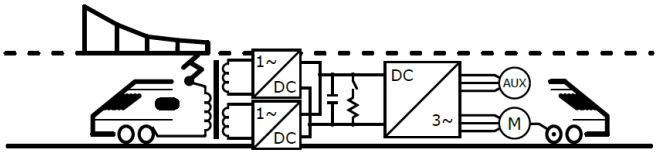


Figure 2.7: Interleaved Traction System. From [10].

2.1.3 The Portuguese Railway System and Rolling Stock

The Portuguese Railway System contains almost 1800 km of electrified railway, which represents approximately 71% of the total length of active railway system. The 25kV AC supply is used on almost all of the different services. This section aims to briefly describe the different services and the fully electric rolling stock that exists on the Portuguese railway system.

Alfa-Pendular Service

The only high-speed service in Portugal is the so called *Alfa-Pendular*. It makes use of the series 4000 electric multiple units, which can reach a top speed of 220 km/h with an AC supply of 25 kV.

Long Distance Services

There are currently three long distance services: the *Intercidades* (inter-city), the *InterRegional* and the *Regional*. The three almost share the same rolling stock, with maximum speeds from 120 to 200 km/h, depending on the coach model in question. As with most of the Portuguese railway line, all of these are fed by a 25 kV AC supply and make use of an AC asynchronous motor , in the case of the series 2200, series 5600, or a DC motor, in series 2600.

Urban Services

The Urban Lines are designed to support the two biggest cities in Portugal, Porto and Lisbon.

The Porto Urban Lines accounts with two different types of coaches, the series 3400 and series 2240, both fed by a 25 kV AC supply with AC motors. The last is also used in the Urban Lisbon Lines as well as in the long distance services.

Regarding the Lisbon Urban Lines there are mainly five different models, again, all fed by the 25 kV AC supply (series 2240, 2300, 2400 and 3500), with the exception of the series 3100/3200 electric multiple units, which work with a 1500 V DC supply and make use of DC motors.

2.1.4 Power Quality Issues on Railway Traction

According to the review of the current power quality related literature it is possible to identify four main factors affecting power quality on AC railway systems [11, 12].

- **Low System Voltage:** With each individual train representing an extra load supplied by the catenary, it is simple to conclude that the more units that circulate on a certain railway line, the higher the voltage drop will be, affecting the trains performance by decreasing the maximum power transmitted along the line. By controlling the train's operating power factor, one can counter this issue.
- **Harmonic Overvoltage:** Harmonic resonance occurs when the frequency value of the current injected by the train matches one of the resonant frequencies of the traction grid. High levels of harmonic currents have a higher probability of exciting the resonance modes of the supply line, adding this excitation voltage to the fundamental voltage which could result in an overvoltage that surpasses the line's nominal value.
- **Loss of Average Voltage:** Older trains use thyristors in the line-side rectifiers, whose commutation induced several crops on the voltage waveform, resulting in the decrease of average voltage. Moreover, low order harmonic distortion is also provoked by the same voltage notching.
- **Characteristic Harmonics:** It is also important to note that there is a fourth issue to be considered in the development of this converter. The PWM switching imposed on the traction converter draws current with harmonics from the catenary. Due to the line impedance, those current harmonics translate into voltage harmonics which not only pose a threat to other equipment on the utility grid, but can also go against the standards for harmonics in

electrical power systems. Despite the decreased number of harmonics in the four quadrant converter solution, the order of those harmonics is higher, when compared to other converter applications in railway.

The line-side converter with bidirectional properties can be used as a tool to mitigate all the issues mentioned above, either through the selection and proper tuning of the AC side filter or through the control method employed in the converter. Hence, although the modern trains do not suffer as much from the second and third problems as the older ones, these issues are still to be accounted for, when it comes to the design of the traction converter system.

As previously mentioned, this work has the intent to explore the first presented issue and present strategies to increase the overhead line capacity, countering the voltage drop that may occur in heavy traffic conditions.

2.2 Voltage-Oriented Control

There are various control methods commonly employed in single-phase grid-connected converters, with two of the most popular strategies being voltage-oriented control (VOC) and direct power control (DPC). This work primarily focuses on the voltage-oriented control.

Irrespective of the chosen method, the control procedure must ensure that the converter rectifies the voltage from the grid to a constant, previously chosen DC voltage value. Moreover, it should also regulate the power exchanges between the grid and the connected equipment (in this case a train) by continuously adjusting both the phase and amplitude of the AC current. Typically, most applications operate at a unity power factor, meaning that the AC current remains in phase with the AC voltage. However, there is also the option to operate at different power factors based on project requirements, as will be further discussed. Nevertheless, it is crucial to prevent poor power quality in the supplied AC current, which can occur due to improper converter operation.

The voltage-oriented control utilizes two cascaded control loops: the voltage control loop and the current control loop. The voltage control loop is the outer loop responsible for regulating the DC bus voltage, while the current control loop is the inner loop that regulates the grid current. These loops are designed with different dynamic characteristics that interfere with each others', therefore, careful design is needed. Furthermore, since the converter is expected to interact with the grid in the various discussed ways, achieving grid synchronization is vital for seamless interface operation. This is done with an extra control architecture, solely dedicated to this objective. Therefore, the control process can then be divided into three main subsystems:

1. Grid Synchronization
2. AC Current Control Loop
3. DC Voltage Control Loop

This section appears with the intent of giving a general overview of the control architecture for voltage-oriented control. Both by describing the functioning and by presenting different solutions for each highlighted control subsystem. In Figure 2.8, a comprehensive diagram of voltage-oriented control is displayed.

As a side note, it is also worth mentioning that both the voltage and current control are directly interconnected with the filter design, since, depending on the chosen configuration and filter parameters, different time constants can be achieved. Hence, there needs to be a balance between high quality filtering and fast dynamic performance.

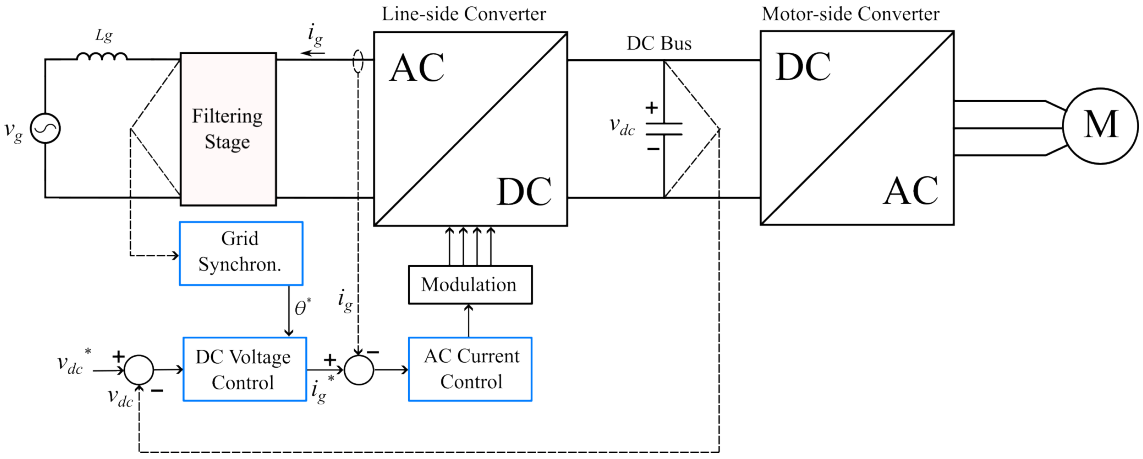


Figure 2.8: Voltage oriented control basic block diagram.

2.2.1 Clarke and Park Transformations

This control method uses the Clarke and Park transformations to perform reference frame transformations, that convert all the AC values to DC in order to allow the use of PI controllers but also simplify the control strategy. It also receives the current reference values generated in the outer loop. Firstly, a stationary, orthogonal referential is generated through the Clarke Transformations, called the $\alpha\beta$, then, the Park transformation is done to create a dq synchronous reference frame, rotating with a frequency, ω, that aligns the reference with the AC voltage (Fig. 2.9). This phase and frequency match is achieved through synchronization techniques such as the utilization of the phased-locked loop, as will be explained later.

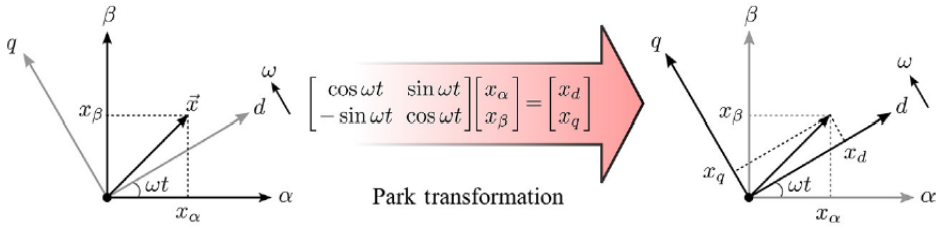


Figure 2.9: Park Transformation Illustration. From [13].

2.2.2 Grid Synchronization

The complexity of electric grids arises from various factors, some described in Section 2.1.4, along with additional ones such as frequent load connections and disconnections, mishandling of grid-connected components leading to equipment failures, or atmospheric events that disrupt the already complex operation of the power grid. Hence, grid variables should not be seen as constant and should be object of continuous monitoring. Also, in respect to the scope of this dissertation, more precisely to the grid connected converter, it will be designed to play an interactive role in their connection with the grid as it can aid to its operation by giving voltage support or by feeding active power back into the line, for instance.

Grid synchronization is an adaptive method of monitoring a given grid variable and generating a synchronous reference signal. It is an important part of the control method used in any line connected converter since it allows for it to work with the grid, without major drawbacks.

2.2.2.1 Phase-Locked Loop

The phase-locked loop (PLL) is a feedback control system that adjusts the phase of an output generated signal to match the frequency of an input signal using an internal oscillator.

In the case of a grid connected converter, its PLL's oscillator should produce a signal with the same frequency of the grid's voltage, that will be used by the control system. The advantages of this technology are related to the control system of the converter - by having a synchronous rotating controller, all the AC variables measured from the grid will be seen as DC ones, at the controller side, which enables the use of low-order controllers, which are easier to tune.

The PLL blocks usually include three blocks, as depicted on Figure 2.10 [14]. The Phase Detector gives an output proportional to the error between the output of the PLL and the input signal. This error is then fed into the Loop Filter block which includes a low-pass filter to target the high order AC harmonics coming from the phase detector block. The last block is the Voltage Controlled Oscillator, responsible for producing an AC signal shifted in frequency with respect to a reference frequency. There are different methods to implement these blocks as well as the whole PLL structure.

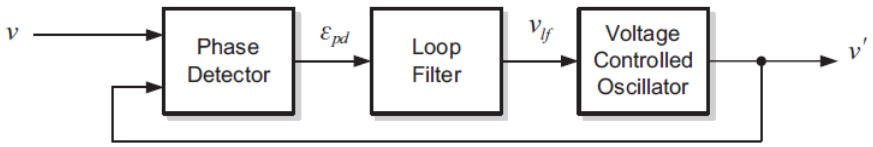


Figure 2.10: Subsystems of a PLL Block. Adapted from [14]

Single-Phase Systems

This section will provide an overview of different PLL system configurations. Their application requires the use of a PI controller, and thus, the use of the Clark and Park transformations.

It is important to notice, however, that these transformations are mainly designed for three-phase applications. Nonetheless, they are still feasible in shingle-phase systems, if a slight modification is employed.

This change includes taking the real phase of the system as the α component and delaying its phase by 1/4 of the grid's period to achieve the component β. As a consequence, when reading the next section, one should always keep in mind that this modifications needs to be added at the input of the presented PLL configurations.

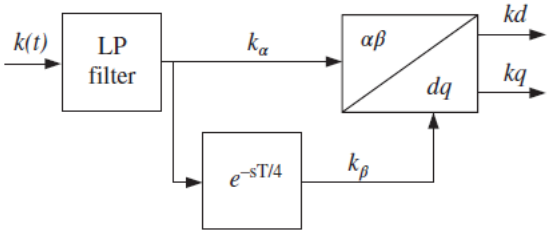


Figure 2.11: Modification for single-phase systems. From [15].

Enhanced Phase-Locked Loop (E-PLL)

By connecting an adaptive notch filter to the conventional PLL is possible to form what is called an enhanced phase-locked loop. This can be done by applying the signal output, in a sinusoidal form, from the voltage controller oscillator as well as the grid voltage signal to the input of the adaptive noise filter. The filter's output depends on the frequency and angle of reference signal and of the grid voltage provided. This configuration improves the PLL's behavior by enhancing the operation of the phase detector block. The placement of the adaptive noise filter makes the input of phase detector be zero, when the grid and the reference signal phase and angles are equal, reducing the oscillations produced by the phase detector. In [14], is possible to observe the major oscillation improvements on the response of the enhanced PLL in comparison with the conventional one.

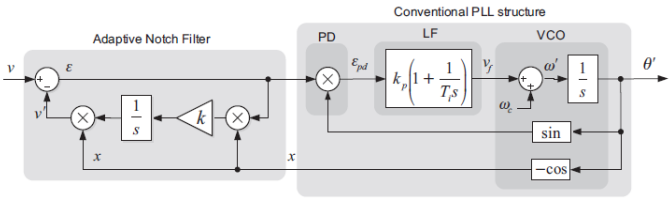


Figure 2.12: E-PLL Diagram. From [14].

Synchronous Reference Frame Phase-Locked Loop (SRF-PLL)

The SRF-PLL is a control block that synchronizes the voltage vector of the *dq* frame with a reference phase from the grid. As represented in the next figure, the *q* component of the *dq* transformed voltage is set to zero through a PI controller, while its output is also integrated to obtain the phase angle which should be used in the previous transformation.

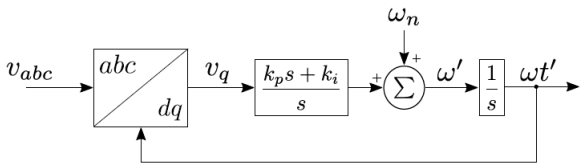


Figure 2.13: SRF-PLL Diagram. From [16].

Double Second Order Generalized Integrator Phase-Locked Loop (DSOGI-PLL)

The DSOGI implementation of the PLL is the adition of two main control blocks, the DSOGI Quadrature Signal Generator and the previously discussed SRF-PLL.
The first is an extension of the SOGI-QSG. The SOGI-QSG is a band-pass like filter with a flexible target frequency that generates two output signals, with a 90° degree delay between them (Fig. 2.14). These signals are nothing more than the result of the filtering of the input signal voltage, which results in its direct and quadrature components. Due to the implied phase difference, the output signals will only differ in magnitude, in the case that the input signal is not on the center frequency. The extension of this control system consists in adding one more SOGI-QSG, which, in unbalanced grid condition, provides the advantage of enabling the rejection of the negative sequence component (Fig. 2.15) [16].

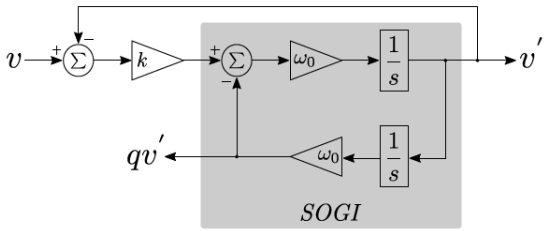


Figure 2.14: SOGI-QSG Diagram. From [16].

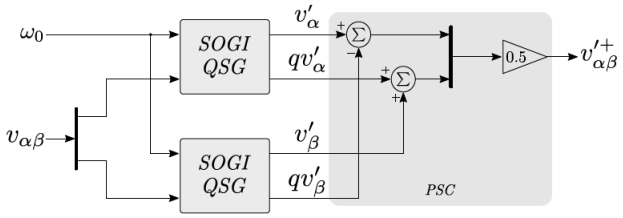


Figure 2.15: DSOGI-QSG Diagram. From [16].

On the DSOGI-PLL control block, the previously discussed SRF-PLL is used to generate a target frequency ω_0 which fed back as an input of the DSOGI-QSG block. The advantage of this block is that the phase error is always kept at zero, even if the grid frequency is experiencing some variations [16]. The resultant PLL block is depicted in Fig 2.16.

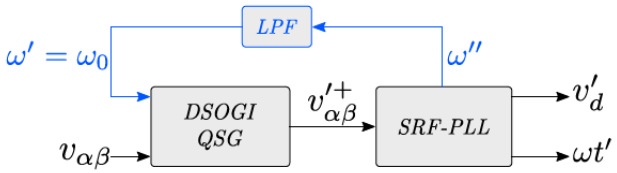


Figure 2.16: DSOGI-PLL Diagram. From [16].

2.2.3 AC Current Control

Two reference current components, provided by an external source (such as other control loops or externally defined references), are compared with measured values and fed to a designed controller. These include the d component of the current, usually responsible for active current and the q component, usually responsible for reactive current control.

For PWM applications the best practice is usually the use of linear controllers, according to [15]. Therefore two types of current control, based on linear controllers, are the proportional-integral (PI) control and the proportional-resonant (PR) control.

PI-based Current Control

The PI controller is a well known solution in all control related fields. It consists of the feed forward sum between a proportional gain and an integrator affected by what is know as the integral gain.

The main disadvantage of this controller is that it can't correctly track AC values, which leads to steady-state error and decreased disturbance rejection capability [14].The use of a PI controller in current control is only feasible if implemented in the *dq* synchronous rotating frame. For this, the transformations explained in 2.2.1, need to be implemented. The next figure illustrates a basic block diagram of the operation of the PI current controller. It should be noted that in this case two PI controllers should be used, for each one of the *dq* current components.

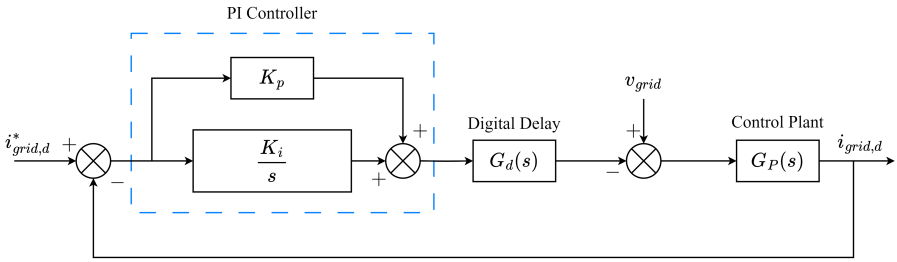


Figure 2.17: PI-based current control loop.

PR-based Current Control

The PR controller is very similar to a PI controller, with a transformation that consists on adding another integrator to create a second order system. Figure 2.18 showcases the diagram of this type of controller. Contrarily to the previous controller, the PR doesn't face the same issues. It can track AC quantities, thus it can be implemented directly in a stationary $\alpha\beta$ reference frame. In addition, the controller showcases an infinite gain at the resonance frequency, as opposed to near-zero gain for any other frequency. Furthermore, another helpful application is the possibility of adding more resonant blocks, in parallel with the K_P and the K_I and transfer function blocks in order to achieve selective harmonic compensation, as related in [17]. This compensation will not affect the dynamic response of the PR. This harmonic compensator inclusion is represented by the dashed line in Fig. 2.18 (ω represents the grid's frequency).

However, an infinite gain can cause stability issues [17]. As such, a non-ideal PR controller can be used, now responding with a finite but still high gain. Moreover, with the inclusion of the parameter ω_c on the second-order portion, it becomes possible to have a broader bandwidth, which reduces the effects that slight grid frequency variations have on the performance of the controller. In Fig. 2.19, an illustrative example of a non-ideal PR-based current control is depicted. To account for signal sampling and PWM update delays, a digital delay control block has been incorporated. The details and considerations regarding this subject will be addressed later on.

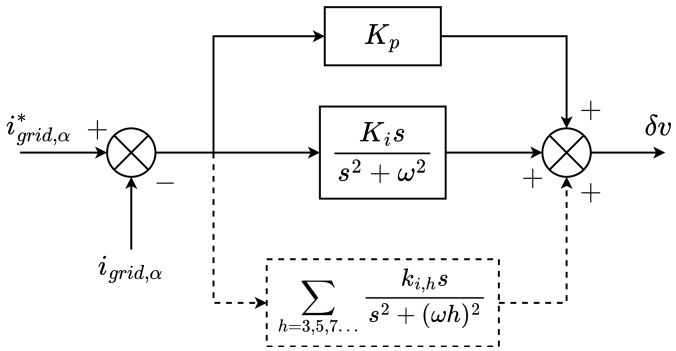


Figure 2.18: Diagram of an ideal PR controller with harmonic compensation.

As this controller can work on a stationary reference frame, the error between the reference and the measured grid currents in their α components is fed to the controller. As seen before, the α component of an AC quantity in a single-phase system is assumed to be the real value of that quantity. As such, the major advantage of the PR controller is that there is no need for any reference frame transformation and the measured current can be used directly in the control system.

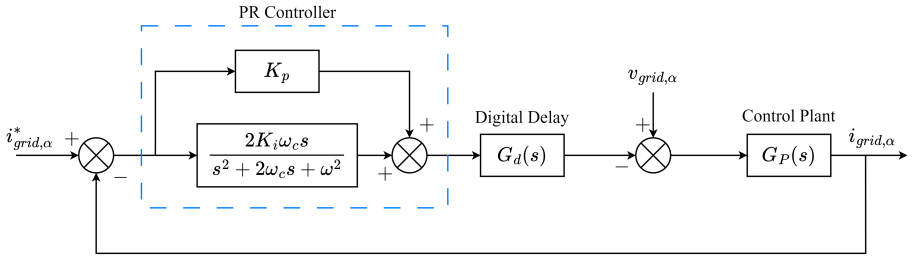


Figure 2.19: PR-based current control loop.

2.2.4 DC Voltage Control

By controlling the power transfers between the train and the catenary line, it is possible to control the DC bus voltage. Power oscillations lead to changes in the voltage levels that need to be compensated by the charging or discharging of the DC link capacitor [14]. However, the control of the power exchanges between the converter and the grid is done either through the control of the AC current or AC voltage. The first will be featured in this document. Therefore, this voltage control loop is not a direct way to control the DC bus voltage since it is actually more of a current reference generator, allowing the control of the DC voltage in an indirect manner.

On the other hand, the implementation of a DC voltage loop comes in handy since the value needs to be stable and so, it is useful to place a desired reference value as input. Moreover, due to this need for stability, the loop should have slow dynamics. Changes in the DC voltage level usually have two possible origins, either through changing the reference voltage that is needed or in the power flow between the grid and the DC-link. The two previously mentioned control loops

emerged from this need, firstly the DC voltage is measured and controlled by a PI controller in the outer loop, which must allow for a stable operation, as referred before. The output is the active current reference value that is then used as input on the inner loop.

It should be noted that the use of a PQ controller on the outer loop, that calculates the active and reactive power, based on voltage and current measurements, is also possible. This enables the regulation of active and reactive power to be done in a direct way. Another possible solution is the use of a "hybrid" outer control loop which includes the voltage control as well as an input for the calculation of the reactive power.

As a general example, in Fig. 2.20, a DC voltage control loop precedes the previously seen PR current control closed loop. It takes the DC voltage as an input, comparing it to a reference value and then generates a direct component grid reference, which is then transformed into the $\alpha\beta$ and fed into the current control loop.

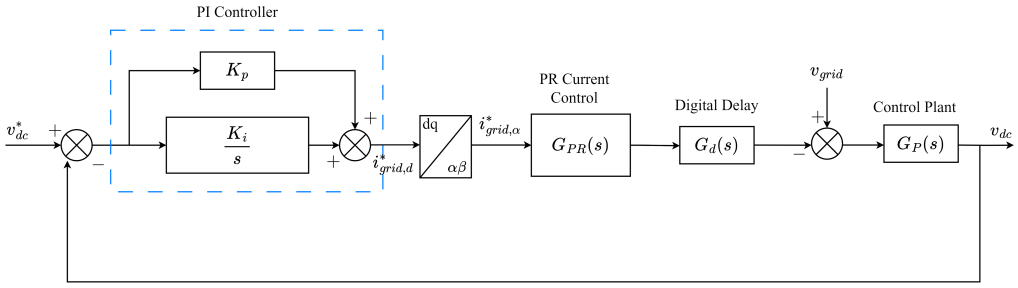


Figure 2.20: PI-based DC voltage control loop in cascade with previous PR current controller.

2.3 Digital Control

In power electronics, precise control of electrical energy conversion is crucial to optimize system efficiency and ensure reliable operation. Analog control techniques, although widely used in the past, often face limitations in terms of accuracy, adaptability, and complexity. For this reason, in the modern times, the application of some of the technologies described before is continuously migrating to the digital world. Therefore, digital signal processing and digital control are areas that are now closely related to power electronics in almost all applications [18]. Digital control harnesses the power of microcontrollers, digital signal processors (DSPs), and advanced algorithms to achieve superior control accuracy and responsiveness.

The need for digital control arises from various factors. Firstly, digital control techniques offer greater flexibility in designing and implementing complex control strategies. Through software programming, control algorithms can be easily modified and fine-tuned to adapt to different operating conditions, system requirements, and control objectives. This flexibility allows power electronic systems to achieve higher levels of performance and functionality. Moreover, it also facilitates a seamless integration with other technologies such as industrial communications, data acquisition, or system monitoring and supervision.

However, the implementation of a discrete control method comes with certain nuances that do not appear in its analog counterpart and must be addressed. This subsection aims to give an overview on some digital control aspects that affect the theoretically predicted results in a practical implementation by discussing some important subsystems that are present in control and are affected by this discretization.

2.3.1 The Digital PWM

In digital control applications, the Pulse Width Modulation (PWM) feature found in microcontrollers is typically either a dedicated peripheral unit or as a reserved function within the timers. The underlying concept involves incrementing a counter, with each clock tick, until it reaches a predetermined duty cycle value. When this condition is met, an interrupt is activated, causing the gate signal (initially set to high at the beginning of the PWM period) to transition to a low state. Figure 2.21 provides a visual representation of this operational principle.

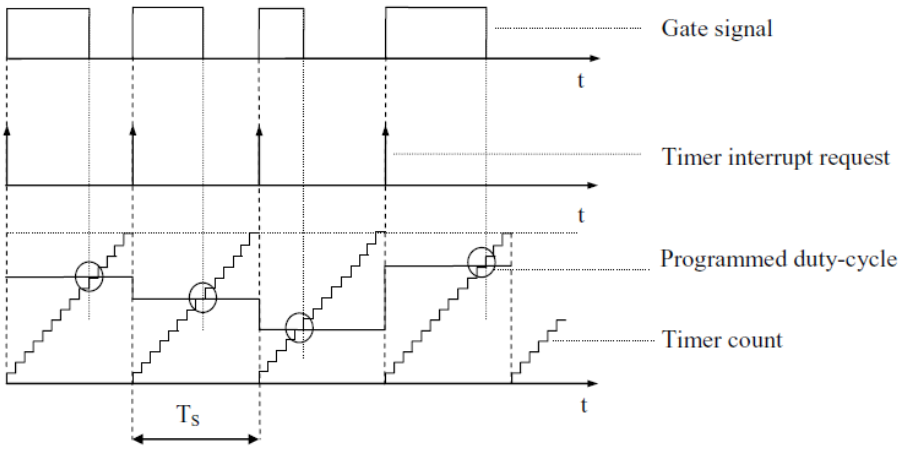


Figure 2.21: Digital PWM scheme. From [18].

Upon careful examination of the provided image, it becomes evident that the modulation signal is updated solely at the start of each modulation period (T_s in the figure). Consequently, any perturbation or desired adjustment in the programmed duty cycle will only manifest in the subsequent modulation period. This inherent characteristic introduces a delay in the response of the modulator. Therefore, when transitioning from analog to digital control, it is imperative to consider this delay and adapt the controller's bandwidth accordingly.

Another noteworthy aspect in digital PWM control is the selection of the sampling frequency (f_s) and the PWM switching frequencies (f_{sw}). As per Shannon's theorem, perfect reconstruction of a sampled signal is unattainable if its bandwidth exceeds the Nyquist frequency ($f_{NY} = \frac{f_s}{2}$), leading to aliasing. Ideally, the highest feasible sampling frequency is chosen. However, since an excessively high sampling frequency poses computational burdens, its value is constrained in practical microcontroller implementations. Nevertheless, this limitation can be advantageous in terms of simplifying the control procedure. When the sampling and switching frequencies

are synchronized, the aliasing of the sampled signal manifests solely as its average value, which is the desired quantity to control. Consequently, in most applications, $f_s = f_{sw}$ or $f_s = 2 \cdot f_{sw}$ if the double update PWM mode is available, as depicted in Fig. 2.21. Regarding the power electronic components, a high switching frequency is also desired, however, high values mean high commutation losses on the semiconductor devices.

2.3.2 Digital Filters

The used control procedure can be hugely affected by signals with significant noise. For a *clean* acquisition of the measured signals, a filtering stage should be added to the remove unwanted frequencies from the signal at the input of the procedure for a stable and correct control operation. The filter operation can be explained by the illustration in Figure 2.22, where the magnitude response of a non-ideal low pass filter can be seen. By observing, it becomes clear that the filter lets low frequencies through, while blocking the ones higher than the cut-off frequency, f_z. The gain of the filter is one until the cut-in frequency, f_p, where it drops significantly.

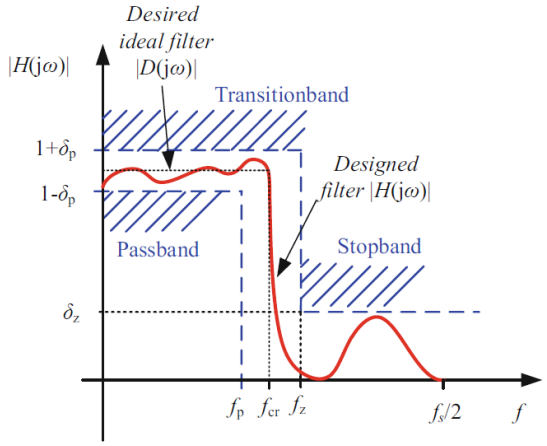


Figure 2.22: Low-pass filter magnitude response. Adapted from [19].

Two main types of digital filters usually used in power electronic applications, each with its advantages and disadvantages. Both will be presented next.

Finite Impulse Response Filter

The FIR filter is a based on simple moving average, where its order represents the number of samples used to calculate the instantaneous average. It is the described by equation 2.1:

$$\begin{aligned} y[n] &= b_0 x[n] + b_1 x[n-1] + b_2 x[n-2] + b_3 x[n-3] + \ldots + b_N x[n-N] \\ &= \sum_{k=0}^{N} b_k x[n-N] \end{aligned} \tag{2.1}$$

FIR filters derive their name from their finite impulse response characteristic, indicating that they rely on a finite number of input samples and operations. This feature may initially seem

advantageous for computational efficiency. However, achieving desired results often requires a higher filter order, resulting in a heavier computational burden. Consequently, FIR filters are not typically well-suited for real-time closed-loop applications as they introduce significant group delay. On the bright side, the absence of a feedback loop ensures their stability. Furthermore, their linear phase response guarantees that the input signal remains unaffected and free from distortion. The usual diagram for a FIR filter in the direct form is shown in Fig. 2.23.

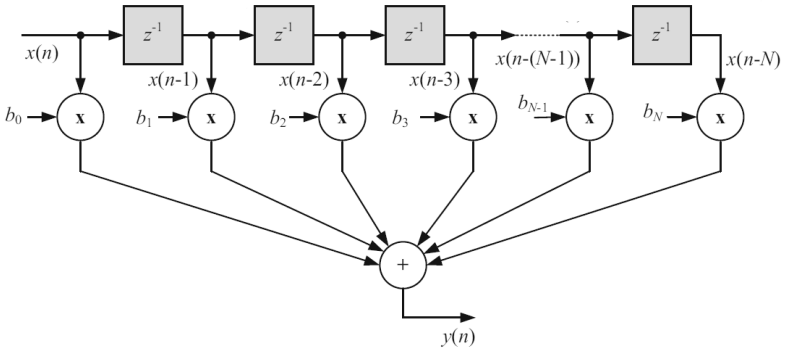


Figure 2.23: N order FIR filter block diagram. Adapted from [19].

Infinite Impulse Response Filters

Contrary to the implementation of FIR filters, IIR digital filters calculate the output based on both the previous inputs and the previous outputs. As such, their behaviour is described by:

$$\begin{aligned} y[n] &= b_0x[n] + b_1x[n-1] + b_2x[n-2] + b_3x[n-3] + \ldots + b_Nx[n-N] \\ &\quad - a_1y[n-1] - a_2y[n-2] - a_3y[n-3] + \ldots - a_Ny[n-N] \\ &= \sum_{k=0}^{N} b_kx[n-N] - \sum_{k=1}^{M} a_ky[n-N]. \end{aligned} \tag{2.2}$$

As a result, the phase response is non-linear which may lead to some amount of distortion of the output signal. Moreover, it also causes it response to be less stable in comparison to their FIR counterparts. Nonetheless, in a real-time application, this type of filter is much more appropriate since it has low latency but also a lighter computational burden since it needs fewer coefficients to achieve a proper result. As a final note, this filter is more complex and requires more effort to design. Nevertheless, it will be the chosen configuration for this work. A block diagram of the general structure of a direct form digital IIR is presented in the Fig. 2.24.

2.3.3 Controller Discretization Methods

For the same reasons as the digital filters, the chosen controllers must also be discretized. In a microcontroller the use of discrete time signals is naturally impossible due to the discrete way in which the signals are acquired. As such in order to achieve an accurate control performance, the controllers must be transformed to the continuous domain. Moreover, an early development of

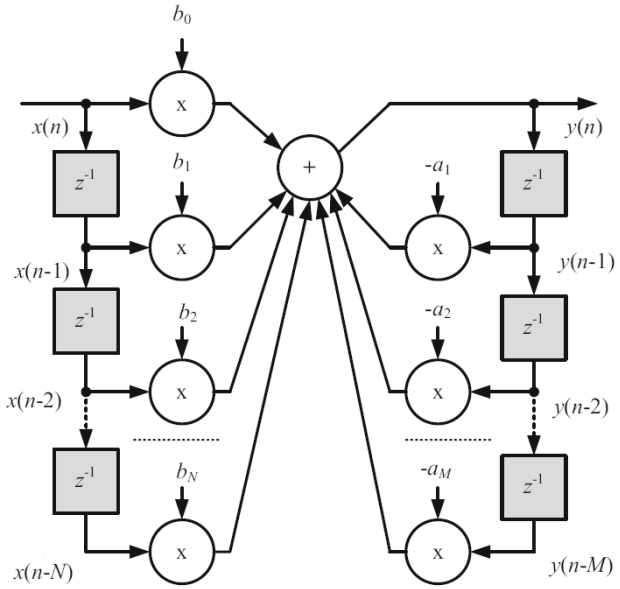


Figure 2.24: N order IIR filter block diagram. Adapted from [19].

discrete time controllers will be a valuable asset for a simulation environment, where the effects of sampling discretization can be analysed beforehand. In the literature, several methods are proposed for discretizing either PI or PR controllers [18, 20]. On the sub section only the Trapezoid (Tustin) and the Euler integration methods will be analysed. The main goal is to transform the continuous time integrals into discrete form, via numerical approximation. The transfer function of a PI controller will be used in both cases to better illustrate the two methods. As already addressed, the characteristic transfer function of a PI controller, in the Laplace continuous time domain is:

$$G_{PI}(s) = K_p + \frac{K_i}{s} \tag{2.3}$$

Trapezoid (Tustin) Integration Method

As the name states, in this method the area below the curve of the measured quantity is approximated with a sum of trapezoidal shaped areas. In the next figure a graphical representation of this approximation is shown:

The z-domain resultant transfer function can be achieved by substituting the independent variable in the continuous domain transfer function by the z-form resultant from the transformation. In the case of this method the z-form is:

$$s = \frac{2}{T_S}\frac{z-1}{z+1} \tag{2.4}$$

By substitution in equation 2.3, it is possible to achieve the z-domain equation:

$$G_{PI}(z) = \frac{K_p\left(1-z^{-1}\right) + \frac{K_i T_s}{2}\left(1+z^{-1}\right)}{1-z^{-1}} \tag{2.5}$$

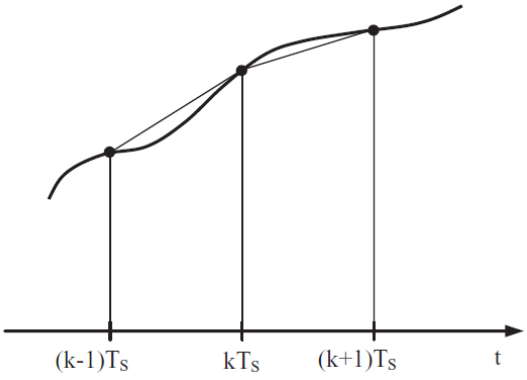


Figure 2.25: Trapezoidal (Tustin) approximation. From [18].

However, this still isn't feasible for a programming implementation, for example in a microcontroller. Therefore the discrete time difference equation must be derived. The transfer function, now on the n domain will be:

$$G_{PI}[n] = \frac{Y[n]}{X[n]} \tag{2.6}$$

Where $X[n]$ and $Y[n]$ represent the input a the output of the controller at the n^{th} sample. By applying the inverse Z-transform, and solving for $Y[n]$:

$$Y[n] = Y[n-1] + K_p(X[n] - X[n-1]) + \frac{K_i T_s}{2}(X[n] + X[n-1]) \tag{2.7}$$

Euler Integration Method

In the Euler integration method, the strategy is similar, only now it is done by calculating the area function of a consecutive sum of samples. This method has two variations: the forward and the backward Euler methods. The main difference lies on the instant that this area is calculated, as can be deducted from the next figure.

Similarly, by taking the Z-form of the backward Euler method:

$$s = \frac{z-1}{z \cdot T_S} \tag{2.8}$$

It is possible to obtain the Z-domain transfer function:

$$G_{PI}(z) = K_p + K_i \cdot T_s \cdot \frac{z}{z-1} \tag{2.9}$$

Once again, the difference equation is obtain and the controller is fully discretized:

$$Y[n] = K_p X[n] + K_i (Y[n-1] + T_s X[n]) \tag{2.10}$$

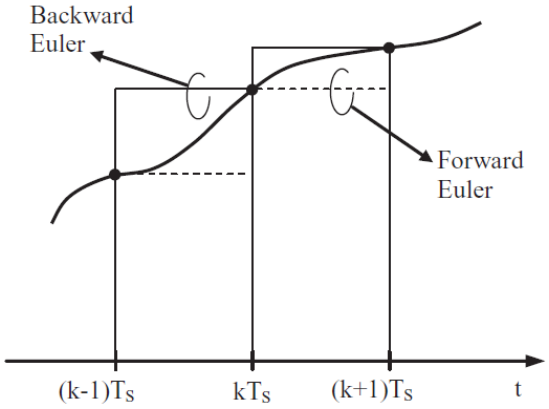


Figure 2.26: Backward and forward Euler approximations. From [18].

PR Controller Discretization

Similarly, the discretization of a PR controller is also needed. Although the methods used for discretization remain the same, the crucial distinction lies in the transfer function of the controller. Notably, the resonant controller is considerably more sensitive to the process of discretization. This heightened sensitivity arises from its characteristic narrow band and infinite gain at the desired resonant frequency. Consequently, even minor design errors or frequency variations can profoundly impact the control operation [20]. With this in mind, Yepes *et al.* conducted an evaluation of various discretization methods for the PR controller, aiming to identify the advantages and limitations associated with each approach. Among the two solutions presented earlier, only the second one demonstrated satisfactory performance at low frequencies. Furthermore, this solution boasted a more straightforward implementation compared to the others, thereby offering a viable and uncomplicated option. Conversely, the Forward and Backward Euler methods were marked as not suitable for resonant controllers as they introduced substantial instability. The transfer function of a non-ideal PR controller's is given by:

$$G_{PR}(s) = K_p + \frac{2K_i\omega_c s}{s^2 + 2\omega_c s + \omega_0^2} \tag{2.11}$$

For a simpler adjustment of the gains, discretizing only the second order function present in the PR controller is a viable solution. Hence, by using the Trapezoid Integration Method, similarly to what was done in the PI controller, one can obtain the difference equation of that second order function. This equation is given by:

$$\begin{aligned} Y[n] = {} & b_0X[n] + b_1X[n-1] + b_2X[n-2] + b_3X[n-3] + \ldots + b_NX[n-N] \\ & - a_1Y[n-1] - a_2Y[n-2] - a_3Y[n-3] + \ldots - a_NY[n-N] \end{aligned} \tag{2.12}$$

Effects of Computational Delay

In a similar fashion to the digital PWM, the computation of the control procedure also has an associated delay, due to the calculation performed. As a result, the control updates the output value, already delayed, and still has to wait for the update delay of the digital PWM. As such, the update of the response to a certain input will not happen in the next PWM cycle, but in the second. When this delays are not considered, a stable operation is not possible, as the controller is always oscillating due to updating its output according to input values that no longer exist. A common solution, is to account for the delays when designing the analog controller. This way and once again, by taking a more conservative control approach, one can reduce the controller's response speed and have a smoother and more precise dynamic operation. Moreover, when this is not enough a reducing of the processing time of the algorithm is also a good measure.

2.3.4 Microcontroller Market

The brains behind the operation of the converter and where all the digital control will be done is the microcontroller. Nowadays, the market of microcontrollers is vast, with an immense amount of choices, which makes the selection a rather time consuming process. The main requirements for a microcontroller on this kind of application are:

- Must have some specific features. Such as fast ADC, DAC, DSP, high-resolution PWM, I/O ports, floating point calculations, real-time clock and timer interrupts. Communication peripherals are advantageous depending on the application;
- Fast clock speed;
- Enough memory for the control program;
- Withstand a relatively high temperature range;
- Integration with an easy-to-use development software is always helpful in order to simplify the job.

A quick search through the main microcontroller manufacturers revealed a list of possible candidates for this type of application.

- Infineon's XMC 4500;
- ST Microcontrollers' STM32H7 family;
- NXP's S32K family;
- Texas Instruments' TM4C123GH6ZXR.

The XMC 4500 will be the one used in the experimental part of this work. It's main features are:

- 512 to 1024 KB Flash, 128 to 160 KB Ram;
- At least two PWM timers;
- Peripherals clock frequency at 120 MHz;

- Core frequency at 120 MHz;
- Temperature range from -40° to 85°/125°;
- Free *DAVE IDE* and *DAVE Apps*.

2.4 Final Remarks

The main goal of this chapter was to provide a clear understanding of the modern technologies that are utilized through the course of this work. Accordingly, the main configurations of electrified railway supply and traction systems were presented as an introductory aspect of railway fundamentals, with utmost care of also giving an overview of the power quality issues that those systems face. Furthermore, several elements of control theory and digital control were explained, predicting the upcoming development and implementation of a controller for a railway traction converter.

Chapter 3

Line-side Converters for Railway Traction

The line-side converter is the first stage of energy conversion and power flow control inside the on-board traction unit of an electrified railway train. It importance in terms of power quality in undeniable since it is responsible for the interface with the railway grid.

Accordingly, this chapter addresses the technological aspects of the line-side converters used in railway traction. It delves into the components utilized in these converters, examines various architectures that can be adopted, and explores interesting modes of operation that can effectively fulfill the objectives of this work.

3.1 Advances in Semiconductor Technology

The first big step in the semiconductor evolution on railway traction systems was in the period of time from the year 1980 to 2000, when there was a large scale adoption of the Insulated Gate Bipolar Transistor (IGBT) technology on trains from all over the world [7]. Before that, line-side rectifiers were either uncontrolled or thyristor based phase-angle controlled, which resulted in poor power factor operations as well as high harmonic production, with a high cooling demands and bulky dimensions. With the adoption of IGBTs, it was possible to increase the maximum switching frequency from 300 Hz to 1500 Hz. Moreover, the use of this technology reduced the noise of the running vehicle, the traction transformer losses and also the weight of the converter, due to a simpler gate driver circuit. A decreased harmonics production led to smaller heat losses and, as a result, to less cooling needs [5, 21].

Recently, a new generation of power semiconductors is being widely researched as an alternative to the IGBTs for general traction applications. The silicon carbide (SiC) semiconductors reveal an outstanding performance when compared to their silicon (Si) counterparts. As depicted by Brenna *et al.* in [22], there are three main advantages when it comes to the use of this technology:

- Lower switching losses means that the converter can work with higher switching frequencies and, as a consequence, it is possible to reduce the size of passive components;
- Ability to resist higher power operations as it features a very high breakdown voltage and very low resistance;
- Capability to withstand higher junction temperatures resulting in lesser need for larger heatsinks.

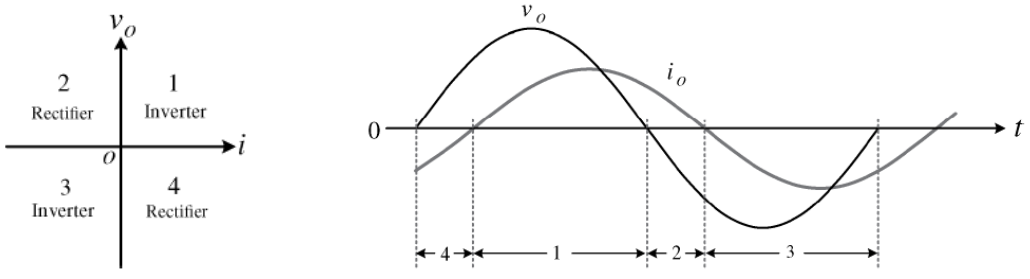
Consequently, SiC devices are the natural evolution of the semiconductor related technology, as they provide such advantages over the Si semiconductors, that allow to increase performance while reducing the overall dimensions of the power converter.

3.2 Common Converter Configurations

Various converter configurations can be employed to establish a suitable interface with the catenary line. The most extensively studied configurations are the multilevel converter, the modular multilevel converter, and the matrix converter. While this work's primary focus is the H-bridge converter, the other configurations will also be object to an overview throughout the course of this section.

3.2.1 H-Bridge Converter

In the modern days, PWM controlled four quadrant single-phase converters, with transistors, are common as a solution for the interface with the catenary. This converter main feature is that it can operate in two different modes, inverter and rectifier, according to the voltage and current waveforms, as shown in Fig. 3.1. In consequence, it is also possible to have control over the real and reactive power exchanges with the grid. In addition, the AC side current is cleaner, with less harmonic content, due to its PWM modulation.



(a) (b)

Figure 3.1: Converter Modes of Operations according to its waveforms. From [1].

As depicted in Fig. 3.5, the converter is connected to the secondary winding of the transformer. Due to the use of PWM, high-frequency harmonics are still produced, although to a much lesser extent. These harmonics can be injected into the catenary and, in an extreme case, into

the main utility grid, resulting in voltage distortions and potentially impairing the functionality of other equipment. Therefore, a filter is typically connected between the secondary winding and the converter, improving the power quality transferred to and from the grid. In this instance, however, the transformer's leakage inductance may itself work as a filter, minimizing its need [7]. Different types of filters for this objective will be addressed later on in this chapter (in section 3.3). The converter has two arms with a pair of GTO or IGBT type semiconductors each. With each of these semiconductor, a diode is also installed in anti-parallel, in order to allow bidirectional power flow. As the converter is pulse-width regulated, one can achieve different DC voltage levels with proper changing of the duty-cycle. Moreover, converters with various configurations can be connected to the DC side, as the example seen in the previous chapter.

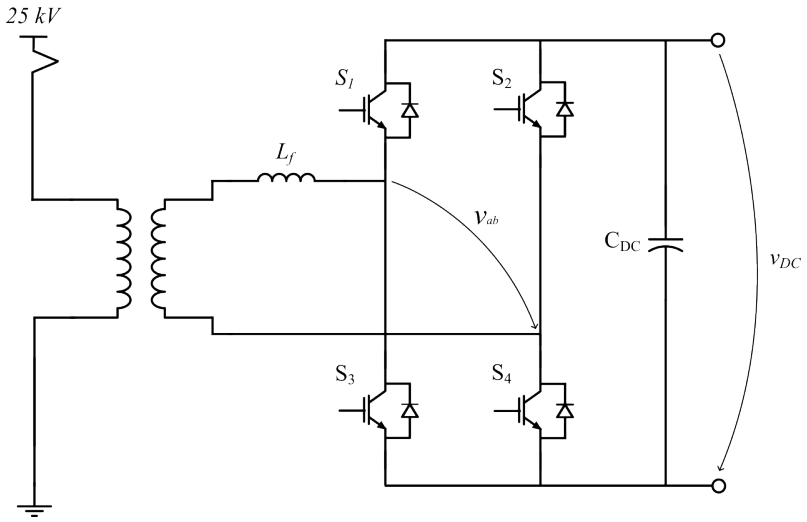


Figure 3.2: Circuit Diagram of a H-bridge single-phase converter.

3.2.2 Multilevel Converter

As discussed in the given overview of the evolution of semiconductor technologies (Section 3.1), current trends in power electronics aim to increase the switching frequency applied to the semiconductors, as it helps to reduce harmonic distortion but also the size of passive components present in the circuit. Nonetheless, higher switching frequencies also give rise to higher losses and stresses on the semiconductors.

Another popular alternative to the conventional H-bridge converter is the multilevel converter. The concept behind this architecture is substituting each semiconductor by two or more. This results in staircase-like output wave, with as many levels as the more semiconductors are added, which naturally, also increases the power quality and allows for an increase in the switching frequency. The main features of the multilevel configurations are [23, 24]:

- Reduced harmonic distortion, due to a high quality output waveform.
- Higher Efficiency.
- Decreased stress on the control components.

However, it also features some downsides, such as a more complex control and higher cost due to the increased component count. There are three architectures that are commonly used, such as the Neutral Point Clamped, the Flying Capacitor or the Cascaded Multi-cell or in the case of the more recent research topics, the Modular Multilevel configuration.

3.2.2.1 Modular Multilevel Converter

The modular multilevel converter (MMC) is yet another configuration that has gained significant attention and is currently the subject of an extensive number of research investigations [25, 26, 27]. This particular configuration involves connecting multiple converters in series on the AC side, while sharing a common DC bus. The modular multilevel converter offers several notable advantages. Firstly, it enables the adoption of higher switching frequencies, which in turn reduces the size of passive components and allows for the possibility of operating without a transformer, resulting in a more lightweight solution. Additionally, this configuration facilitates the increase of output levels, and since all converters share the same DC bus, simpler gate drivers can be utilized [25].

Moreover, the modular nature of this converter design provides enhanced flexibility for maintenance purposes but also to easily adjust the system to different voltage ratings. However, the implementation of this converter configuration does come with certain difficulties, as highlighted by the authors [25]. For instance, when working with high catenary voltages, a significant number of modules would be required, which, in turn, necessitates a high number of PWM command signals. To address this issue, multiple microcontrollers could be employed to control the entire system, with a potential solution being the utilization of one microcontroller per module in a Master-Slave configuration. Figure 3.3 below offers a simplified illustration of the modular multilevel configuration.

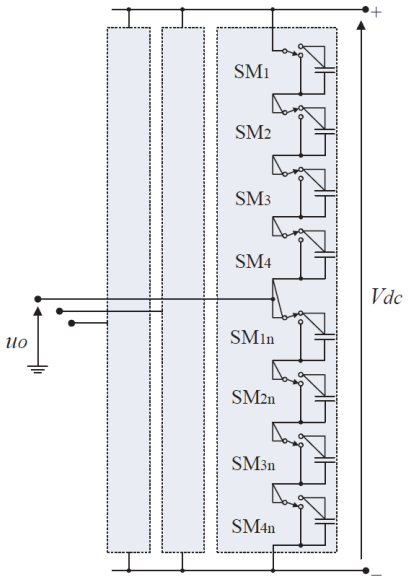


Figure 3.3: Simplified MMC block diagram. SMx represents a specific sub module. From [28].

3.2.3 Matrix Converter

As discussed numerous times throughout this study, the progression of power electronics in various domains, including railway applications, consistently involves an increase in switching frequency. The matrix converter represents an alternative configuration that can be utilized for this purpose. However, it distinguishes itself as a distinct architecture, functioning as a single-stage AC/AC converter. In the context of railway traction, this topology is extensively investigated and often associated with the implementation of a power electronic transformer (PET), in contrast to the commonly employed low-frequency transformer. Remarkably, it is the second most studied converter configuration for such applications [29, 30]. The PET offers advantages such as reduced size and increased operating frequency, typically ranging from hundreds to tens of kilohertz. Nevertheless, its adoption requires connecting the line-side converter directly to the catenary, subjecting it to significantly higher voltages. This highlights the need for matrix converters.

The matrix converter comprises an arrangement of bidirectional switches arranged in an m by n array, depending on the number of phases in the source (m) and the load (n) [31]. Its main benefits include a simpler and more compact circuit, sinusoidal input and output currents, bidirectional capabilities, and the ability to operate with a unit power factor.

In [29], another application of a matrix converter in conjunction with a power electronic transformer is presented (Fig 3.4). The proposed system employs a cascade connection of multiple single-phase matrix converters to interface with the catenary line. The authors successfully implemented this system and obtained favorable results under various operating modes and line conditions, demonstrating its viability as a solution for employing medium frequency transformers. However, the current limitations of available semiconductor power and voltage ratings pose a significant constraint on the widespread adoption of this application. Only through advancements in this technology can the proposed system become more widely utilized.

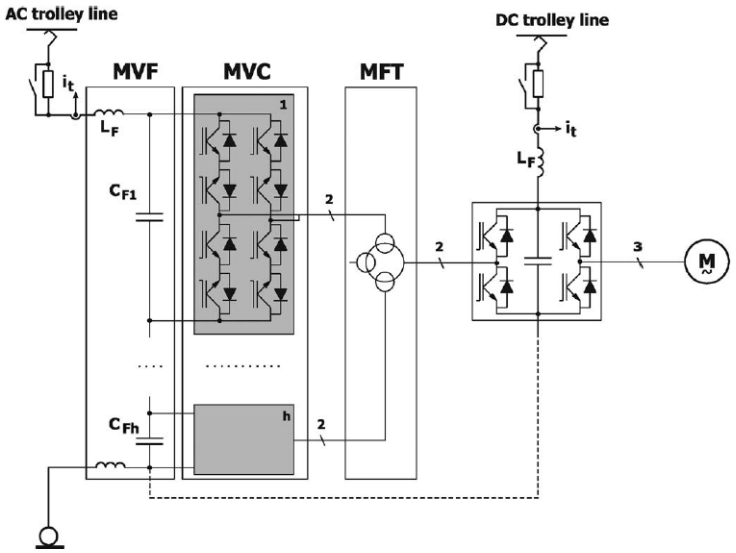


Figure 3.4: Cascaded matrix converter (labeled as MVC). From [29].

3.2.4 Interleaved Configuration

Another option currently in use is the interleaving of multiple converters. Interleaving consists in placing two or more converters in parallel, independently controlled by PWM generated signals with different phases. This allows the system total output current to be the sum of the currents of each separate converter, hence reducing output current ripple.

Modern trains for high-speed AC lines or electrical multiple units usually feature two or four line side converters that can be interleaved. As discussed in [1], the phase difference between each converter must be 1/2 or 1/4 of the switching period, respectively, for a correct interleaving operation. In consequence, the frequency of the output current is double or quadruple of the switching frequency a higher output frequency, with smaller and easier to filter amplitudes. The correct phase shifting between the current output of both converters also leads to decreased harmonic content.

This can be confirmed in the study carried by Brenna *et al.*in [32] that contemplates the harmonic analysis of the current absorbed at the pantograph for the use interleaved four quadrant single-phase convertersin a high-speed AC train in comparison with a generic standalone four quadrant converter.

The simulation registered a considerable third and a high tenth order harmonics, the first due to the difficulty in following the sinusoidal reference with a low switching frequency and the last corresponding to the switching frequency. In fact, the Fourier analysis of the current output in the case of four interleaved converters revealed that the tenth order harmonic is no longer noticeable, while the third harmonic is still present, due to the reasons stated before.

The interleaved configuration also makes the system redundant, ensuring that it will continue to function even if one of the converters fails. Three interleaved converters were used in a different case study to test the system's redundancy. It was observed that although the switching frequency is not entirely cancelled as in the prior case, the results are still superior to those obtained when using a single converter.

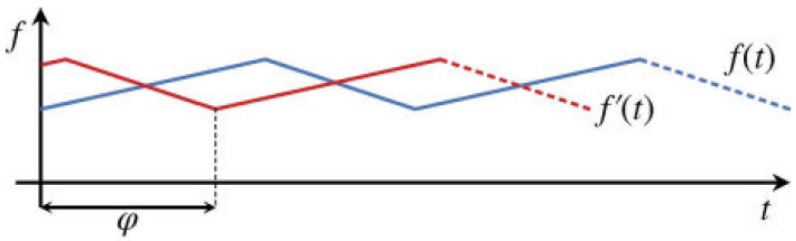


Figure 3.5: Output current waveforms from two interleaved converters. From [32].

3.3 Filter Design

AC Side Filter

As previously depicted, the grid side filter is rather important for the quality of the current injected into the grid. It has mainly two jobs, the first is to ensure the appropriate working of the line-side converter, consequently, if connected to a voltage source, it should have an inductive behaviour. Moreover, as mentioned before, the harmonic content produced by the converter due to the PWM may induce voltage distortion in the line, hence, the grid filter can also be used to suppress these and other types such as the resonance harmonics. It is also possible, however, that the transformer's leakage inductance may work as a filter, minimizing its need [1].

Different choices of filter exist for this objective, such as L, LC or LCL type filters. According to [14], the most preferred typologies to mitigate the voltage degrading harmonics:

- L Filter: is the simplest filter configuration used to mitigate PWM harmonics.
- LC Filter: the filter targets chosen harmonics from the whole spectrum that need to be reduced. The filter needs to be tuned to reduce a specific harmonic frequency, with care not to place its resonance frequency too close of the switching frequency.
- LCL Low-pass Filter: targets only high order harmonics, which might not be suitable for systems with low switching frequency. It reaches the whole harmonic spectrum, however, one should be careful not to place its resonance frequency too close of the switching frequency.

DC Side Filter

As related in [14], the energy retained at the AC side by the passive components is only less than 5% of the the total energy stored, with the DC link being the side that retains more energy. This means that a filter is also fundamental for the DC side. A capacitor is usually used in order to reduce voltage ripple.

The filter design also influences the control of the converter, with the response of the AC and DC waves being affected by the filters' time constant.

3.4 Pulse Width Modulation

The modulation technique enables the coordinated commanding of the switches of the converter to generate the desired output voltage and frequency. Sinusoidal PWM is one of the modulation methods most frequently used in power electronic solutions. Two variations of this method will be discussed along with their primary differences in this section.

Bipolar PWM

In this method, a sinusoidal wave v_{sin}, usually named modulating wave, is compared with a triangular wave v_{tri}, named carrier wave. The switches are turned on and off in pairs, which alternates the voltage at the AC side of the converter (V_{ab}), as follows:

Table 3.1: Switch commands in bipolar PWM.

Condition	S_1	S_2	S_3	S_4	V_{ab}
$v_{sin} > v_{tri}$	ON	OFF	OFF	ON	V_{dc}
$v_{tri} > v_{sin}$	OFF	ON	ON	OFF	$-V_{dc}$

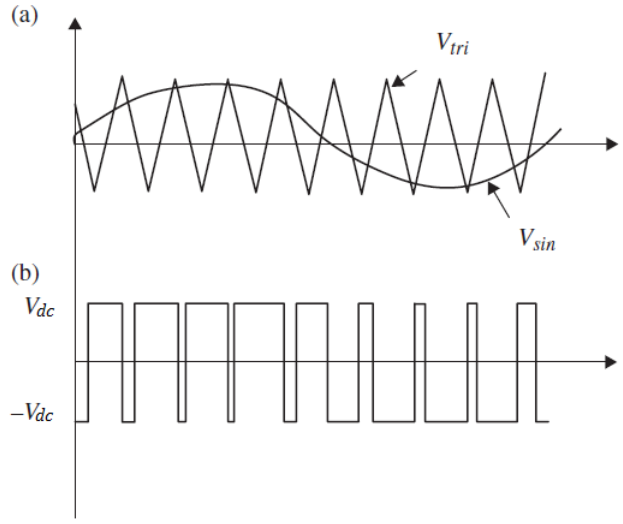


Figure 3.6: Bipolar PWM: modulating and carrier wave signals, (a) and resulting output wave at the AC side, (b). Adapted from [7].

Unipolar PWM

Alternatively, a widely used strategy is also the unipolar PWM. The main difference to the bipolar switching presented before is that this technique uses two sinusoidal modulating waves, which results in different switch commands and an AC voltage waveform with three levels, as follows:

Table 3.2: Switch commands in unipolar PWM

Condition	S_1	S_2	S_3	S_4	V_{ab}
$v_{sin} > v_{tri}$	ON	OFF	OFF	OFF	V_{dc}
$v_{tri} > v_{sin}$	OFF	ON	OFF	OFF	0
$-v_{sin} > v_{tri}$	OFF	OFF	ON	OFF	0
$-v_{tri} > v_{sin}$	OFF	OFF	OFF	ON	$-V_{dc}$

It is important to acknowledge that in this case, the AC side voltage level corresponds to the subtraction between the voltages of each branch in relation to the ground, hence V_{ab} will not only vary from V_{dc} to $-V_{dc}$, but will also be 0 at the stages where V_a is equal to V_b (Fig. 3.7) and hence the "unipolar" designation. Consequently, this technique doubles the switching frequency when compared to the bipolar PWM (as depicted in Fig. 3.7), which is naturally desirable as it improves the quality of the resultant waveform.

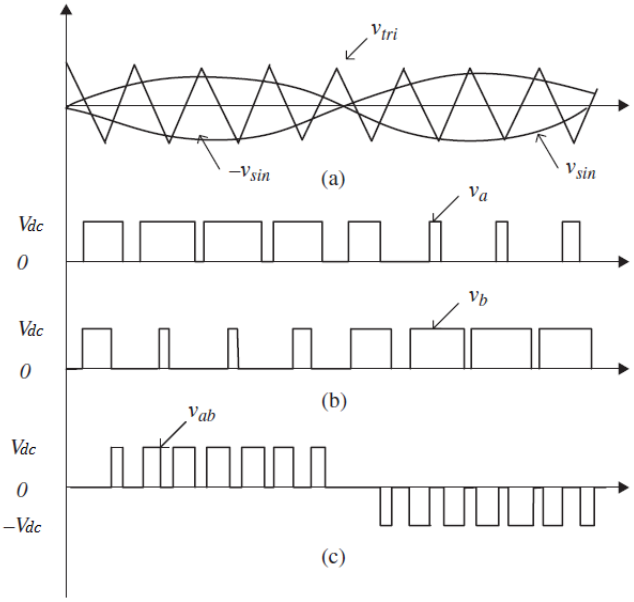


Figure 3.7: Unipolar PWM: modulating and carrier wave signals, (a), output in relation to the ground, (b), and resulting output wave on the AC side, (c). Adapted from [7].

3.5 Regenerative Braking

The substantial size and weight of a fully operational train lead to the generation of a significant amount of energy during braking. Railway systems employ various braking techniques, from pure mechanical, having all the energy dissipated in the disks and pads, to rheostatic, where the motor acts as generator and the energy is dissipated at on-board resistors. However, advancements in power electronics technologies have made it possible to recover and reuse this energy rather than dissipating it. This is achieved through a different braking method known as regenerative braking.

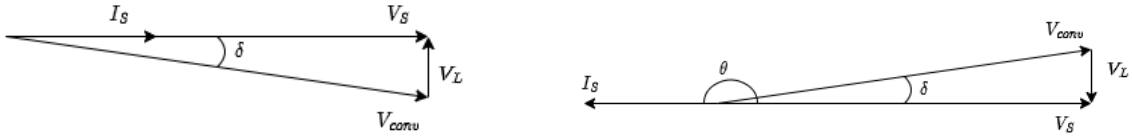
While regenerative braking has gained considerable attention in recent times, particularly due to the rapid proliferation of electric four-wheeled vehicles, it has already been extensively researched and implemented in the railway industry for a considerable period.

Although there are more, the most commonly related strategies to harness the energy originated in braking in the literature are [25, 33]:

- Feedback to the feeder line.
- On-board energy storage system;
- Wayside energy storage system;

Within the context of this dissertation, these three alternatives prove to be the most captivating due to their direct relation with the line-side converter for injecting energy back into the grid. With regards to the first option, the primary concept is to simply redirect the braking energy to the supply line. However, a direct power transfer between trains is not always feasible, as it necessitates the proximity of another train capable of consuming the injected power. One potential solution involves coordinating the departure and arrival of two consecutive trains at the same station [25]. Alternatively, a reversible traction substation could transmit the energy to the medium voltage grid, allowing it to be utilized by other devices. The remaining two options center around the utilization of energy storage systems. The second option involves an on-board solution, enabling the train to operate on a catenary-less railway or selectively feed energy back into the overhead line when necessary. The last option entails storing energy in an off-board battery located beside the track, which can then be utilized by another vehicle when required.

Since the line-side converter offers bidirectional capabilities, it is possible to control the direction of the active power flow, hence during braking, the train would supply active power to the grid instead of consuming. This can be done through the control of the magnitude of the converter's output voltage and its phase angle relative to the mains voltage. As the example in Fig. 3.8, when working with unitary power factor, by varying the angle δ it is possible to achieve one of the two different operation modes for the converter: the rectifier *(a)* or inverter *(b)* modes depending on the direction of the current.



(a) (b)

Figure 3.8: Phasor diagrams for the converter's operations with unitary power factor: rectifier operation (a) and inverter operation (b).

3.6 Reactive Power Compensation

One of the important factors to consider, when addressing power quality issues on electrified railways, is the overhead line capacity. Heavy railway traffic on the supply line leads to low operating voltage on the catenary, which in turn causes high reactive power demand from the supply line. In consequence, several methods of reactive power compensation, such as static VAR compensators (SVCs) or static synchronous compensators (STATCOMs), have been used with the aim of countering the issue of low system voltage. However, these types of compensators are static and have poor performance in cases where the train is far from their position [6].

An interesting solution, also regarding the earlier discussed current control, is the use of the line-side converter as an active and mobile compensator. More precisely, due to its bidirectional operation, reactive power compensation is possible as a solution to regulate the system voltage to nominal, without suffering from the disadvantages of being static.

According to the deduced equations on the study made in [34] and following the line of thinking of the previous section, if the real power demand is assumed to be constant, the reactive power can be controlled mainly with the amplitude of the converter voltage and also with the its phase difference to the grid voltage, δ.

As a result, the variation of those parameters leads to different power factor operations. The two different operations are depicted in Fig. 3.9, with the leading power factor (b), being the one which depicts reactive power injection into the grid. The reactive power operational range, however, is limited by the interval of values of the controlling parameters, magnitude of V_{conv} and δ.

Nevertheless, it should be said that in a real application for this converter the real power will not be constant since it will depend on the motor's operation, as a consumer or producer of active power, as seen in the previous section. The constant real power condition was only used on that study to demonstrate the effects of varying the reactive power parameters. In the simulation and experiment, the manipulation of those parameters should be carefully made, since they also affect the active power transfer.

The reactive power controller can be done with the use of a PI controller that takes the error between a reactive power reference and the corresponding measurement, and generates the orthogonal reference for the AC current, i_q, that should be then fed to the current control scheme.



(a) (b)

Figure 3.9: Phasor diagrams for the converter's operation with different power factor: lagging power factor (a) and leading power factor (b).

Despite some trains work with a fixed power factor, which is feasible and compensates for possible voltage drops, the conditions of the line are not always the same, since the train is moving, and other rolling stock can also affect the quality of the supply. As such, a more interesting solution is the use of the line parameters as a way to generate variable reactive power setpoints in a closed loop manner, leading to a more effective compensation.

3.6.1 Strategies for Catenary Voltage Support

Determining the amount of reactive power to inject into the catenary, however, is not a simple task. In fact, there are a number of variable factors that affect the catenary line conditions and that should be taken into account. Although the amount of research into on-board reactive power compensation for overhead line voltage support is somewhat limited, the remainder of this section will provide an overview of several algorithms and methods documented in the literature on this subject, and more specifically how the reactive power setpoint is generated.

Standard PI Controller

As the intent is to give support to a catenary line under low voltage condition, the intuitive main input variable would be the line voltage. As a first simple solution, a PI controller using the catenary line voltage as input and the 25 kV standard value as reference would generate a reactive current reference i_q that would then be fed to the current control subsystem.

Nonetheless, the always changing conditions of a railway supply line turn this into a more complex multivariate problem. For instance, the presence of an increased number of trains, each drawing a certain amount of reactive power from the line, can result in a reduction of the supply voltage measured by the train under consideration. Furthermore, as the train moves along the line, the measured line voltages vary, with lower voltages observed as the distance to the nearest substation increases. Consequently, a conventional PI controller, designed for nominal conditions, may not be capable of accurately tracking the reference value across different scenarios.

Gain Scheduled PI Controller

In [12], Bahrani *et al.* present PI controller with adjustable gains as a solution. It involves estimating the catenary line's impedance beforehand and iteratively adapting the controller's gains for effective reactive power compensation in different train positions between two traction power substations.

This method's initial step is to determine the catenary's inductance, which will indirectly change depending on the train's present position. The process begins with the injection of the 7.7th harmonic current at an arbitrary frequency (as long as it doesn't interfere with any other systems), after which the correspondent harmonic voltage and current at the point of contact are measured. To implement the suggested approach in this study, a SOGI-PLL tuned to this particular harmonic may be used to derive the $\alpha\beta$ voltage and current components from the measured values at the point of contact (Equation 3.1 and 3.2). Following that, the value of the 7.7th harmonic impedance is also determined (Equation 3.3). Then, to obtain more exact values, a real-time identification technique, with the introduction of a factor that acounts for measurement errors, was used. Since it may deteriorate the voltage at the site of contact, the harmonic current injection shouldn't be done continuously.

$$\|V_{pc,7.7}\| = \sqrt{V_{pc,7.7,\alpha}^2 + V_{pc,7.7,\beta}^2}, \tag{3.1}$$

$$\|I_{t,7.7}\| = \sqrt{I_{t,7.7,\alpha}^2 + I_{t,7.7,\beta}^2} \tag{3.2}$$

$$\|Z\| = \frac{\|V_{pc,7.7}\|}{\|I_{t,7.7}\|} \tag{3.3}$$

The Ziegler-Nichols frequency response method was employed in order to calculate the different PI gains according to the changes in the line inductance. It was observed that, while the integral gain remained constant for all train distance points used in the calculation, the propositional gain was accessed to be inversely proportional to the estimated inductance.

The study then proceeded with three simulation tests: one without compensation, one with a single train and two substations performing reactive power compensation, and one with two trains and three substations, again with reactive power compensation. In the first test, it was evident that the voltage drop at the contact point increased as the distance from the substation increased, reaching its peak value precisely at the middle point between two substations. Conversely, in the second and third tests, the authors observed a nearly constant AC voltage, indicating precise adjustment of the PI gains and effective compensation of reactive power. These findings demonstrate the feasibility of the proposed method for catenary voltage support. Additionally, the method showcased its capability to operate in network solutions with multiple substations and vehicles.

However, it should be noted that when multiple trains are operating simultaneously, one train's compensation may affect the performance of the other. In terms of inductance estimation, it is crucial to define unique harmonic frequencies for each train to prevent interference in the calculations of both systems.

Optimization Based Strategies

Although the previous method demonstrated stable performance and effective reactive power compensation, it also possesses certain limitations. As mentioned in [35], the continuous injection of harmonic currents for parameter estimation can introduce noise and contamination to the catenary voltage, which is undesirable. Moreover, if there is a failure in accurately estimating the line's inductance, it can result in incorrect gain adaptation and subsequently lead to inadequate reactive power compensation. Therefore, it is essential to explore alternative solutions. In this regard, the literature also presents two optimization-based approaches that are worthy of being adressed.

Higher Order Controller

In [35], an alternative higher-order controller is proposed to replace the previously mentioned PI controller. This control method involves minimizing the error between a set of open-loop transfer functions and the desired transfer function.

The usual initial step in designing higher-order controllers is to acquire a model of the plant, which represents the system to be controlled. As described by the authors, due to the unavailability of a parametric model, a non-parametric model utilizing convex optimization techniques is employed to design the proposed controller. Firstly, the transfer function of the plant is determined by utilizing the estimated voltage magnitude obtained from the SOGI-PLL, along with the output of the controller, which is the orthogonal component of the AC reference current:

$$\mathbf{G}(j\omega) = \frac{v_d(j\omega)}{i_{q,\mathrm{ref}}(j\omega)} \tag{3.4}$$

Subsequently, a non-parametric model can be obtained at a specific position of the train. The method for obtaining this model consists in determining the magnitude and phase of the transfer function at specific frequencies. A more detailed explanation can be consulted in the paper [35]. As previously mentioned, as the train moves further away from the nearest traction substation, the line inductance measured in the point of contact changes. Consequently, the family of models considered for the controller design encompasses two extreme positions of the train: the position with minimum inductance, situated next to a traction substation, and the position between two substations where the maximum inductance is observed. Subsequently, the authors proceeded to identify the appropriate order for the controller. The minimum value was determined to ensure stable operation at both the maximum and minimum inductance values. For the study case presented in the article, the authors found that a fifth order controller showed good dynamic response for the minimum value, and a stable operation for the maximum.

Afterwards, an optimization problem was formulated to minimize the error between the family of transfer functions derived from the two extreme positions and a desired transfer function. The solution obtained through this optimization process was then tested in both a simulation environment and experimental setup. The results confirmed that the proposed system effectively supports the catenary line's voltage, stabilizing its operation under various conditions based on the train's position.

Optimal Area Control

Another optimization-based approach is proposed in [34, 36]. The author acknowledges that the power loss in the system is proportionally influenced by both the square of the voltage variation and the square of the reactive power variation (Eq. 3.5. Therefore, reducing transmission losses and improving the voltage profile are two significant objectives that can be integrated into a single objective function, with its main variable being the reactive power of the train. The objective function represents the power loss for an entire catenary section and includes constraints on the maximum and minimum reactive power available for a single train. Additionally, this objective function can be obtained through the sum of the power loss functions of each subsection.

The algorithm employed in this approach involves an iterative process of creating and solving the optimization problem using the steepest descent method. Through this iterative process, the optimal values for the train's reactive power are determined, aiming to minimize power losses and improve the voltage profile of the catenary system.

$$P_{\text{LOSS}} \propto |\Delta V|^2 \propto \Delta Q^2 \tag{3.5}$$

$$\underset{q^{\min} \le q \le q^{\max}}{\text{minimise}} f(q) = \min_{q^{\min} \le q \le q^{\max}} \sum_{k=1}^{L} P_{\text{LOSS},k} \tag{3.6}$$

Prediction Based Strategies

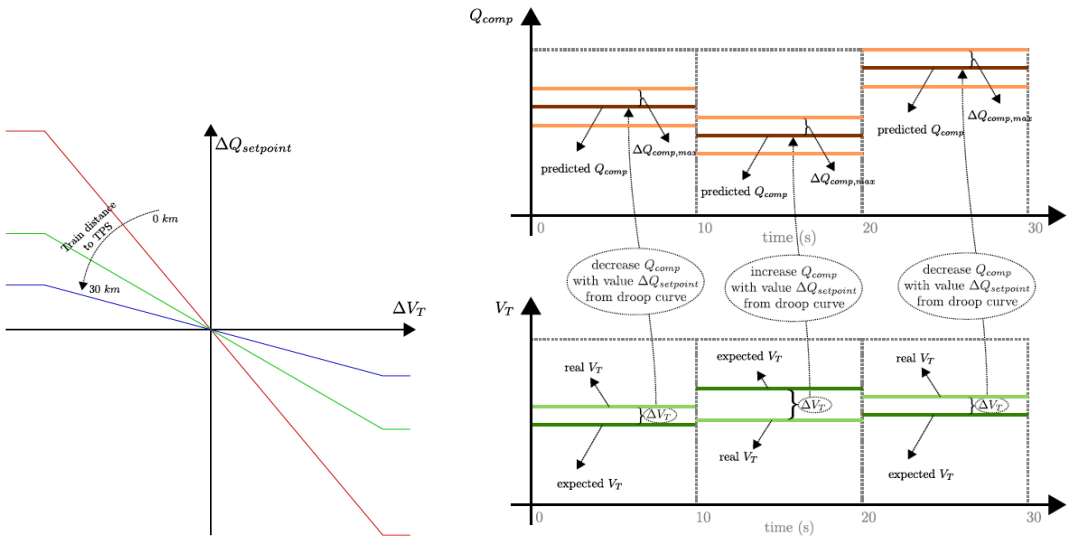
Unfortunately, the implementation of the aforementioned optimization-based approach requires a ground station to receive real-time data on onboard power flow and train position measurements for performing the calculations. Additionally, the generated reactive power setpoints must be sent back to each train. This number of actions must all be done instantly for a stable operation, with no time delay, which isn't feasible in a real world application.

Nonetheless, in [37], the authors build upon the previously introduced optimization algorithm and propose a smart power flow management strategy with a prediction method. This strategy aims to forecast future power consumption and generate reactive power setpoints, taking into account the inherent time delay in data transmission. Moreover, the strategy includes the capability to predict the resultant voltage after compensation. By comparing the predicted voltage with the measured train voltage, the algorithm can further adapt and verify the accuracy of the generated setpoint, making any necessary adjustments as needed. This approach enables the algorithm to account for the time delay in data transmission and improve the overall stability and performance

of the system.

Additionally, a droop strategy is presented as a way to achieve a more stable reactive power control, by continuously correcting the reactive power setpoint and thus, further improve the proposed method. In Fig. 3.10 it is possible to observe the droop characteristic curve for three different scenarios. The referential has as axis ΔV_T, it being the difference the real and predicted train voltages and $\Delta Q_{set\,point}$, which is the output of the droop curve and, consequently, the needed correction to add to the predicted reactive power setpoint.

It is important to acknowledge that the inclination of the curves varies in accordance with the train's distance from the traction substation. Upon careful observation of the image, it becomes evident that as the train moves farther away from the traction substation, the corrective factor for the reactive setpoint diminishes. Furthermore, as the disparity between the measured and predicted voltage increases, the corresponding correction required also escalates, naturally. In the next figure shows an example of how this strategy should work and improve the overall stability in reactive power compensation.



(a) (b)

Figure 3.10: Droop control strategy: droop characteristic curve (a) and basic display of this strategy (b). From [9].

3.6.2 Standard EN 50388-1

The technical guidelines provided in Standard EN 50388-1 facilitate smooth interaction between power supply and rolling stock entities [38]. The standard addresses the power factor of a traction unit and regenerative braking, among other topics.

Regarding the power factor, the traction units should achieve a power factor close to unity. However, two cases of operation are considered: inductive or capacitive power factors. The following guidelines are outlined:

In the first case, where the traction unit operates with an inductive power factor:

- When the line voltage is below a specified maximum limit, the inductive power factor should always exceed 0.95. This prevents loss increases and further reduction of the line voltage.;
- During regenerative braking, the inductive power factor can be adjusted within specific line voltage limits to provide stability to the operation.

For the case where the traction is producing reactive power:

- A capacitive power factor of 0.95 can be used for voltage support, or even lower, only if the line voltage is under its nominal value;
- In regenerative breaking, a power factor adjusted to one is to be employed, in order to facilitate the operation.

Moreover, in a more general sense, the maximum reactive power value for a traction unit, inductive or capacitive (consuming or producing), should always be 30% of its maximum active power.

3.7 Final Remarks

In this chapter a general overview of the key aspects of the line-side converter was given. Firstly, a study of different converter typologies was made, comparing the advantages and disadvantages of various configurations utilized or proposed for use in railway traction systems. Moreover, other important features such as the modulation or specific operations that can be enabled through the converter's control (regenerative breaking and reactive power compensation) were also addressed as a proposed solution. In the scope of this dissertation, several developed methods for reactive power compensation through the proposed converter were also depicted.

Chapter 4

Modelling and Simulation

4.1 Introduction

A software simulation, using *PSIM*, was conducted with the aim of better understanding the behaviour of the converter described in the previous chapter, but also with the intent of predicting possible outcomes of the incoming experimental validation.

The system's architecture should follow the established H-bridge converter model discussed in the preceding chapter. Moreover, the system should also incorporate a pre-charge circuit and three contactors: the main contactor (K_{MAIN}), the pre-charge contactor (K_{PC}), and the DC-link contactor (K_{DC}). These provide safety in case of exceeding values of voltage or current. Also, the motor load shall be simulated with a resistor at the nominal value placed at the DC bus. The subsequent illustration depicts the proposed circuit configuration.

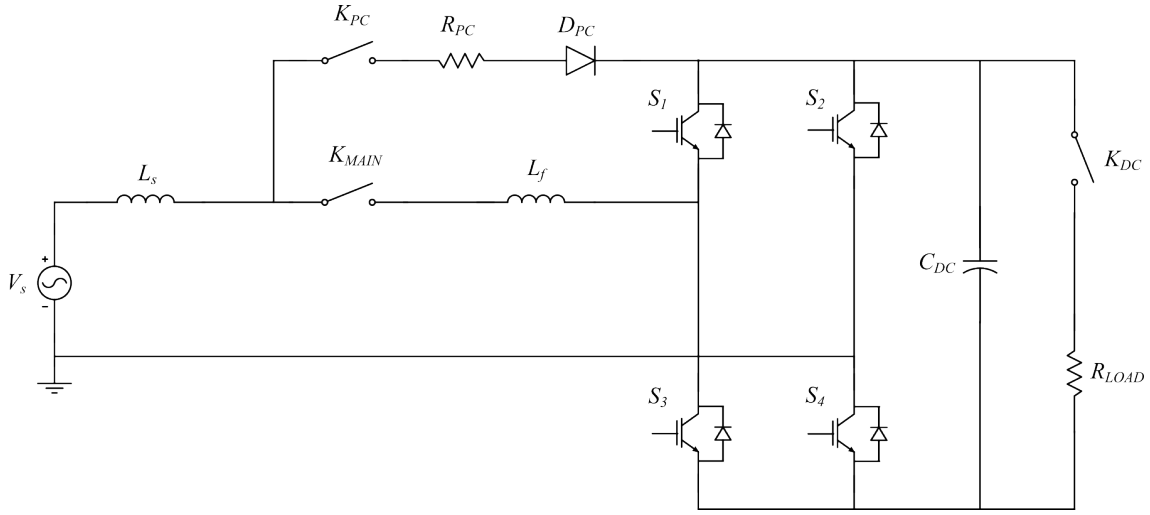


Figure 4.1: Diagram of proposed power circuit.

The parameter values, based on the CP Series 2300/2400 Electric Multiple Units, include the AC line voltage, the DC bus voltage, the nominal power and the switching frequency. In addition, the nominal peak current and the filter inductance were thereafter calculated. All are represented in Table 4.1.

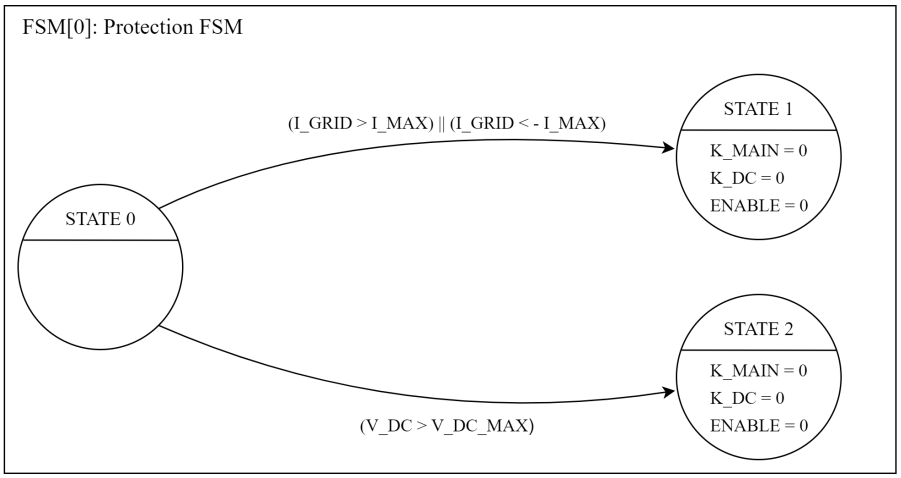
Table 4.1: Parameter values used in the simulation.

AC line voltage (rms)	1200 V
DC bus voltage	2100 V
Nominal power	700 kW
Switching frequency	2 kHz
Line inductance (L_s)	1 mH
Nominal peak current	583 A
Filter inductance (L_f)	3.2 mH
Filter series resistance	0.02 Ω

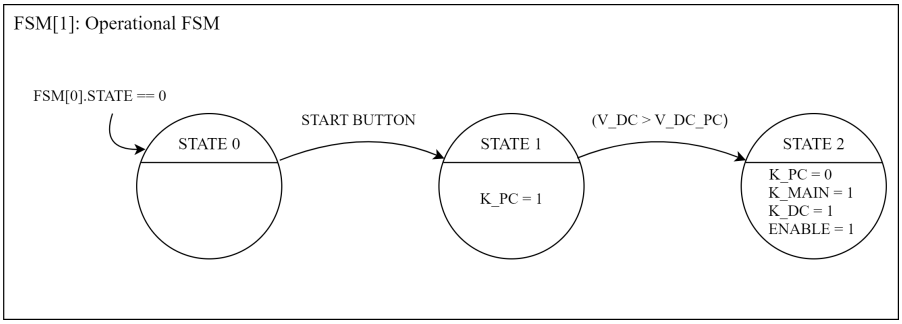
4.1.1 Supervision

Prior to implementing the system, it is necessary to address certain aspects related to its supervision, particularly with regards to its protection and operation. The three contactors serve the purpose of providing safety in the event of current or voltage overload, while also facilitating the pre-charging of the DC bus capacitor. Therefore, the contactors need to be integrated into a state machine logic, along with the control of the converter. Consequently, two finite state machines (FSMs) have been developed - the protection state machine and the operation state machine, which are depicted in Fig. 4.2.

Through the analysis of the FSM diagram, it is clear that the protection state machine continuously monitors whether the voltage or current exceeds the maximum defined limits. If these limits are surpassed, the contactors are opened, and the control and modulation of the converter are disabled. The operational state machine coordinates the pre-charging of the DC side capacitor, which initializes after the press of a start button, after which the corresponding contactor closes. Once the pre-charge is completed, the system transitions to the next state, where the main and the DC contactors close, control and modulation are enabled, and its normal operation commences. It should be noted that the protection state machine takes priority over the state machine responsible for the operation of the converter. Thus, if any type of faulty behavior is detected by the protection state machine, the converter will not be able to operate.



(a)



(b)

Figure 4.2: State Machine Diagrams: protection FSM (a) and operational FSM (b).

4.1.2 Workplan

This simulation was divided into six consecutive stages, in order to simplify and validate each subsystem as the work progressed:

1. AC Current Control
2. Grid Synchronization
3. DC Voltage Control
4. Reactive Current Control
5. Discrete Implementation
6. Final Case Study

The purpose of this chapter is to provide a detailed description of each of the enumerated stages. The initial four stages were designed under ideal conditions, while stages 6 involved discretization and the implementation of a control algorithm in C code, respectively. These stage was carried out to validate and predict the outcomes of future real-life experiments that took place. Ultimately, all of these stages converged in a final case study, which intends to demonstrate the

converter's ability to provide support to the catenary voltage, validating the main reasoning of this work in a simulation of a real scenario.

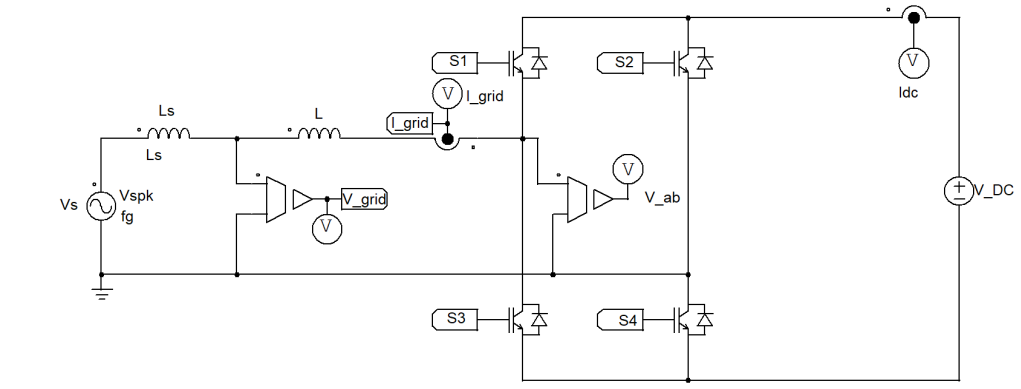
4.2 AC Current Control

The purpose of first stage of the simulation experience was to successfully implement the AC current control loop. Accordingly, three main goals were defined at this step:

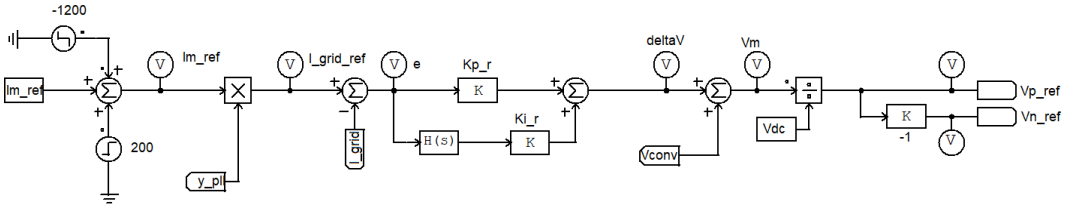
- Correct implementation and tuning of the PR controller;
- Implementation of the current control closed-loop;
- Validation of the operation of the whole system for different AC current references.

As the objective was to only validate the current control, two simplifications were introduced into the previously proposed system. First, as the DC voltage isn't controlled at this stage, a fixed DC voltage was imposed in the DC bus, by means of the placement of a fixed voltage source. Also, concerning grid synchronization, the standard PLL block present in the *PSIM* software was used. The resultant power and control circuits can be consulted in Fig. 4.4.

Regarding the control system, it is implemented according to the previously discussed PR-based current control, in Section 2.2.3. A sum of reference currents, starting at the nominal one was inserted to evaluate the control's performance. It is then compared with the actual input current and fed directly to the PR controller, whose output is later added to DC bus voltage. The resultant signal is then fed to the SPWM generator.



(a)



(b)

Figure 4.3: *PSIM* Diagrams: power circuit (a) and control circuit (b).

The tuning procedure for the non-ideal PR was made using a manual method of continuously adjusting the controller's gains based on the effects observed from each one:

1. Proportional Gain: the effects of the proportional gain were observed by maintaining the integral gain at a zero value. It is well-established in common PI controller applications that the proportional gain significantly influences the speed of response of the controller. However, since the PR controller directly accepts AC signals as inputs, evaluating its dynamic response is not as straightforward. The objective is not to verify the plant's capability to reach a constant value, but rather to accurately track a constantly changing value. Therefore, the value of the proportional gain, denoted in the figure as K_{p_r}, was progressively increased until the AC current waveform closely resembled a sinusoidal waveform, with amplitudes approximating the generated AC reference. With a $K_{p_r} = 10$, a sinusoidal waveform with the correct amplitude was observed. Nonetheless, a considerate phase delay between the measured and the reference signals was still noticeable. However, the further increase of the proportional gain only introduced distortions on the waveform, failing to resolve this issue. Consequently, at this point the focus was shifted towards adjusting the integral gain.
2. Integral Gain: the expected effects of increasing the integral gain, denoted as K_{i_r}, are the reducing of the steady-state error. Therefore, by increasing its value the response speed of the controller is increased but also has a smoothing effect when compared to the proportional gain. Utilizing an integral gain of $K_{p_r} = 320$, the controlled AC current demonstrates no phase delay relative to the reference current.
3. The last step was to validate the control loop for various reference currents. A test with two different reference current values (positive and negative) and with the chosen controller gains, revealed that the controlled AC current achieved the correct amplitude and phase. The current stays perfectly in phase with the AC voltage or maintained an exact 180 degree phase difference, in the case of a negative reference is given (Fig. 4.4).

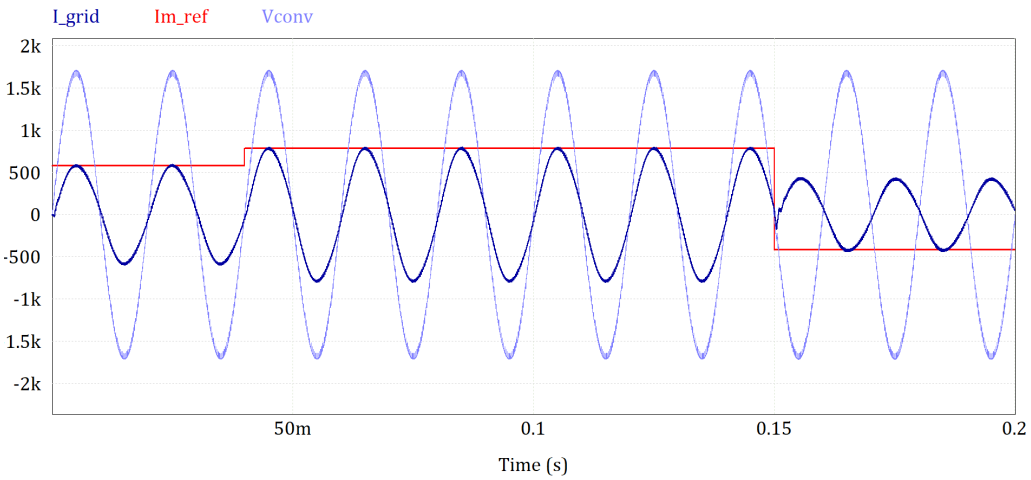


Figure 4.4: Resultant waveforms: I_s in blue, $I_{m,ref}$ in red and V_{conv} in lighter blue.

4.3 Grid Synchronization

Contrary to the previous simulation stage, if the control is to be implemented in a microcontroller unit, the main constituent blocks of the PLL must be designed and validated separately, rather than using a simple pre-built block. Therefore, a separate simulation was performed to verify the operation of a block-by-block implemented FFSOGI PLL.

The fixed frequency SOGI-PLL is another grid synchronization system, different from those presented in section 2.2.2. The main advantage of this configuration is that it isn't affected by frequency variations and still provides accurate synchronization in those cases. It uses phase error compensation to account for the discrepancy between the actual estimated phase angle and the ideal one. This provides stability to the system with a simple implementation as shown below.

The objective for this stage is to validate the output variables of the FFSOGI-PLL in relation to an AC input, usually the grid voltage or current. In addition to a voltage synchronized angle, synchronous and orthogonal components of the voltage, it is also capable of delivering other variables that might be of use, such as the voltage magnitude and estimated angular frequency. As shown in the diagram of Fig. 4.5, a 230 V 50 Hz voltage (depicted as V_{grid}) was connected to the input to simulate an ideal grid voltage. The FFSOGI, on the left-hand side, is then responsible for generating the synchronous and orthogonal components (v_{alpha} and v_{beta}), with the use of the Park transformation. The value of the direct component is the magnitude value of the input voltage. Naturally, the quadrature component is forced to zero, hence it is used directly on the input of a PI controller. By adding the grid fundamental frequency to the output it is possible to obtain its estimated frequency. By further integrating it the result is estimated phase angle which is then corrected as previously explained. The proposed diagram, illustrated in Fig. 4.5, is based on the studies made on [39] and [40].

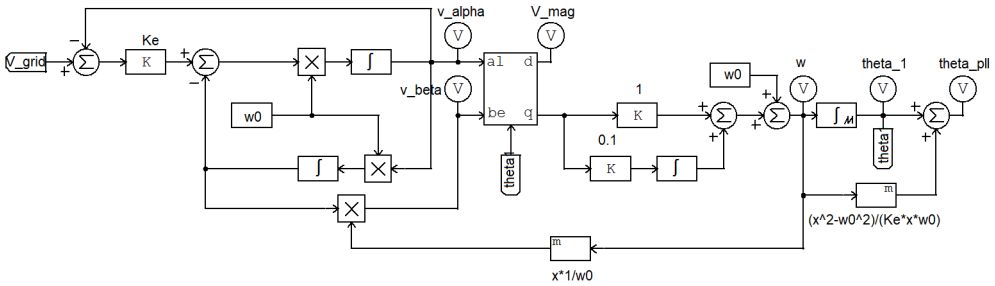


Figure 4.5: FFSOGI-PLL diagram.

Upon examination of the obtained waveforms (Fig. 4.6), it becomes evident that the generated angle, denoted by *theta_pll*, is synchronous with the sine wave. Additionally, the amplitude of the voltage, in red, coincides with the peaks of the grid voltage waveform, while the estimated angular frequency, indicated in dark blue, is slightly below it, as it corresponds to $2*\pi*50$, as expected.

Since this FFSOGI-PLL test was successful, it shall be adapted and used in the further stages of this simulation.

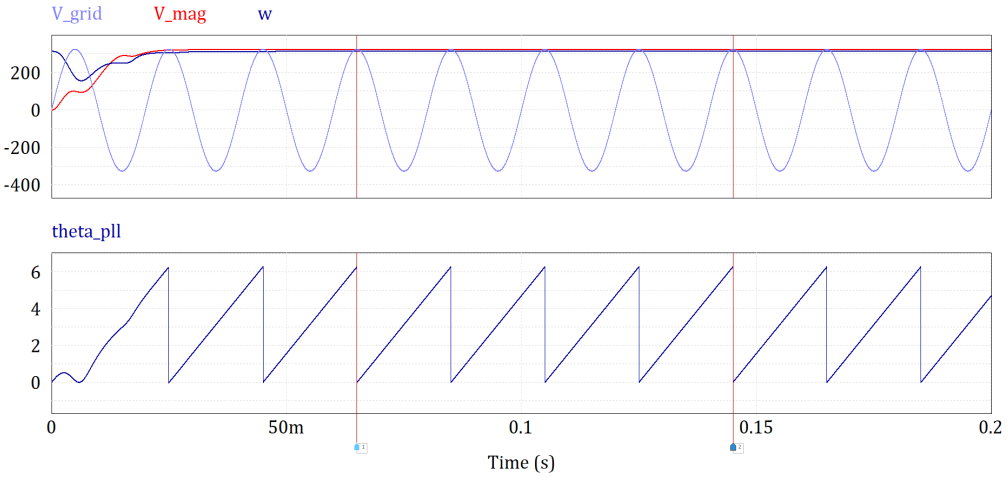


Figure 4.6: Resultant waveforms: V_{grid}, V_{mag}, w on the graph above, and the estimated angle, $theta$, on the graph below.

4.4 DC Voltage Control

With the PLL being synchronous with the AC converter voltage, the next step was to implement a controller capable of generating an AC current reference that should be fed to the PR controller. Moreover, this should guarantee a constant 2100 V on the DC bus as the imposed DC voltage is now replaced by a capacitor filter, with the aim of reducing the voltage ripple and a resistive load, at nominal value, to emulate the motor load's effect on the DC bus.

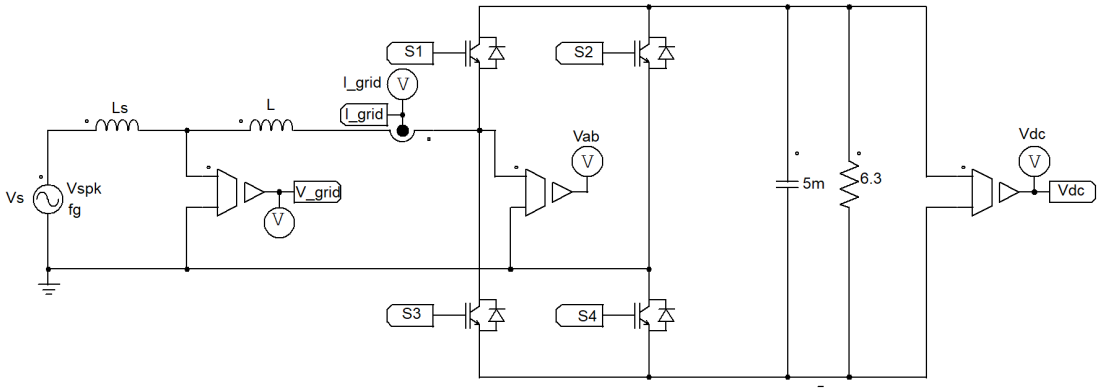


Figure 4.7: Resultant power circuit.

Regarding the implementation of the controller, a PI controller was selected due to its capability to track DC references effectively. The controller receives an error signal between the measured and the reference DC bus voltages, and generates a continuous active reference current as its output. This output is subsequently utilized as the d component in a dq to $\alpha\beta$ transformation to derive an AC reference current, which is compared to the measured current to generate the error signal for the PR controller.

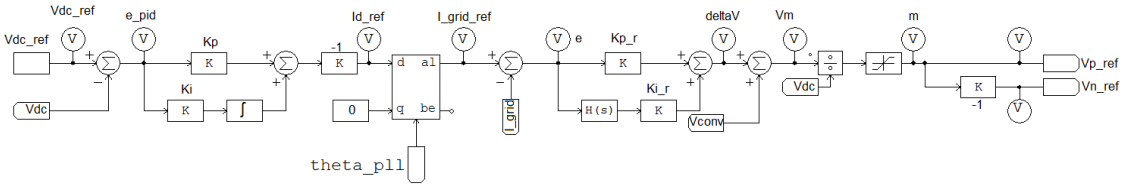


Figure 4.8: Control circuit diagram with the DC voltage control loop.

According to the following figure (Fig. 4.9), the DC voltage waveform exhibits minor oscillations around its average value of 2100 V, which is the intended behavior. The oscillations are due to the power exchanges with a 50 Hz grid . The PI controller was adjusted using the same try-error method, and the optimal values were determined to be $kp = 0.53$ and $ki = 33.33$. Regarding the current waveform, it still follows the reference current pattern. It is to note that a pre-charge circuit is typically utilized in real implementations of this converter to charge the DC-side capacitor, preventing the negative current peak a current at the beginning of the operation, this circuit will be addressed later on. Accordingly, an initial capacitor voltage was set, to simulate a previously charged capacitor. Moreover, further tests were conducted where a sudden change on the DC load was provoked in order to observe the controller's response in for different load values. Consequently, the change from 10% to 100% (at $t = 0.5s$) of the nominal power naturally alters the behaviour of the DC voltage and AC current waveforms. Nonetheless, the DC voltage controller is capable of adjusting its output to a rapid variation in power demand, quickly achieving a new steady-state at the desired value. Also, the current controller is capable of tracking the reference currents, now given by the previous controller.

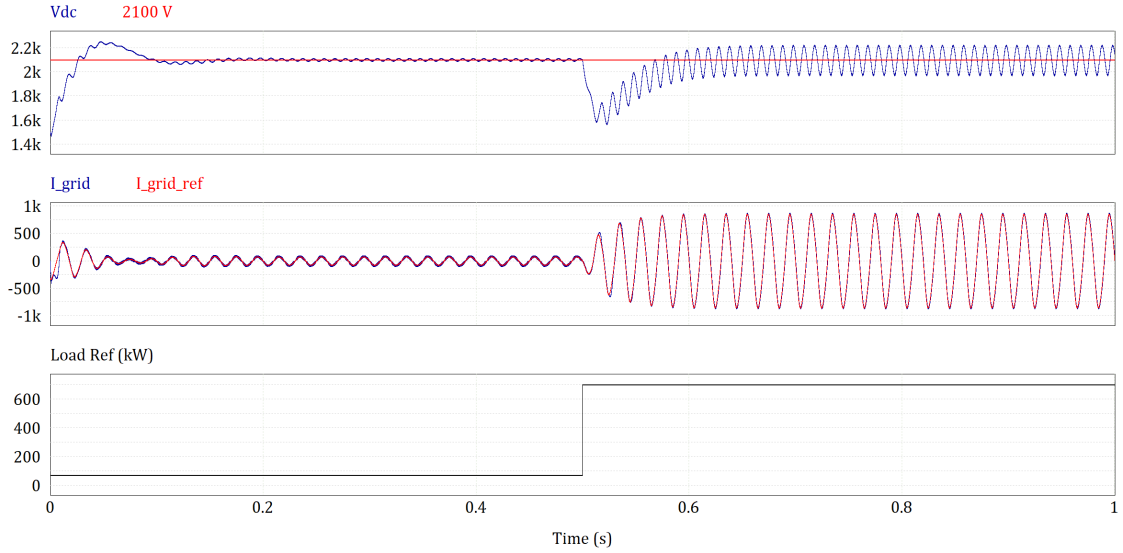


Figure 4.9: DC voltage (above), AC current (middle) and respective references, in red. Load power reference change (bottom).

4.5 Reactive Power Control

According to the Instantaneous Power Theory, provided by Akagi *et al.* in [41], it is possible to obtain the instantaneous values of active and reactive power through the so called instantaneous space vectors of the grid's current and voltage, in the coordinates $\alpha\beta$, as presented in the following equation.

$$\begin{bmatrix} p \\ q \end{bmatrix} = \begin{bmatrix} v_\alpha & v_\beta \\ v_\beta & -v_\alpha \end{bmatrix} \begin{bmatrix} i_\alpha \\ i_\beta \end{bmatrix} \tag{4.1}$$

As the voltage components were already determined in the SOGI block of the PLL system, the next step was to modify this subsystem in order to also generate the i_α and i_β components. Accordingly, another SOGI instance was added after the corrective factor of the estimated angular frequency, with the same working principle, but now with the grid's current being used as an input. Using the resultant components from the current with equation 4.1, one can calculate the instantaneous values of the active and reactive powers:

$$\begin{cases} p = v_\alpha i_\alpha + v_\beta i_\beta \\ q = v_\beta i_\alpha - v_\alpha i_\beta \end{cases} \tag{4.2}$$

As already stated, the reactive current control is made through the q component of the current. As such, another PI controller was introduced to regulate the reactive current.

As referred, the output of the controller serves as the reference for the quadrature component of the AC grid current. Hence, it needs to be integrated into the dq to $\alpha\beta$ transformation module. Consequently, the module should generate an AC current reference that allows for the inclusion of a reactive current component, as opposed to the previous experiment where a default value of zero was utilized.

Regarding the controller implementation in the context of this study, a substantial rate of change in the transfer of reactive power between the power grid and the train in operation will lead to instability in the voltage supply. Therefore, quick changes in reactive power operation are to be avoided. Consequently, the PI controller was adjusted to exhibit slow dynamics. The best response was achieved by setting the values of K_p and K_i to 0.001 and 0.05, respectively.

Several tests were conducted in order to validate the correct operation of the designed control loop. In the first, two references of reactive power (-250 kVAR and -600 kVAR) were fed to the input of the controller. It is important to note that the reason behind the use of negative values is to force the converter to inject reactive current into the grid, and validate its operation with leading power factor. It should also be noted that for testing purposes, the Standard EN 50388-1, as presented in 3.6.2, was not considered.

In Fig. 4.10 illustrated the response of the converter to the variations to the given references. The reactive power was calculated through the previously depicted formulae (Eq. 4.2).

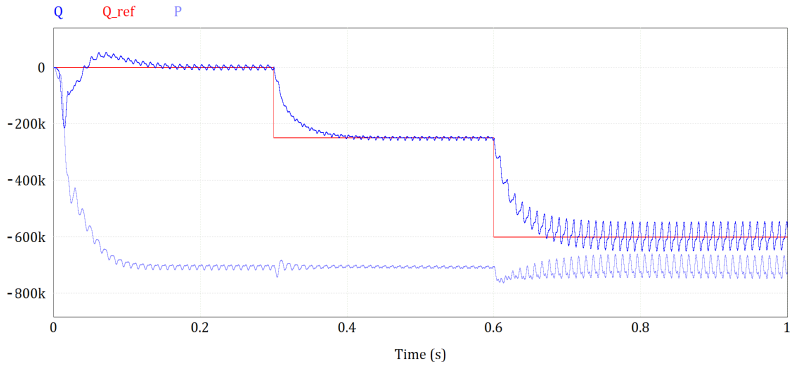
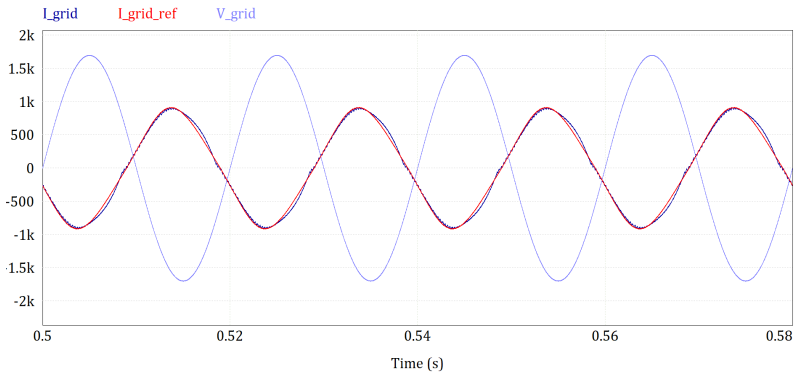


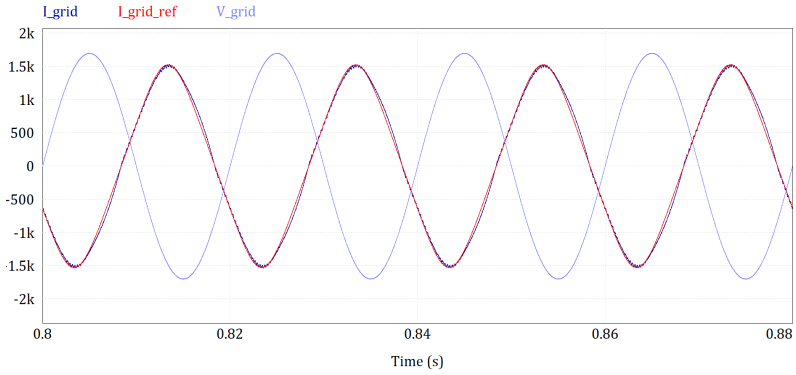
Figure 4.10: Reactive power response with leading power factor, in blue and reactive power reference, in red.

The converter's operation can be further validated through the analysis of the behaviour of the AC current. In the first case, is clear that it is leading the voltage waveform with an increasing phase difference with the increment in reactive power, as expected for leading power factor operation. This fact is depicted in Figure 4.11.

It should also be noted that, for the second case, where the converter is operating with a 0.75 power factor, the AC current became distorted. This occurs because the converter doesn't feature the capability of working with such low capacitive power factor, thus, the controller is also not able of correcting the measured current to follow the reference one. One possible solution is taking this into account when designing the converter. Accordingly, another test was conducted, where 500 V were added to the reference given to the DC voltage controller ($V_{DC} = 2600$ V), increasing the converter's active power. As a result, the behaviour of the current significantly improves, as shown in 4.11 (b). Naturally, the power factor also increases, but the main goal which is injecting 600 kVA into the grid is fulfilled.



(a)



(b)

Figure 4.11: AC current and voltage waveforms for both cases. With 0.95 (a) and 0.87 (adjusted) (b) leading power factors.

In a similar way, the symmetric reference values for reactive power (250 kVAR and 600 kVAR) were used to test the system with a lagging power factor. Once again, the reactive power correctly followed the reference values, as shown in Fig 4.12.

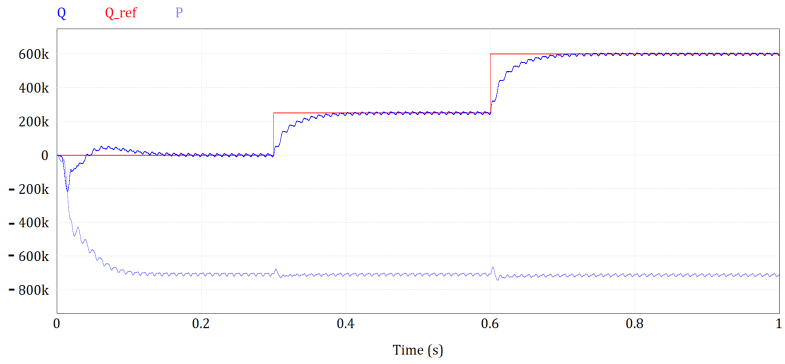
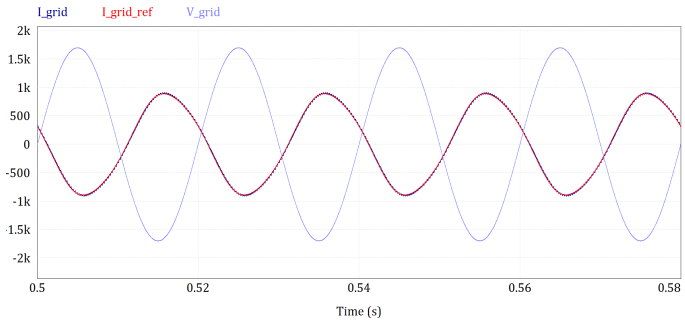
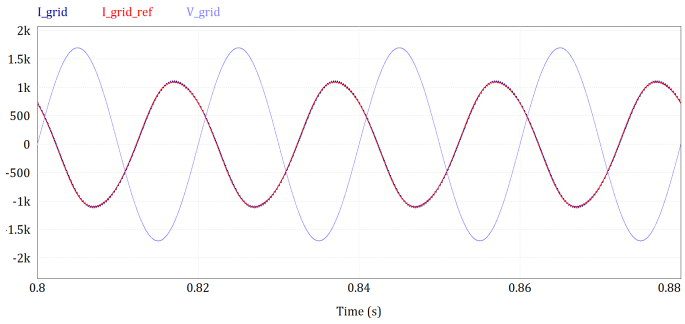


Figure 4.12: Reactive power response with lagging power factor, in blue and reactive power reference, in red.

Once again, by observing the AC side waveforms, it is possible to access that the current is lagging the voltage. The reactive power increase has the same observed effect on the phase difference between the two quantities.



(a)



(b)

Figure 4.13: AC current and voltage waveforms for both cases. With 0.95 (a) and 0.75 (b) lagging power factor.

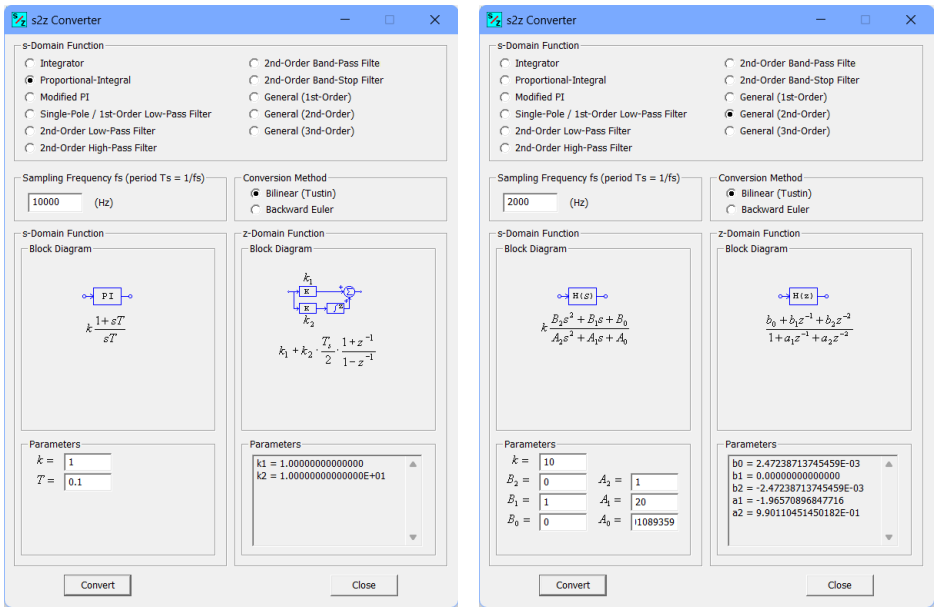
4.6 Discrete Implementation

As mentioned earlier, due to the experimental scope of this dissertation, the simulation must be conducted in highly realistic conditions in order to anticipate the possible effects of a physical implementation of the system. Consequently, the following phase outlines the approach employed to attain effective digital control, specifically by simulating an implementation in C code. Key aspects such as controller discretization and digital filter design are addressed, resultant from the preceding discussion on digital control. Additionally, the design of a code structure utilizing interrupt routines is implemented as a way to accommodate the future implementation of the comprehensive control system on a microcontroller board. This structure represents the final result of integrating all the aforementioned systems, including control, filters, and supervision.

4.6.1 Controller Discretization

Regarding all the elements of the converter circuit discussed in the previous chapters, the main elements that should be discretized are the FFSOGI-PLL, the PI and the PR controllers. The discretization of these control components was done using the *s2z Converter* utility, present on the *PSIM* software. This provides a straightforward way of discretizing of various types of s-domain functions, either by the Bilinear (Tustin) Method or by the Backward Euler Method. Both are explained in 2.3.3, however, the former was chosen for this simulation.

In the subsequent illustration, two instances of discretization are provided. The left-hand side illustration corresponds to the PI controller within the PLL, whereas the second example shows solely the discretization of the transfer function of the PR current controller, in order to facilitate any necessary gain adjustments.



(a) (b)

Figure 4.14: *PSIM s2z Converter* tool: PI (a) and PR (b) controllers discretization example.

Recalling the discrete control overview given in 2.3.3, it is still necessary to transform the Z-domain transfer functions of each controller into their respective discrete form.

Concerning the PR controller, the implemented difference equation of its second order transfer function is given by Equation 4.3, where e corresponds to the vector of the current and previous error values fed to the controller while y stands for the vector of current and previous outputs of the controller. The result should then be multiplied to the integral gain and later added to the proportional gain, according to the previously given PR configuration.

$$y[n] = b_0 e[n] + b_1 e[n-1] + b_3 e[n-2] - a_1 y[n-1] + a_2 y[n-2] \tag{4.3}$$

Regarding the PI controller for the PLL, the DC voltage and reactive current controllers, the difference equation is given by Equation 4.4. Here, the same principle applies, with the current and previous values of the error and outputs being used. Also, the previously seen variable T_s, resembling the sampling period, is now changed (only in name) to c_t, representing the cycle time. This only serves to better demonstrate the way the code is structured in preparation for a real microcontroller implementation. In such application, the implementation shall be based on the use of interrupt routines. As a consequence, the cycle time, represents the periodicity in which the interrupt routine should be called. For the case of the PI presented in the PLL a 10 kHz sampling frequency is to be used, whereas in the case of the converter control PIs, a sampling frequency of 2 kHz will be used, in line with the PWM frequency. The cycle times are then different for each of the subsystems.

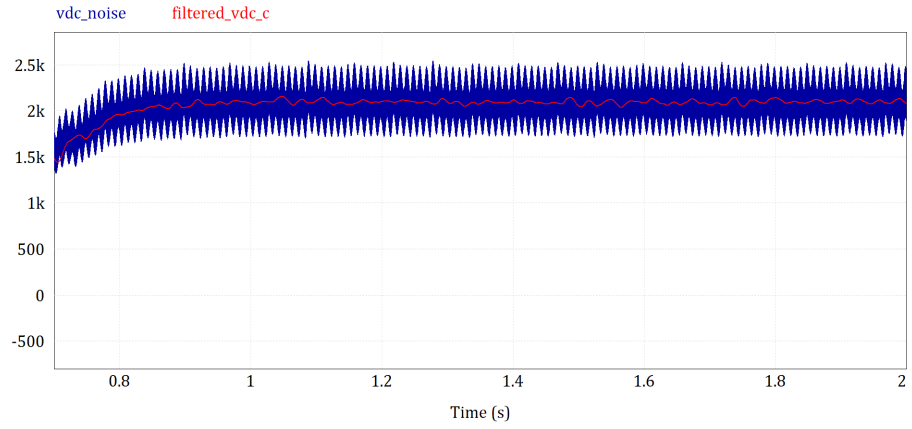
$$y[n] = y[n-1] + K_p(e[n] - e[n-1]) + \frac{K_i c_t}{2}(e[n] + e[n-1]) \tag{4.4}$$

The controllers were then ready to be implemented in C code. However, considering the previously mentioned delay inherent to discrete implementations, slight adjustments were made to the controller gains to achieve improved results.

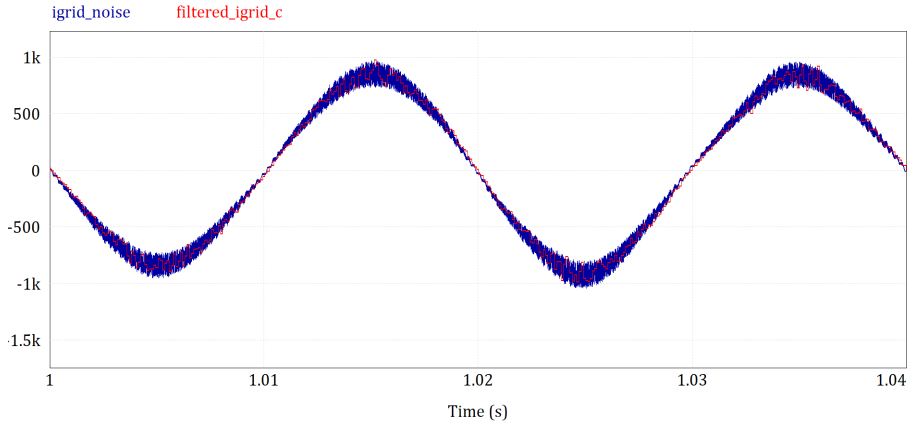
4.6.2 Digital Filters

To evaluate the discrete implementation of an IIR filter, the measured DC voltage and grid current signals were multiplied by randomly generated signals to replicate the effects of high-frequency noise in real-world applications, as depicted in Figure 4.15.

The design of the two IIR filters was performed using the *Filter Designer* app available in *MATLAB*. This tool proved to be highly useful as it allowed for the specification of the parameters of the filter such as filter type, order, and cut-off frequency, enabling the extraction of the coefficients and obtain a transfer function of the type shown in Section 2.3.2. For the DC bus voltage, a 6th order Butterworth IIR filter with a cut-off frequency of 50 Hz was selected. For the AC grid current, a 2nd order Butterworth IIR filter with a cut-off frequency of 4 kHz was chosen. Both filters operated at a common sampling frequency of 10 kHz. Following the extraction of the coefficients, the difference equations were implemented.



(a)



(b)

Figure 4.15: Noise and filtered signals: DC voltage (a) and AC current (b).

4.6.3 General Code Structure

The general code structure is then divided into two different routines, as depicted in Fig, 4.16. This separation brings an early depiction of a real microcontroller code implementation. Not only do the effects of using two different routines at different frequencies become evident, but also the translation process from *PSIM* to the microcontroller is simplified, as the majority of the code is already written with a code structure very close to the one which will be implemented.

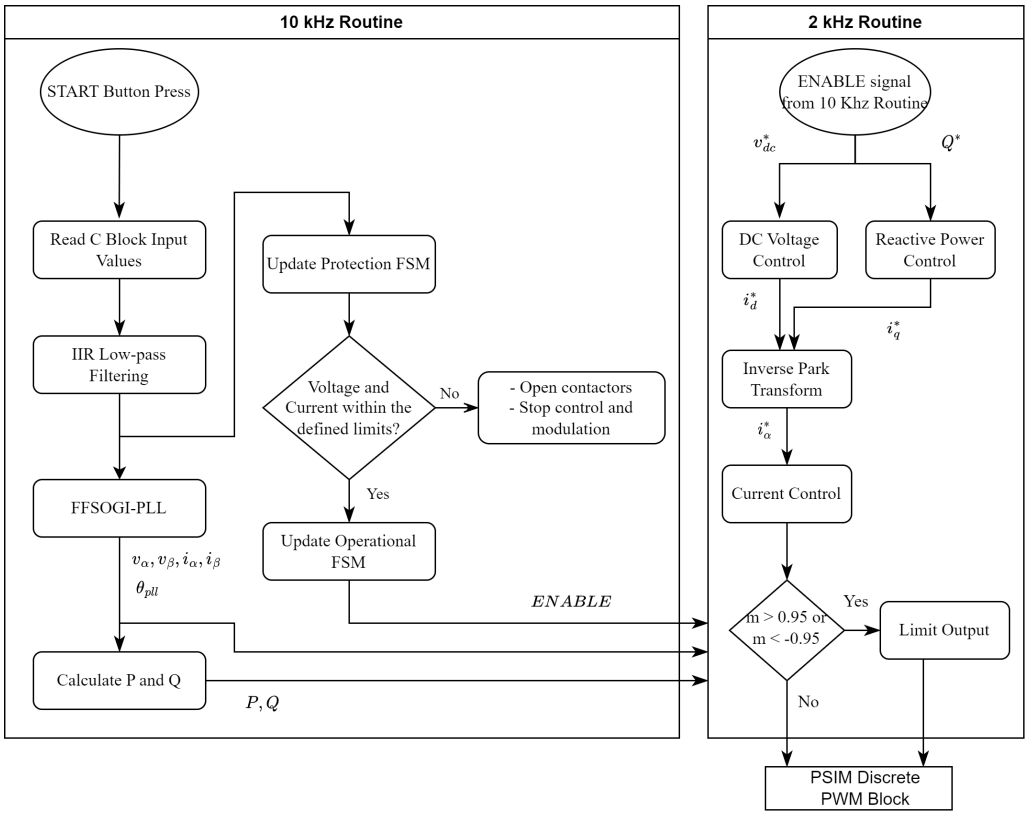


Figure 4.16: General Code Structure.

4.6.4 Obtained Results

With all the different systems discretized and placed inside a designed code structure, it becomes now possible to test it in a new simulation stage. This simulation consisted in the previous converter architecture with the added pre-charge circuit. As such, all contactors were included and the power circuit is now the same as the depicted in Figure 4.1. This way, it was then possible to validate the operation of the design state machines, in cooperation with the developed control system, now in its discrete form. Moreover, the previous reactive power experience was repeated with the same reference values. Through the study of the DC voltage waveform in Fig. 4.17, it is possible to validate the operation of the operational state machine. As displayed in 4.2, in the operational FSM starts at State 0. At instant $t = 0.05$ s the START button is pressed, and the FSM transitions to State 1, where the DC bus pre-charging operation takes place. The defined value of pre-charge was 1500 V. When the DC voltage matches this value, the FSM transitions to State 2 where the control and modulation are enabled, and the converter normal operation begins, as can be proved by the regulation of the DC voltage to 2100 V immediately after that. Furthermore, the reactive power control still maintains its operation, as depicted in Fig. 4.18.

By closely inspecting the current waveform, it is possible to observe the effects introduced by the sampling, as the waveforms now display a staircase-like appearance, due to the sample and hold delay present in the acquisition. Also, due to the previous adjustment of the controllers, in

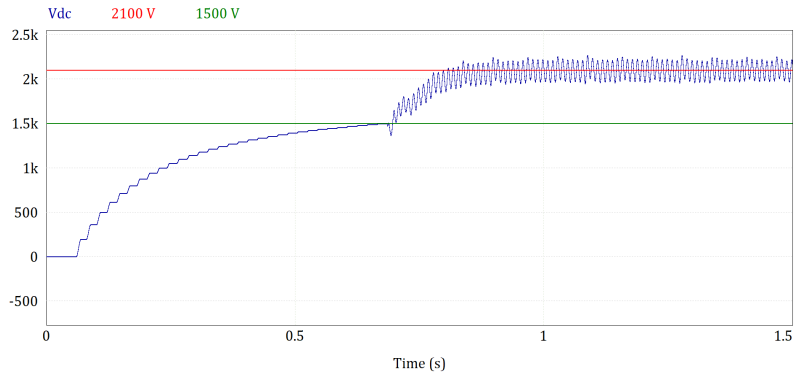


Figure 4.17: Pre-charge and control of the DC bus.

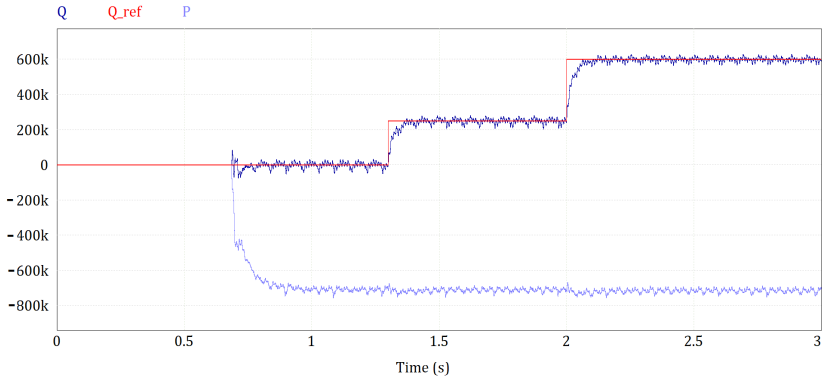


Figure 4.18: Reactive power response with lagging power factor, in blue and reactive power reference, in red.

order to compensate for the digital control delays, the results are satisfying with the PR controller being capable of correctly tracking the reference current values, as illustrated in Fig. 4.19. It should be noted that, regarding the PWM scheme, although the unipolar PWM shows better results in terms of the quality of the waveforms, in the C code implementation, the bipolar PWM was used, in order to mimic the limitations of the microcontroller's PWM timer, which will be used in the experimental portion of this work.

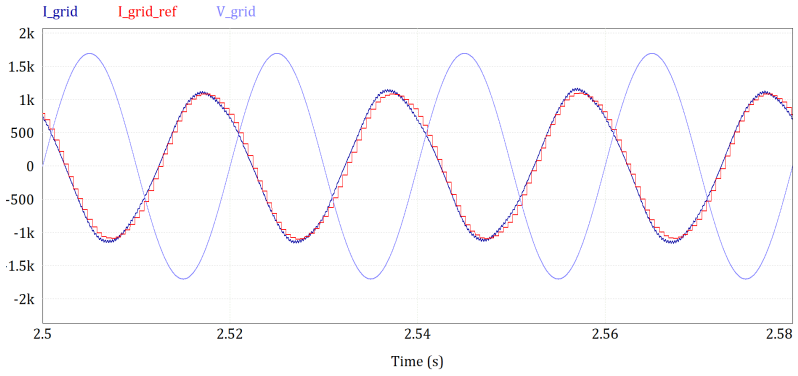


Figure 4.19: AC current and voltage waveforms for a lagging power factor.

4.7 Case Study

The proposed case study aims to validate the control of the reactive power transfer between a train containing the proposed converter and the overhead line, as a way to support and maintain a regulated supply voltage for other running trains.

Accordingly, in the developed case study, a 25 kV AC line is modeled in *PSIM* along with two other trains (*Train 1* and *Train 2*).

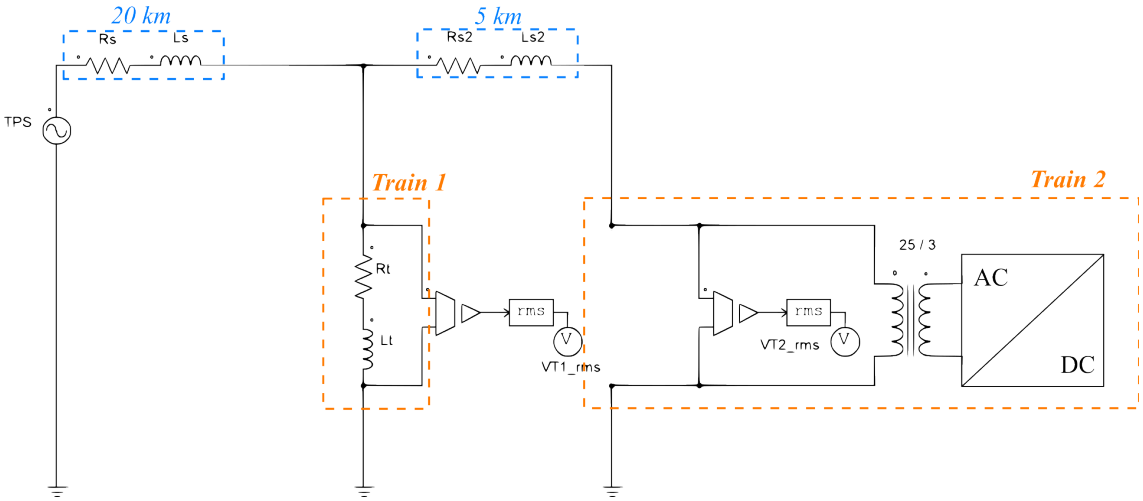


Figure 4.20: Diagram of the modelled case study.

On the left hand side of the diagram presented in Fig. 4.20, a traction power substation (TPS) supplies the whole system with 25 kV 50 Hz. The first train is positioned 20 km away from the substation while the second, which contains the proposed line-side converter, is at 25 km of distance from the substation. The starting values used for the parameters of the line impedance and of the trains are:

Table 4.2: Case study parameters.

Line Impedance	$X_s = 0.45\,\Omega$/km with $X/R = 3$
Train 1	$S_{nom} = 4$ MVA with $cos(\phi) = 0.98$
Train 2	$S_{nom} = 700$ kVA with $cos(\phi) = 0.98$

To evaluate the performance of the converter two tests were conducted: the first with a reactive power reference set to 0, and the second with the converter injecting 700 kVAR into the catenary line.

As referred through the course of this document, it is clear that the distance of both trains to the traction substation greatly affects the line voltage, with the voltage drop increasing with distance. Moreover, the addition of more trains to the same line, would increase it even further.

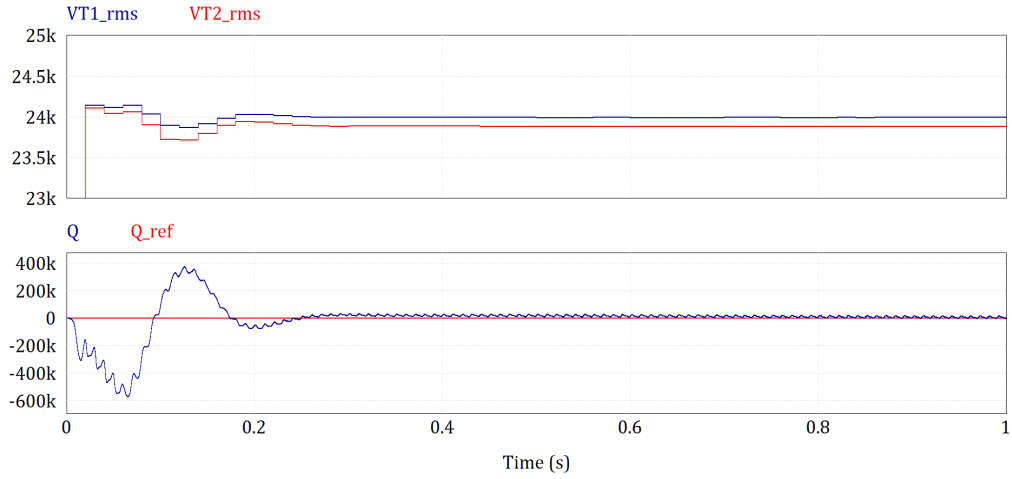
The following figure shows the rms value of the supply voltage measured at each of the trains. The obtained results show that with no reactive power compensation from the second train, the supply voltage of both trains is reduced due to the effects of line impedance (Fig. 4.21 (a)). Moreover, the second train registers a lower value than the first one due to the impedance of both the 5 km section between them and the impedance of the $700\,kVA$ train.

In the second case (Fig. 4.21 (b)), a $700\,VAR$ capacitive reference was given to the converter present on *Train 2*. This setpoint was introduced at the instant $t = 0.4s$, so it was easier to observe the change in the voltage levels. As a result, not only the *Train 2* but also *Train 1* experienced an increase in the supply voltage level. This result confirms that the use of reactive power compensation on on-board traction converters can be used to stabilize the voltage levels on the catenary line both for the train that is doing the compensation but also for other vehicles nearby. However, the effectiveness of reactive power compensation also depends on distance.

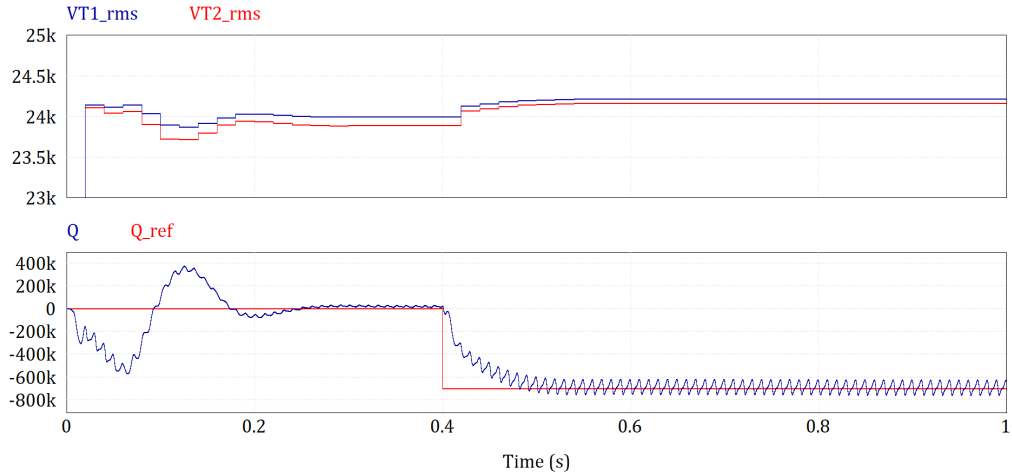
In Table 4.3, the obtained results are presented in terms of the rms supply voltage before and after compensation, as well as voltage drop (in relation to the nominal voltage) and voltage increase percentage after compensation for each train. It is worth noting that *Train 2* registered a larger increase in its supply voltage than the first, verifying the fact that the reactive power compensation also depends on the distance that a specific train is from the point of compensation. As a side note, it is important to address the fact that *Train 2* is operating at a 0.7 power factor, which is already a low value and is only possible for low voltage conditions, as presented in 3.6.2. Even so, this isn't enough to restore the voltage back to its nominal value. Naturally, the purpose of this strategy is that it can be applied to more than one train. Also, trains with higher nominal power will have a greater capability of compensating for higher voltage drops.

Table 4.3: Obtained results for both simulation cases.

		Reactive Power Setpoint		
		Q = 0	**Q = -700 kVA**	
Train 1	**RMS Voltage**	23.99 kV	24.22 kV	
	Voltage Drop	1.01 kV	0.78 kV	22.7 % **decrease**
Train 2	**RMS Voltage**	23.89 kV	24.16 kV	
	Voltage Drop	1.11 kV	0.84 kV	24.3 % **decrease**



(a)



(b)

Figure 4.21: Rms supply voltage of the two trains (top) and reactive power response (bottom) for each case: with zero (a) and 700 kVA capacitive (b) reactive power setpoints.

4.8 Final Remarks

This chapter proposes a H-bridge configuration for the line-side converter installed in the traction unit of a train. A simulation was carried out in several steps to validate the theoretical control concepts presented earlier when applied to this converter. Additionally, a discrete control implementation was validated, resulting in a C code program that closely resembles the operational structure of a microcontroller. This successful simulation and control implementation served as a precursor to the upcoming real-life application, which will be discussed in the next chapter.

Furthermore, to address the research questions initially defined, a case study was conducted, emulating a real-life scenario. The results demonstrated that the converter effectively supported the operation of the catenary's power supply, particularly under low voltage conditions. This operation benefited not only the train equipped with the converter but also other vehicles in its vicinity.

Chapter 5

Experimental Validation

5.1 Introduction

The proposed objectives for this dissertation also included a practical implementation of the proposed control algorithm in a real converter. Therefore an experimental validation was developed. Four practical steps were defined in order to observe the full operation of the converter. Starting with grid synchronization, moving to active and later reactive currents control, and after DC bus voltage control, as depicted in Table 5.1. For all these experiments and minor tests occurring inside each one, a respective simulation was conducted in order to successfully predict the outcomes of such implementations. These will be omitted as they depict aspects that were already dicussed.

Moreover, two software tools were utilized in order to continously validate the outputs of such experiments, *Micrium* and *PicoScope*. While the first allows the user to observe and manipulate variables of the programmed code in real-time, the second being an USB oscilloscope that allows the graph visualization to be done on a personal computer, served as a way to confirm the results shown on the first and observe the real measured quantities. An example of the user interface of both tools is present in Appendix C.

Table 5.1: Conducted experiments and main goals.

Experiment	**Objective**
A	Grid Synchronization.
B	Active Current Control.
C	Reactive Current Control.
D	DC Voltage control.

5.1.1 Experimental Setup

In order to complete all the test stages, the experimental setup needs to guarantee specific conditions that are dependent on the objective of each test. As such, the testbed was developed with not only the proposed converter but also with other elements including all the contactors previously described in the simulation phase, a pre-charge circuit, a diode rectifier connected to the DC bus, a three-phase variable autotransformer (variac) in order to adjust the DC voltage according to the requirements of each test, and two transformer providing isolation from the grid. Moreover, the acquisition of the signals was done with a PCB board developed by *Nomad Tech* specifically for the control of the power converter. The microcontroller would the be placed on this acquisition board. In addition to *Micrium*'s interface, two more button panels were used to start the converter and to pre-charge the DC bus. Fig. 5.1 shows a general diagram of this setup. It is important to note that the current sensor is now placed with a opposite direction of the one used in a simulation stage. The power flow direction now presents different polarities with the positive representing power transfer from to grid to the converter. Moreover, despite the diagram practically staying the same for the full duration of the experience, some values and configuration changed in order to test some specific parts of the system. As such, at the beginning of every section, the used values and configuration will be shortly addressed.

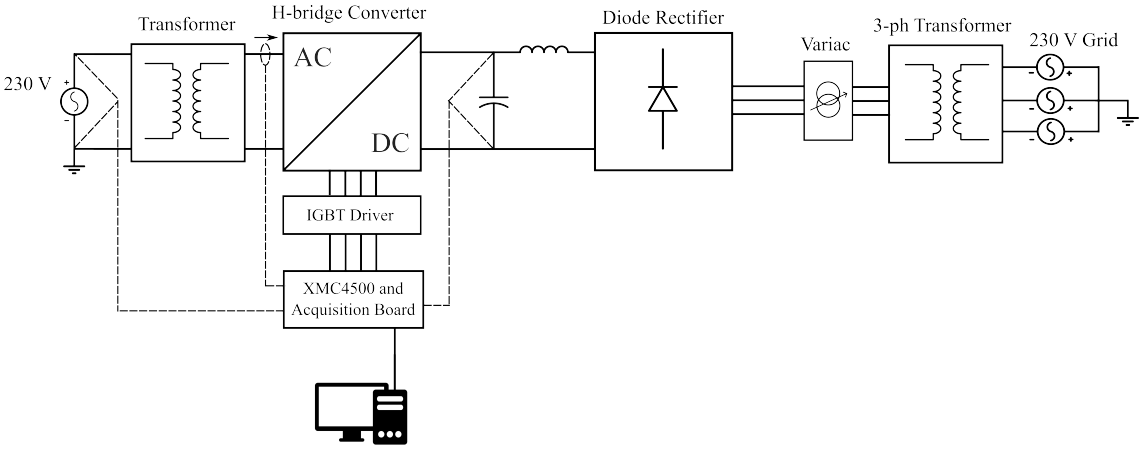


Figure 5.1: Diagram of the experimental setup.

5.1.2 Updated Code Structure

The code developed in the simulation portion of this work was designed with the intent of simplifying the transition to the XMC microcontroller. While it certainly achieved this goal, some modifications were still needed, namely the addition of another routine to the overall code structure. The PWM routine which was done by simply using a PWM block in *PSIM*, now needs to also be developed under a timer interrupt in order to directly generate the duty-cycle from the microcontroller to the IGBT drive circuit. Some considerations concerning the operation of the

built-in PWM firmware had to be addressed. Accordingly, Fig. 5.2 depicts the upgraded code structure from what was explained in the previous chapter.

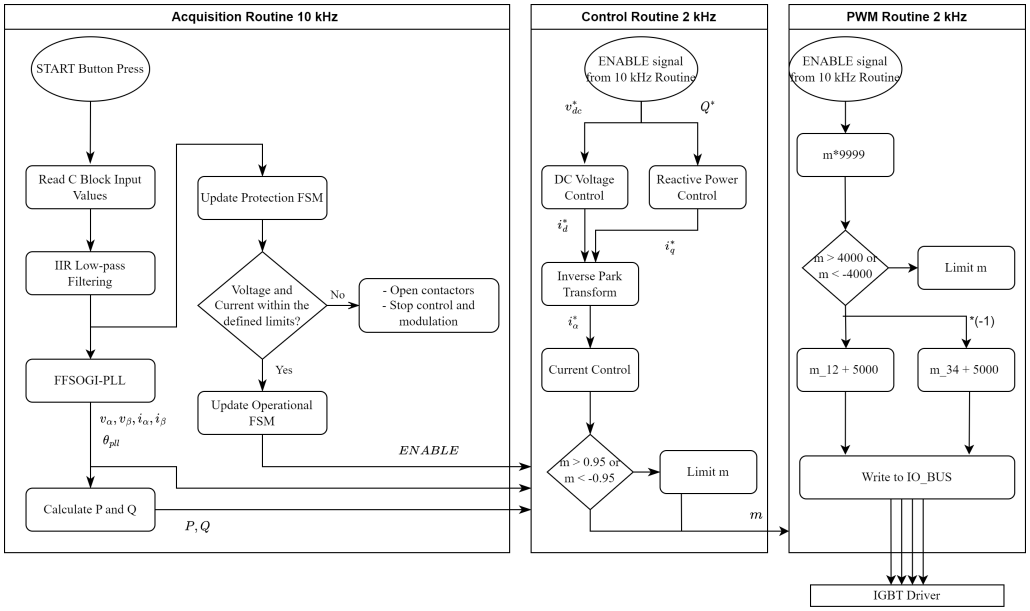


Figure 5.2: Updated Code Structure.

5.1.3 Filtering

Before starting the proposed experiments two important safety and operation aspects were validated, the digital filtering and the operation of the developed finite state machines.

As an example, Fig. 5.3, shows the comparison between the raw and the filtered DC bus voltages. As done before, a 100 Hz second order filter was applied.

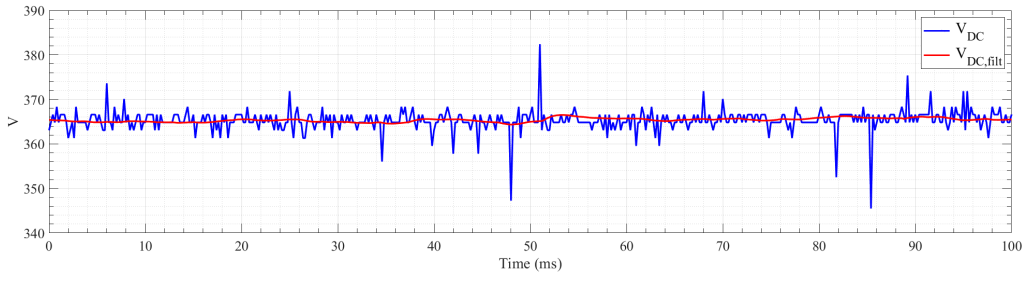


Figure 5.3: 100 Hz digital filter implemented for the DC bus voltage measurement.

Furthermore, on the next experiences it is possible to observe the operation FSM working with the control only starting at time instant 50 ms.

5.2 Experiment A

Grid synchronization was the first experiment to be implemented. It was done seperately, with a different testbed as the PLL is an independent subsystem, that only depends on its input voltage. As such the FFSOGI-PLL was developed inside the 10 kHz acquisition routine.

The testbed consisted of a voltage transducer connected to the acquisition board and consequently to the XMC microcontroller. The voltage transducer was connected to the grid. The programming was done in a very similar fashion of what was previously implemented in simulation environment. The results depicted in Fig. 5.4 were obtained with *Micrium* software, where the execution variables in the microcontroller are sampled at 10 kHz.

In Fig 5.4a, the outputs of the FFSOGI are depicted. It is clear that the α component is synchronous with the grid voltage waveform, while the β component represents its orthogonal component. Furthermore, in the next figure (5.4b), the estimated phase angle is also synchronous in respect to the grid voltage waveform, with values between 0 and 2π. At last, in Fig. 5.4c, the estimated amgular frequency, depicted as ω, and the estimated voltage magnitude, V_{mag}, are represented. The PI controller present in the PLL was continuously adjusted in other to obtain the better performance possible, with the final gains being $K_p = 5$ and $K_i = 10$. Accordingly, the average values of each waveform are according to the expected values: 314.38 rad/s in the case of the estimated frequency and 326.93 V for the voltage magnitude.

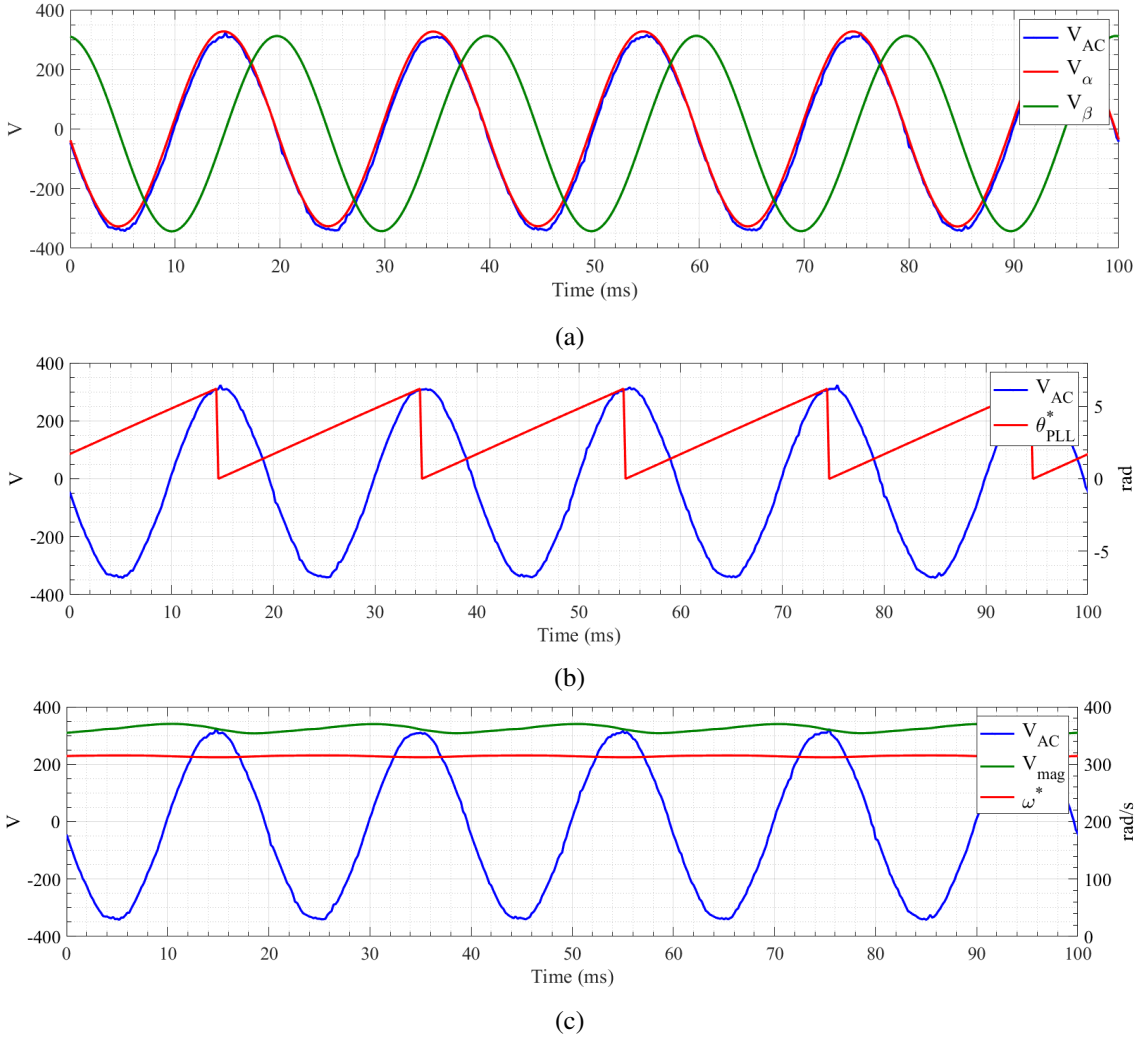


Figure 5.4: FFSOGI-PLL resultant waveforms: α and β components (a), phase angle θ_{PLL} (b), estimated frequency ω^*_{PLL} and voltage magnitude V^*_{mag} (c).

5.3 Experiment B

The next practical validation step was the implementation of the current control loop, working only with active current references. In order to achieve the desired results, this experiment was further divided into two separated validation stages, as depicted below. The objective was to confirm the correct operation of the constituent parts of the current control system in a separate way.

In this experiment, the experimental setup depicted in 5.1.1 was slightly changed: on the AC side a 1 Ω resistor is placed to act as a load, leaving the grid connection for later experiments. Moreover, the DC bus capacitor was pre-charged to aproximatelly 50 V. The *PicoScope* oscilloscope and user interface are used to compare the waveforms visualised in *Micrium* with measured signals for the reasons mentioned before.

B1. PWM Validation

The primary objective of the initial procedure was to validate the correlation between the modulation index (m) and the variation in current amplitude. Additionally, the generation of PWM for the IGBT driver was also verified.

Using the *Micrium* software, a graphical interface was developed to facilitate real-time modification of code variables. This allowed assigning specific values to the variable m. Instead of the PLL, an internally generated saw-tooth wave with a frequency of 50 Hz and an amplitude ranging from 0 to 2π was employed for open-loop control. The resulting angle was used to derive a sinusoidal modulation signal with amplitude m. To ensure compatibility with the microcontroller board, this modulating signal was normalized between 0 and 10000, representing the range of values from 0 to 100%. Subsequently, the signal was utilized to generate a duty cycle at the PWM output bus of the XMC.

An initial test was conducted to determine the operational limits of the duty cycle. Beyond these limits, the AC current waveform deviated from its sinusoidal shape due to saturation of the filter inductance. In this particular scenario, the maximum and minimum duty cycle observed was 4000 and -4000. Therefore, this values should serve as limits for the duty cycle.

Furthermore, a validation of the PWM operation also took place by analysing the voltage drop at the terminals of one IGBT with *PicoScope* (Fig. 5.5). It is clear that the PWM is working as intended with the result being a pulsated wave with a series of high and low voltage levels, with the maximum value corresponding to that of the DC bus voltage, in this case 50 V. In this experiment there was no control of the AC current.

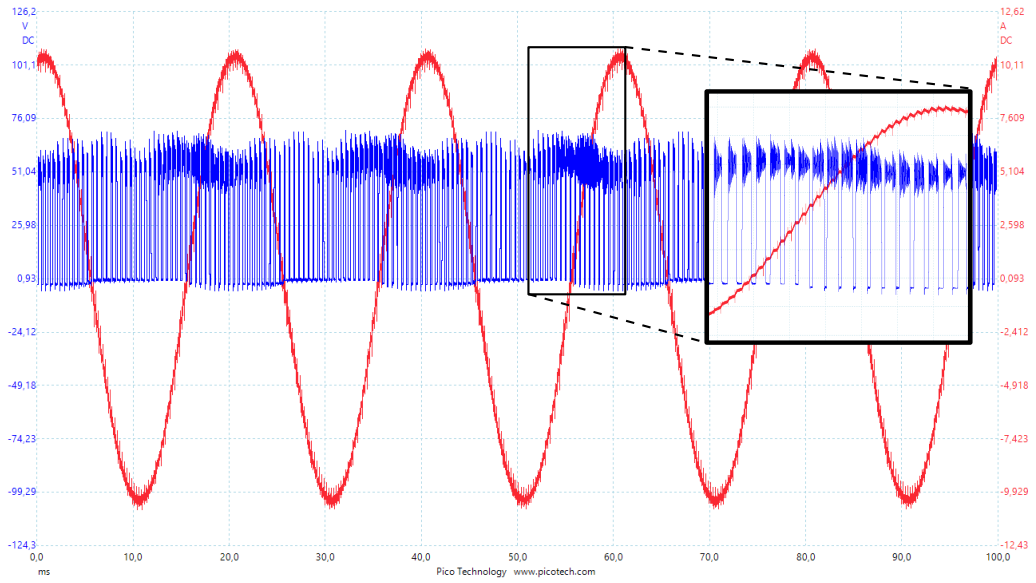


Figure 5.5: Voltage drop at the terminals of an IGBT, in blue and corresponding AC current, in red.

B2. Closed-loop Current Control

The second stage of this experiment aimed to validate the developed PR controller. As such, and still with a internally generated angle, an amplitude reference for the AC current was given to the current control system. The PR was then adapted in an iterative way, following the same approach used simulation environment and explained in Section 4.2. The final selection of gains was $K_p = 5$ and $K_i = 15$. With these gains and an input reference of 10 A the PR controlled demonstrated accurate performance in tracking the AC current reference, as depicted in Fig 5.6.

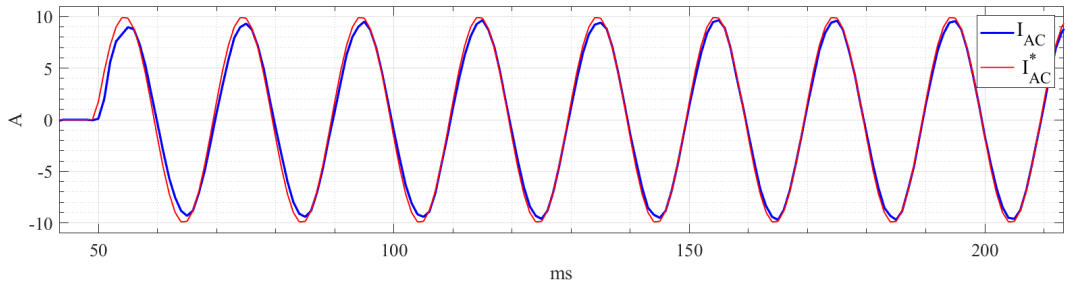
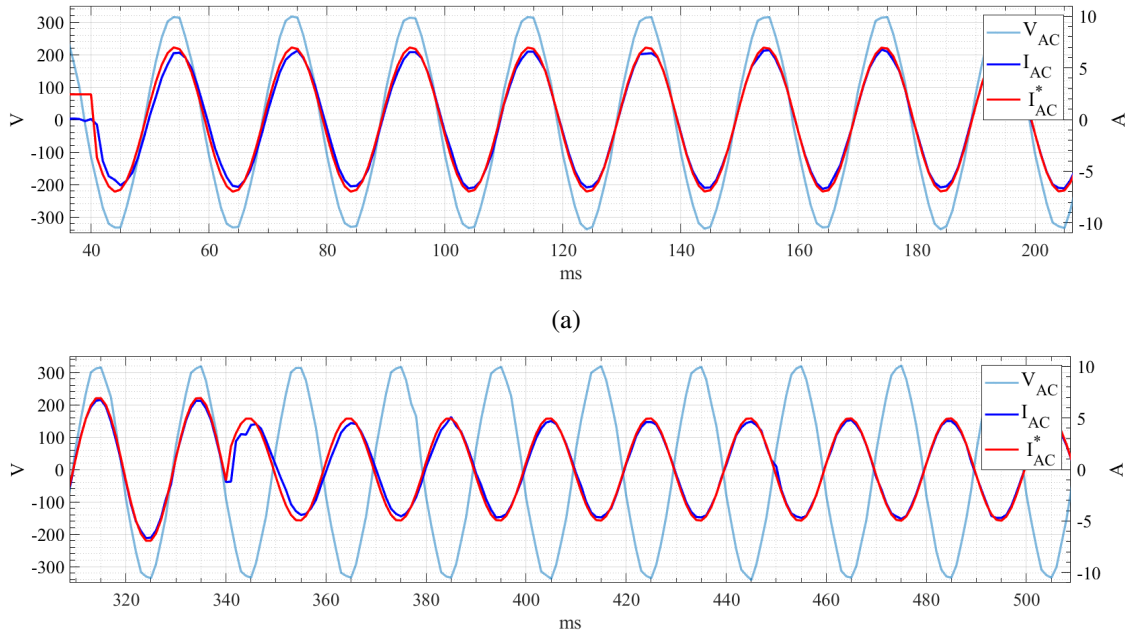


Figure 5.6: PR controller response with internally generated angle.

The next phase involved incorporating the signal generated by the PLL to achieve an AC current control synchronous with the grid. The grid voltage was independently measured directly from the mains. Additionally, a second reference change was introduced to evaluate the controller's response to a negative reference. Specifically, input references of 7 A and -4 A were utilized for the current controller. As illustrated in Fig 5.7, the controller accurately tracked the given references in both cases. Notably, the current is in phase opposition to the voltage in the second scenario, as expected.



(a)

(b)

Figure 5.7: PR Controller response with grid synchronization: from the starting point of operation (a) and after a reference change (b).

5.4 Experiment C

For the third experiment, the power circuit was modified to incorporate connection with the grid. The final circuit configuration is the same as described in the introduction of this chapter, the load resistor was replaced with a connection to the grid through an isolation transformer (Fig. 5.1, left-hand side). Furthermore, the DC bus voltage was set to 200 V, and the AC voltage, due to the transformation ratio, was 90 V_{rms}.

To ensure the correct operation of the previously developed current control system with the grid connection, Experience B was repeated with success, only altering the gains of the PR controller. Once this validation was successful, the response of the controller to a given reactive current reference signal input was analyzed. Multiple tests were performed to examine the variations in AC current amplitude and phase in relation to the AC voltage for different i_q^* values while keeping i_d^* fixed. The completed tests and their corresponding illustrations can be found in the following table (Table 5.2).

Table 5.2: Figure correspondence for different reactive reference currents.

i_d^*	1	1	1	1	1	1	1	1
i_q^*	-2.5	-5	-7.5	-10	2.5	5	7.5	10
Figure	5.8a	5.8b	5.8c	5.8d	5.9a	5.9b	5.9c	5.9d

Through the analysis of the first set of figures (Fig. 5.8), it is possible to observe the correct controller response, for different negative reactive current reference values. This means that the direction of reactive power flow is from the converter to the grid as the current waveform is leading the voltage's. Moreover, when the reactive current references were changed to positive values (Fig. 5.9), it was possible to observe that the current waveform was lagging the voltage waveform, in this case the converter was consuming reactive power from the grid. Furthermore, and validating the current control loop, the AC current also increases in magnitude with the increment on the reactive current reference.

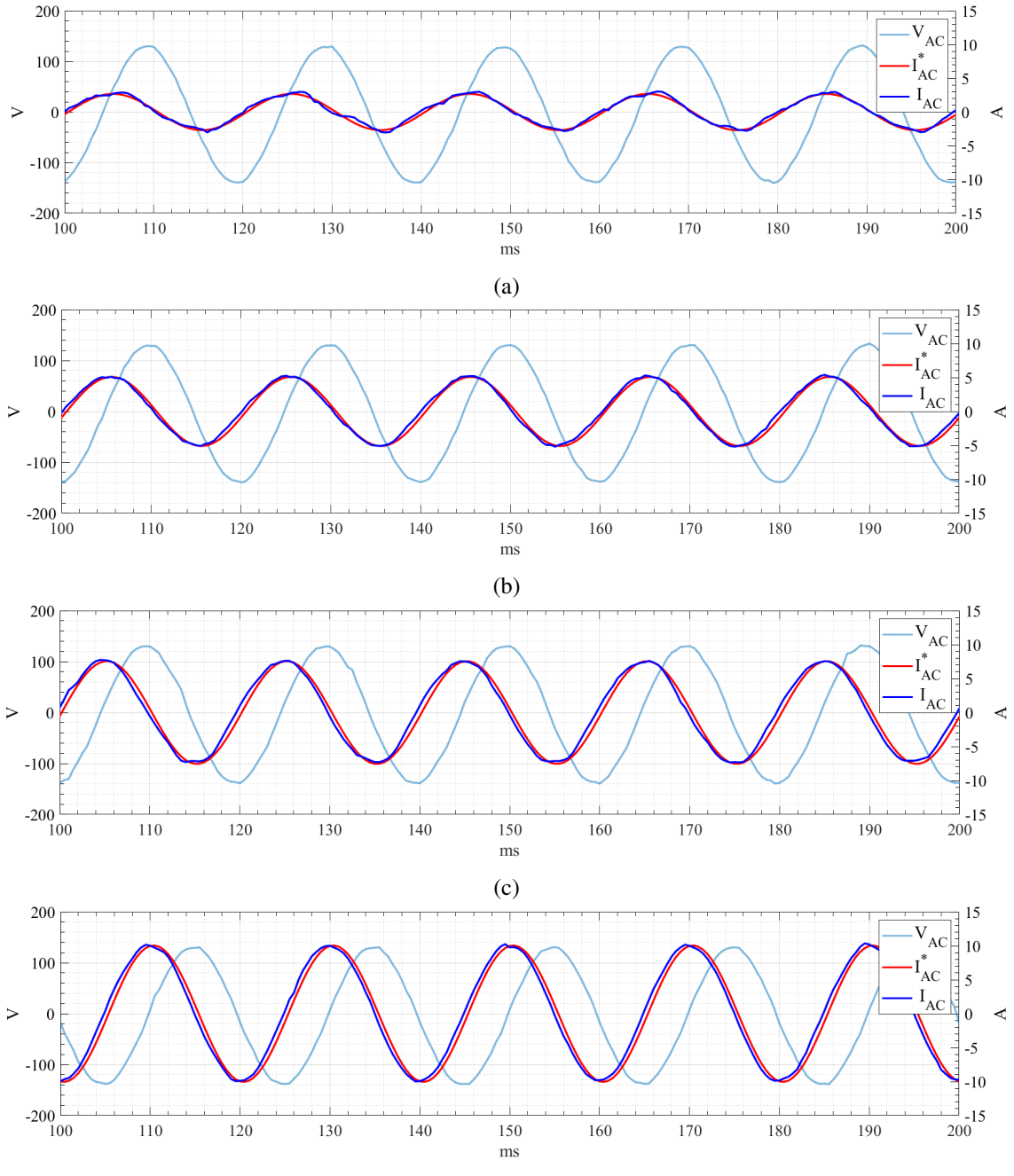
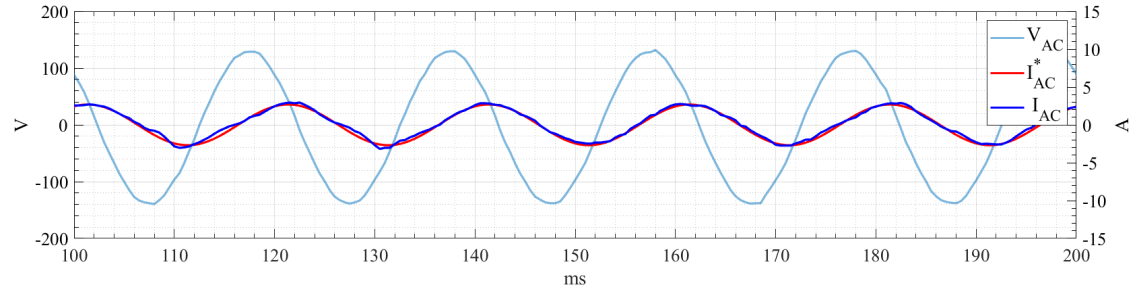
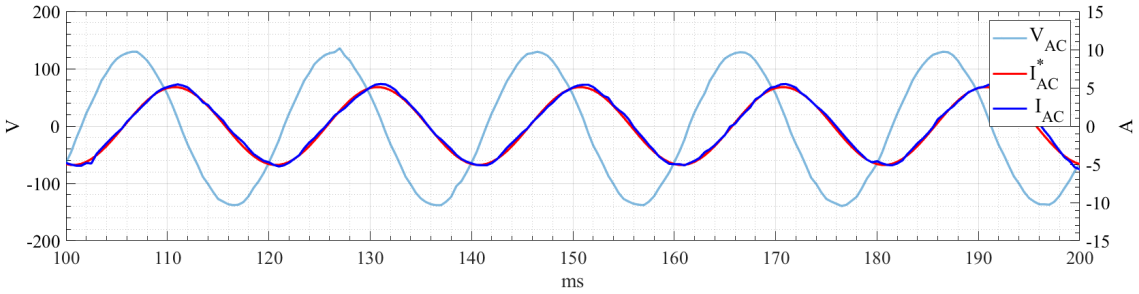


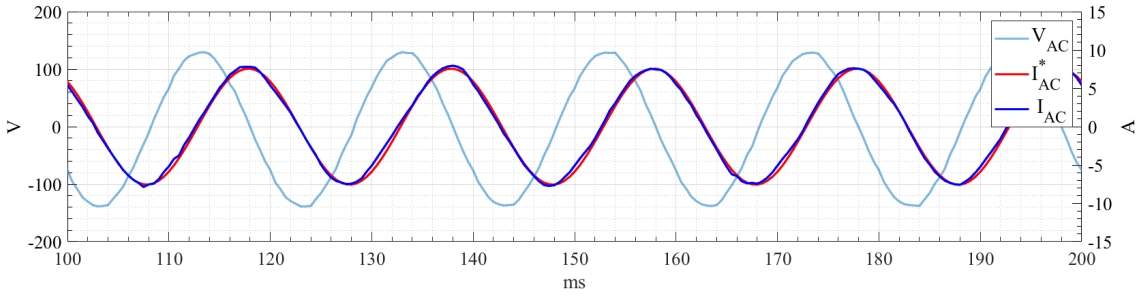
Figure 5.8: System response with different negative reactive current references.



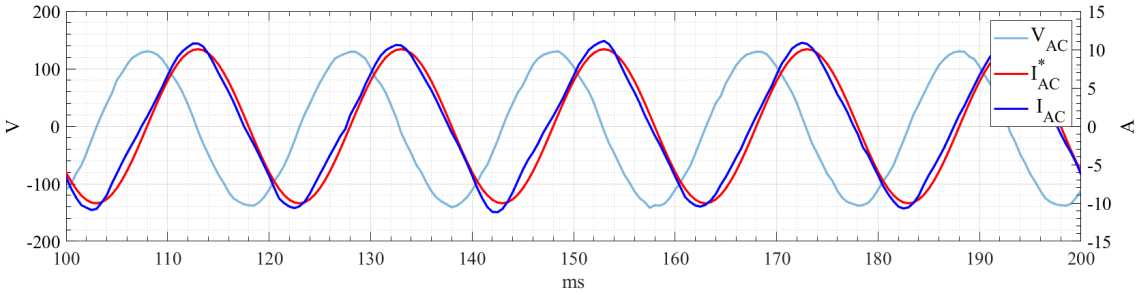
(a)



(b)



(c)



(d)

Figure 5.9: System response with different positive reactive current references.

5.4.1 Reactive Power Controller

For a direct reactive power control, another PI control loop was designed, similarly to what was done before. To achieve the values for both active and reactive power, an additional SOGI instance was also implemented, with the objective of estimating the $\alpha\beta$ components from the measure AC current used in the calculations of the instantaneous power values. The choice of the different reactive power reference values was based on the application of the instantaneous power calculations on the previous test (without utilizing the reactive power control loop). Therefore, by utilizing the previous test of Fig. 5.9c, the calculated instantaneous power and reactive power are presented in Fig. 5.10. The latter presents an average value of approximately 500 VA.

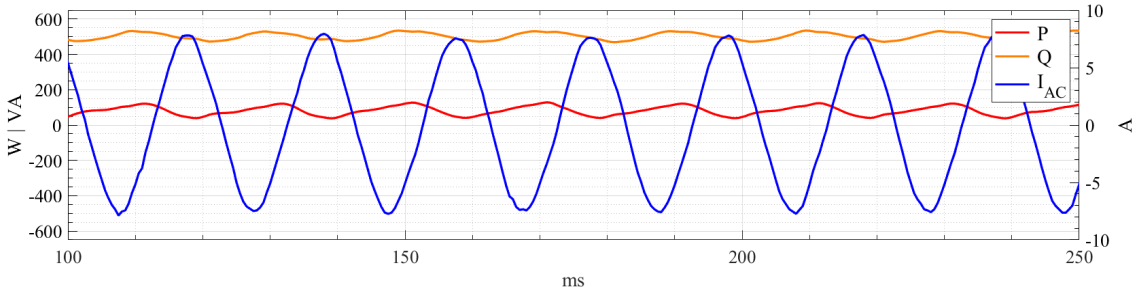


Figure 5.10: Active and reactive power calculations for $i_d^* = 1$ A and $i_q^* = 7.5$A.

In Fig. 5.11, the results for two symmetric references are displayed. It is possible to observe that the calculated reactive power is correctly controlled, taking values according to the given reference. By the assignment of negative reference values, the converter operates with leading power factor, injecting reactive power to the grid, with positive values, the contrary is observed as the converter operates with lagging power factor. Moreover, by assigning the reference reactive power a value of 500 VA and keeping the active current reference, i_d^* at zero, the controller generates an AC current reference with magnitude value 7.5 A, totally corresponding to the reactive current reference i_q^*. This validates the operation of the reactive power control loop as it produces the correct reference values according to the previous PQ calculation test.

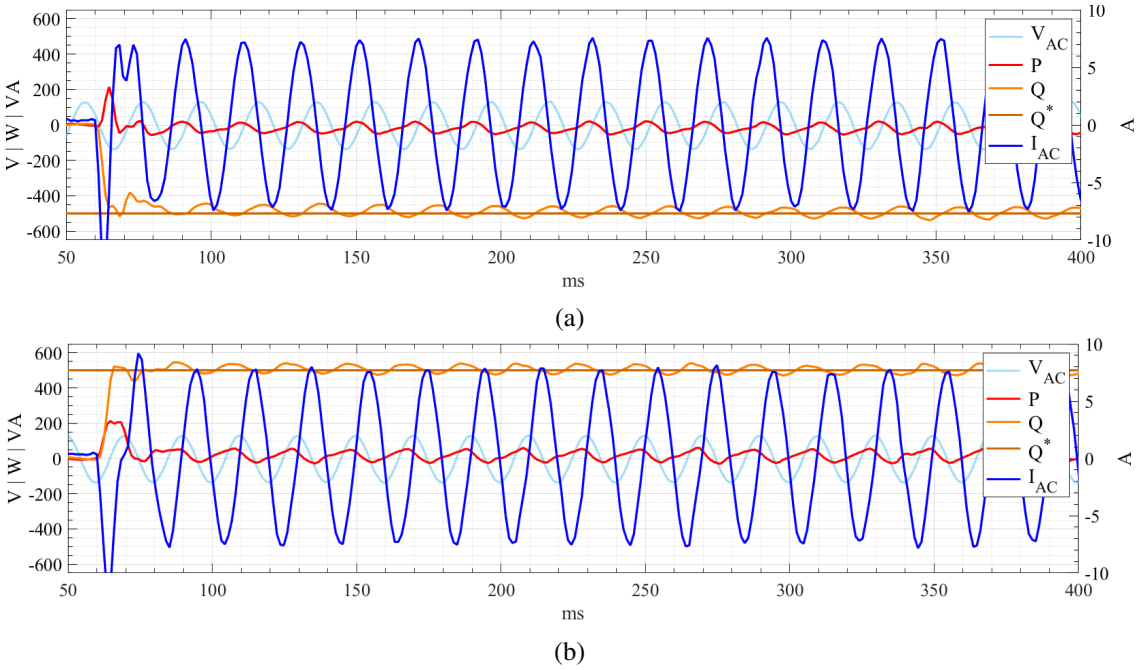


Figure 5.11: System response for -500 VA (a) and +500 VA (b) reactive power references.

5.5 Experiment D

The last experiment was the control of the DC bus voltage. The objective was to raise the DC voltage from a fixed value imposed by the rectifier, after the pre-charging of the DC bus capacitor, to a higher value, in this case from 400 V to 450 V. In order to successfully carry out this experiment without making significant alterations to the control algorithm, a 50 mH inductance was added on the AC side of the circuit, thereby providing approximately the same inductance as that of the transformer. The outcomes of this experiment are depicted on Fig. 5.12. As demonstrated, the AC current is controlled to have its direct component in phase with the AC voltage, which signifies a flow of power from the grid to the DC bus, charging the capacitor and consequently raising the DC voltage. Also, a permanent quadrature component can be observed, since the amplitude of the AC current waveform is constant and doesn't decrease after the reference voltage level is reached.

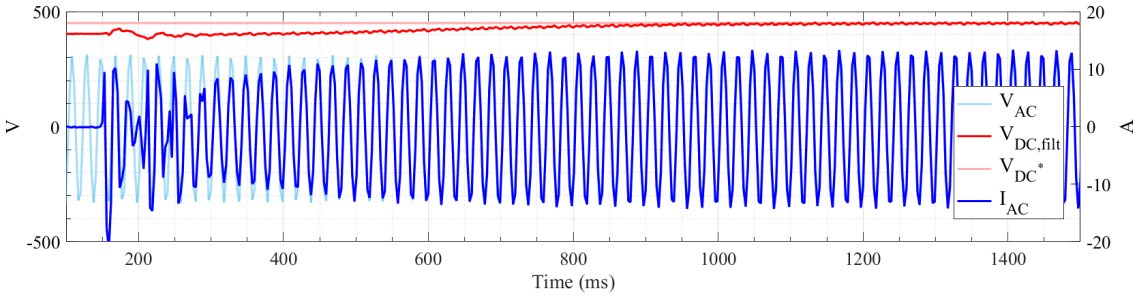


Figure 5.12: DC voltage control.

5.6 Final Remarks

This chapter addressed the complete procedure of the experimental validation of the proposed converter and control scheme. The several systems that were previously simulated, were validated physically, further supporting the hypothesis that this converter can be used as a reactive power compensation device, stabilizing the catenary voltage. Although not shown, it should be noted that for each small test conducted in the experimental portion of this work, a simulation was also done. The objective was to confirm the proposed methodology for the converter in question before the actual implementation. Moreover, when the practical results were not satisfying, the software simulation provided an extra study environment, where tests could be done in order to easily identify the root causes of any eventual problem.

Chapter 4 proposed a set of control algorithms to demonstrate the voltage stabilization in electrified railway systems using simulation tools. Only with the experimental demonstration of each of those control algorithms it is possible to support the hypothesis of this dissertation. Accordingly, this chapter has successfully shown the expected behaviour of the power converter while being controlled by the proposed algorithms from an experimental standpoint.

Chapter 6

Main Conclusions and Future Work

Through the research developed across this study, it became possible to identify the main issues related to power quality degradation in electrified railway systems, as well as methods to mitigate them, with further validation through simulation modelling and physical testing.

6.1 Summary and Contributions

Firstly, a brief overview of the most common railway system configurations is presented, more precisely of different supply and traction systems. An identification of the main power quality problems affecting the supply lines was also made and is described in this document, responding to **Q1**.

The further review of the literature associated with the topic revealed the interesting and less featured in the literature method of reactive power compensation through the on-board line-side converter. This comes as a solution to increase the catenary line capacity and stabilize the supply voltage levels in electrified railway systems. Accordingly, the line-side converter of the traction system, it being the main component responsible for this operation, was analysed with greater detail concerning possible typologies, electrical component choosing and adequate control methods, theoretically answering to **Q2**.

Thereafter, a software simulation was conducted in order to understand the behaviour of the system's components as well as the importance of their modeling and discretization to emulate their operation on a future implementation. This simulation also modelled a study case which consisted in a real-life scenario where the proposed strategy was tested on the proposed converter. This proved the developed strategy to be cabable of performing stabilization of the catenary voltage, where the voltage drop can be reduced by 24.3% in the presented case study with the adaptation of the train grid-side converter controller, thus answering to **Q3**.

Finally, a experimental validation was conducted in order to demonstrate the applicability of the proposed and simulated methods in a real converter operating with reactive power compensation control, as proposed in **Q4**.

As a final remark, it is left to conclude that, with all the previously formulated questions now answered, the use of the line-side converter with modern semiconductor technologies can be used to reduce the issue of low voltage on catenary lines. Moreover, the use of advanced control methods, such as the one presented on this dissertation, also features great relevance in the efficiency improvement of this specific converter operation. The proposed solution, although it is not a target to a lot of scientific research nowadays, certainly has its earned place on modern and future applications of power electronics control for railway traction systems.

6.2 Future Work

Although the proposed study has revealed to be very complete in terms of proving the proposed hypothesis at the beggining of this document, the are still improvements that can be worked on an thus shall be identified in the section. Considering the technologies addressed throughout this document, some possible future developments include:

- Converter Configuration: The power converter topology that was utilized was the H-bridge. Nonetheless, several other typologies and configurations were also depicted, along with the respective advantages and disadvantages of each one. As such, the development of power converters according to these configurations can be target of further study.

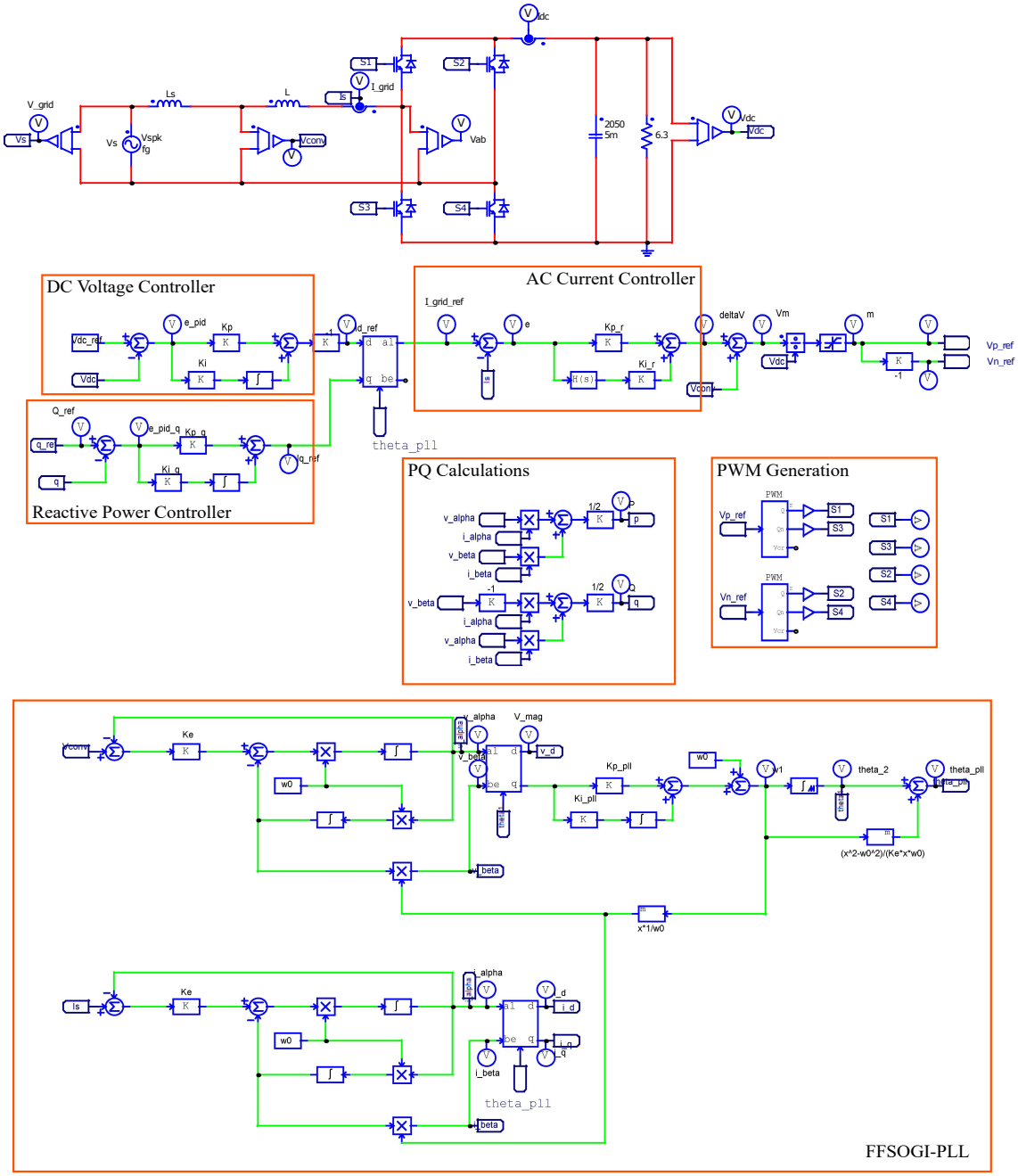
- Harmonic Compensation and Filtering: As previously depicted, the PR controller possesses the advantage of simple selected harmonics compensation. As such, identifying which harmonics need to be filtered and compensated for and applying it to both different configurations of AC filter design and to the PR controller can be a solution to improve the power quality of the proposed converter.

- Algorithms for Reactive Power Compensation: The proposed strategy for line voltage stabilization utilized a single reactive power PI controller, where certain setpoints were given arbitrarily. However, due to the ever changing conditions of the catenary line, this solution is not the most optimized possible. A possible target of future development can either be the application of one of the mentioned strategies, which is already a big improvement towards optimizing the operation of catenary voltage stabilization, or the further development of yet another strategy that aims to improve the results of the ones already illustrated.

Appendix A

Simulation Diagrams

A.1 Complete Circuit Diagram


Vdc
S1
S2
S3
S4
V_grid
Vs
Ls
L
Vspk
fg
Vconv
I_grid
Is
Vab
2050
5m
6.3
Vdc
DC Voltage Controller
Vdc_ref
e_pid
Kp
Ki
K
Vdc
d_ref
d al
q be
theta_pll
AC Current Controller
I_grid_ref
e
Kp_r
Ki_r
H(s)
deltaV
Vm
m
Vconv
Vp_ref
Vn_ref
Q_ref
q_ref
e_pid_q
Kp_q
Ki_q
q
Reactive Power Controller
PQ Calculations
v_alpha
i_alpha
v_beta
i_beta
1/2
P
Q
PWM Generation
PWM
Vp_ref
Vn_ref
S1
S3
S2
S4
Ke
w0
V_alpha
V_mag
V_d
Kp_pll
Ki_pll
w1
theta_2
theta_pll
(x^2-w0^2)/(Ke*x*w0)
x*1/w0
Is
i_alpha
i_d
i_q
i_beta
FFSOGI-PLL

Appendix B

Experimentation Figures

B.1 Experimental Setup

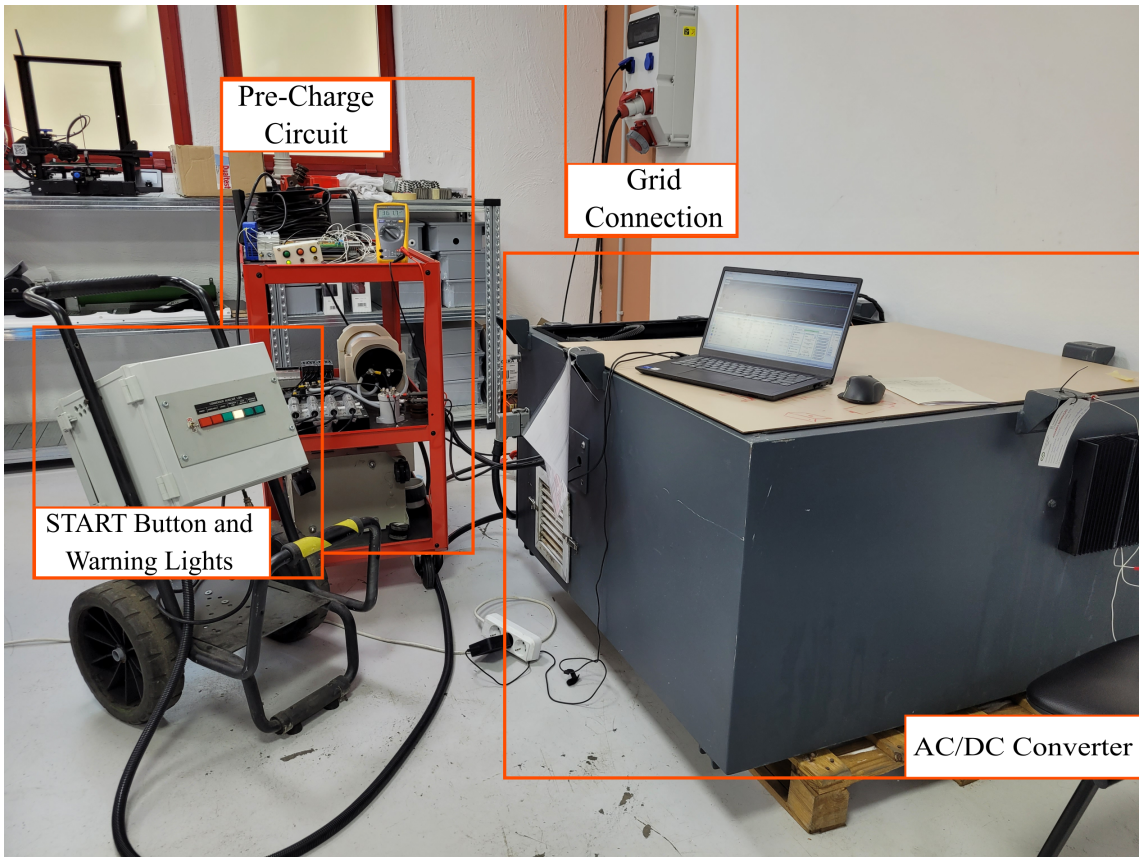


Figure B.1: Full experimental setup.

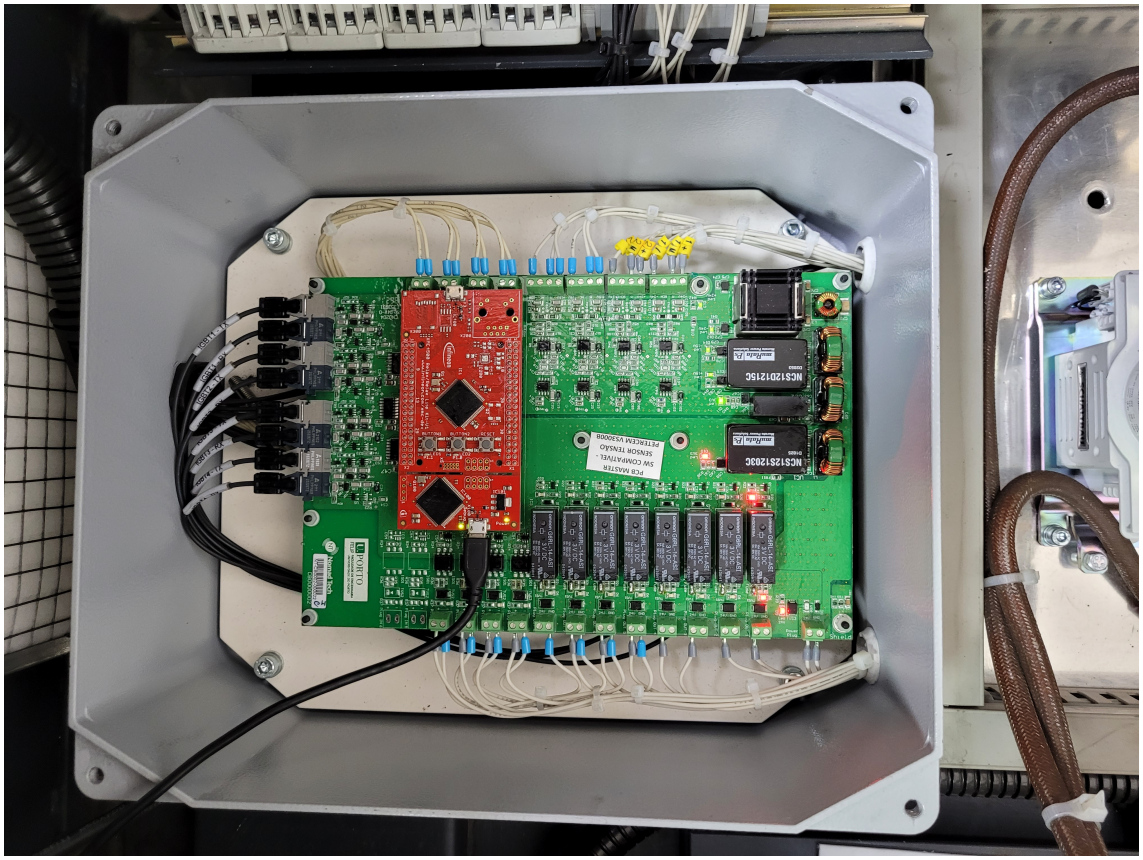


Figure B.2: XMC and Acquisition Board.

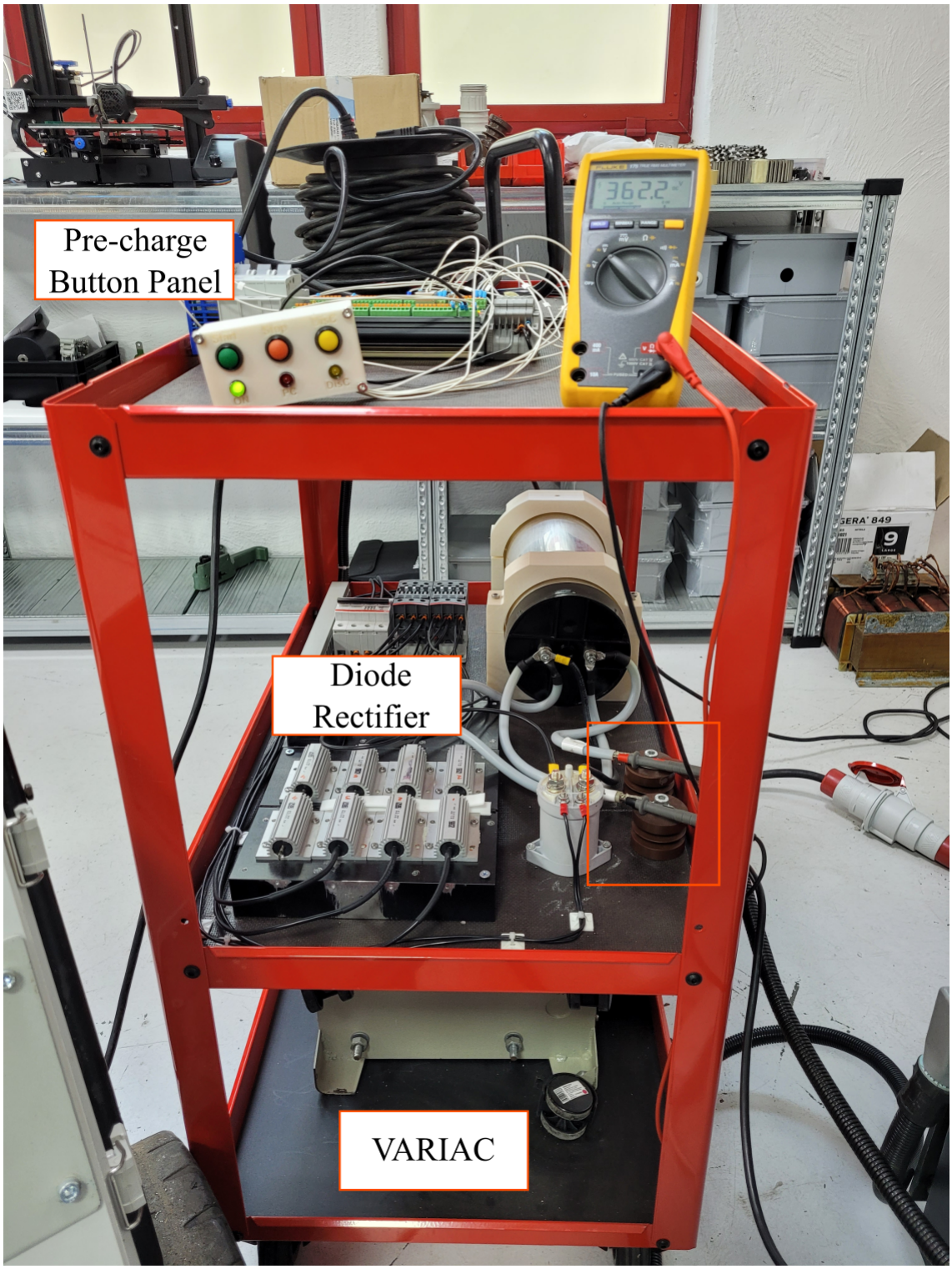


Figure B.3: Pre-charge circuit.

Appendix C

Utilized Software Tools

C.1 *PSIM*

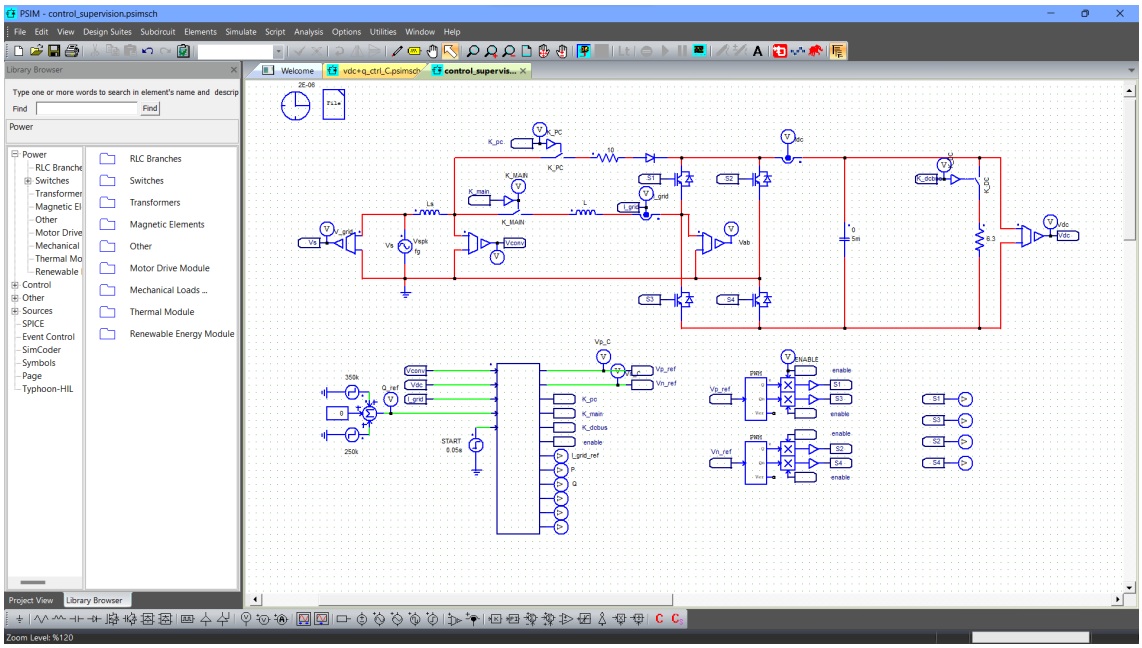


Figure C.1: User interface of *PSIM* simulation software.

C.2 *Dave IDE*

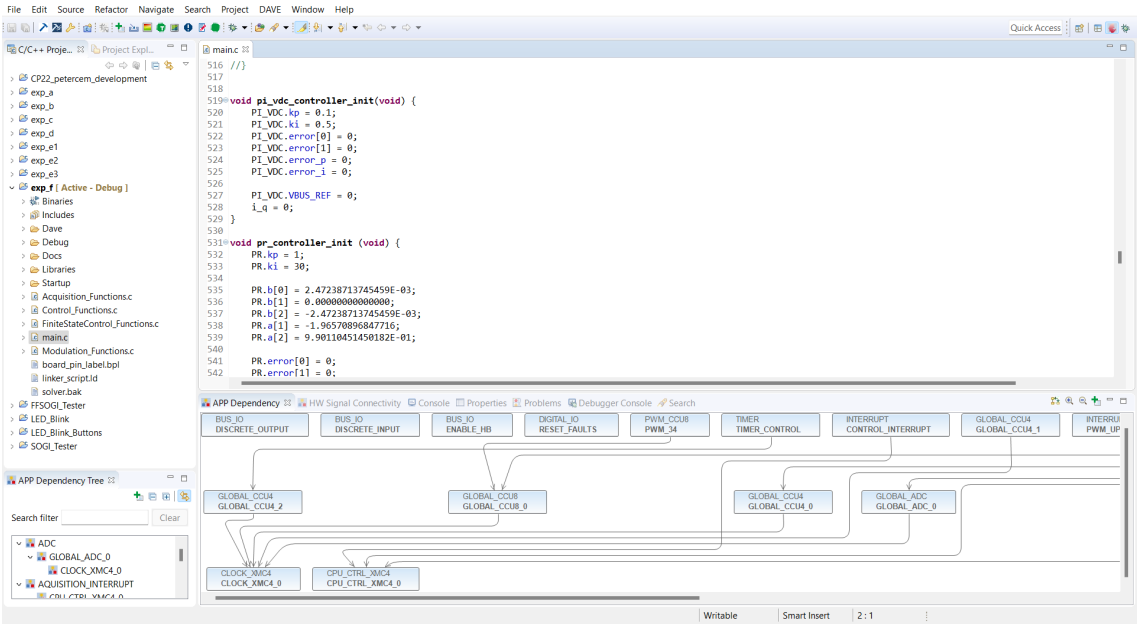


Figure C.2: User interface of *Dave IDE*.

C.3 *Micrium uC/Probe XMC*



Figure C.3: User interface of *Micrium*: code oscilloscope view.

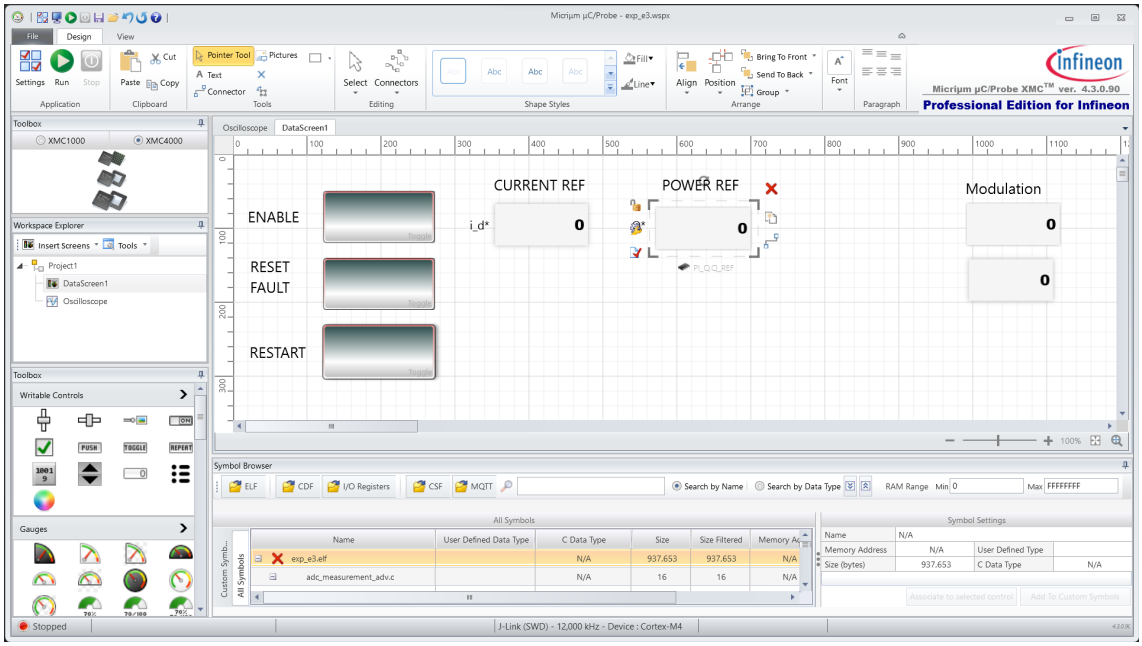


Figure C.4: User interface of *Micrium*: created HMI to introduce reference values and control the FSMs.

C.4 *PicoScope*

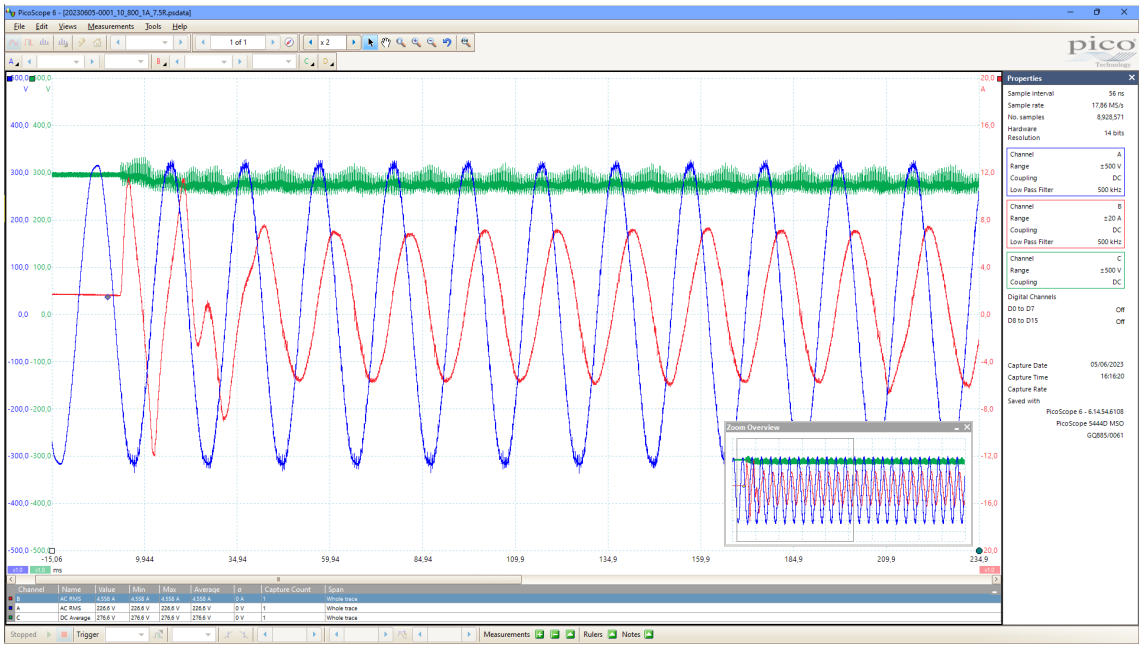


Figure C.5: User interface of *PicoScope*, extracted during Experiment C.

C.5 *MATLAB*

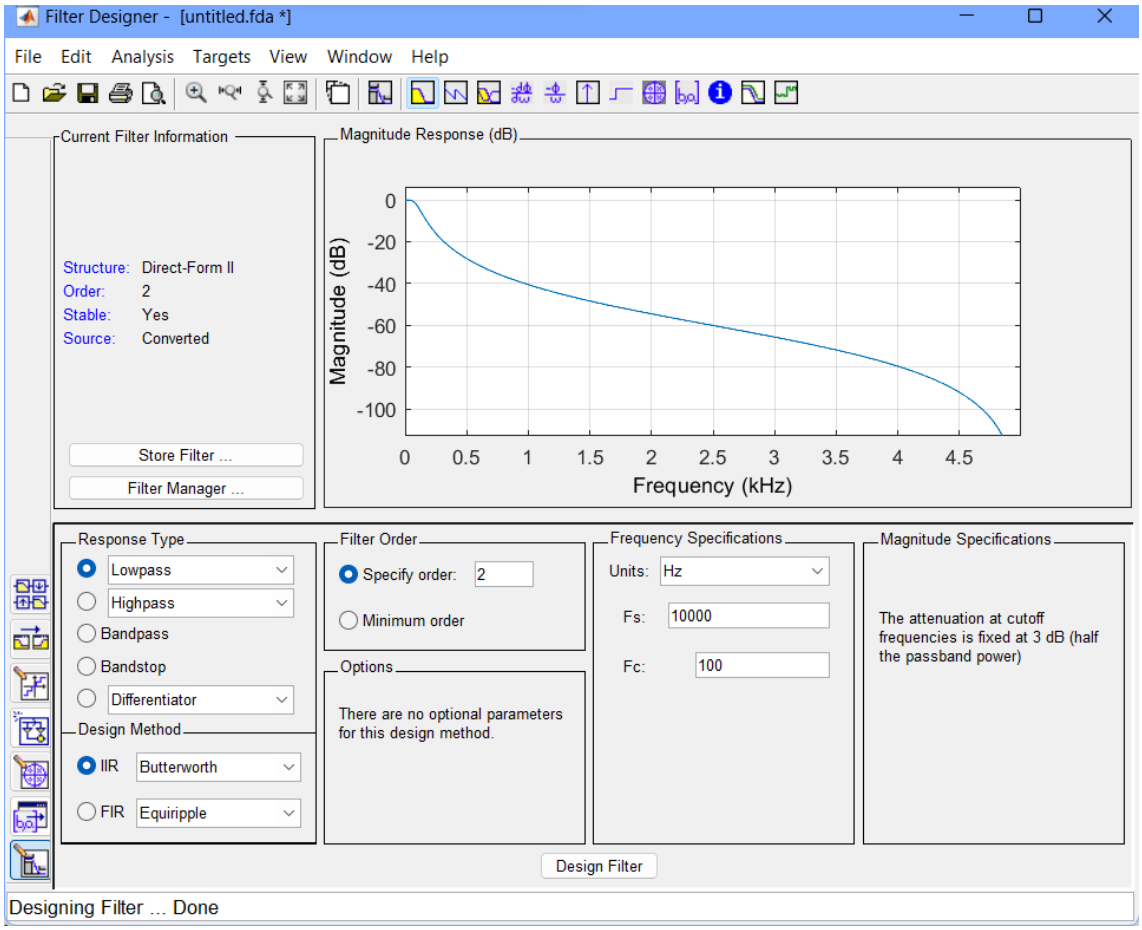


Figure C.6: User interface of *MATLAB*'s *filterDesigner* app

References

[1] M. Brenna, F. Foiadelli, and D. Zaninelli. Electrical railway transportation systems, 2018. https://doi.org/10.1002/9781119386827.

[2] International Energy Agency (IEA). The future of rail - opportunities for energy and the environment. 2019 [Online]. Available at: https://www.oecd.org/publications/the-future-of-rail-9789264312821-en.html. Accessed: 2022-10-22.

[3] Rail - fuels & technologies. Available at https://www.iea.org/fuels-and-technologies/rail Accessed: 2022-10-15.

[4] Shift2Rail Joint Undertaking. Shift2rail multi-annual action plan. Technical report, Shift2Rail, 2015 [Online]. Available at: https://rail-research.europa.eu/publications/multi-annual-action-plan/.

[5] D. Ronanki, S. A. Singh, and S. S. Williamson. Comprehensive topological overview of rolling stock architectures and recent trends in electric railway traction systems. *IEEE Transactions on Transportation Electrification*, 3:724–738, 9 2017. https://doi.org/10.1109/TTE.2017.2703583.

[6] I. Krastev, Tricoli, Pietro, Stuart Hillmansen, and Minwu Chen. Future of electric railways: Advanced electrification systems with static converters for ac railways. *IEEE Electrification Magazine*, 4(3):6–14, 2016. doi:10.1109/MELE.2016.2584998.

[7] G.Abad. Power electronics and electric drives for traction applications, 2016. https://doi.org/10.1002/9781118954454.

[8] S. Frey. *Railway electrification systems engineering*. White Word Publications, 2012.

[9] V. A. Morais. *Tools and Strategies for Power Flow Management in Smart Railways*. PhD thesis, Universidade do Porto, 2021.

[10] A. Steimel. *Electric Traction-Motive Power and Energy Supply-Basics and Practical Experience*. Oldenbourg Industrieverlag, 2014.

[11] R. E. Morrison. Power quality issues on ac traction systems. *Proceedings of International Conference on Harmonics and Quality of Power, ICHQP*, 2:709–714, 2000. https://doi.org/10.1109/ICHQP.2000.897765.

[12] A. Rufer B. Bahrani and M. Aeberhard. Catenary voltage support: Adopting modern locomotives with active line-side converters. *IEEE Transactions on Smart Grid*, 3:377–387, 3 2012. https://doi.org/10.1109/TSG.2011.2163090.

[13] F. Blaabjerg. Control of power electronic converters and systems. volume 1. Academic Press, 2018. https://doi.org/10.1016/C2015-0-02427-3.

[14] R. Teodorescu, M. Liserre, and P. Rodríguez. Grid converters for photovoltaic and wind power systems, 2007. https://doi.org/10.1002/9780470667057.

[15] M. Malinowski H. Abu-Rub and K. Al-Haddad. Power electronics for renewable energy systems, transportation and industrial applications, 2014. https://doi.org/10.1002/9781118755525.

[16] J. Pinto, A. Carvalho, A. Rocha, and A. Araújo. Comparison of dsogi-based pll for phase estimation in three-phase weak grids. *Electricity*, 2:244–270, 7 2021. https://doi.org/10.3390/electricity2030015.

[17] R. Teodorescu, F. Blaabjerg, M. Liserre, and P. C. Loh. Proportional-resonant controllers and filters for grid-connected voltage-source converters. *IEE Proceedings: Electric Power Applications*, 153:750–762, 2006. https://doi.org/10.1049/ip-epa:20060008.

[18] S. Buso and P. Mattavelli. Digital control in power electronics, 2006. https://doi.org/10.2200/S00047ED1V01Y200609PEL002.

[19] K. Sozański. *Power Systems Digital Signal Processing in Power Electronics Control Circuits Second Edition*. URL: http://www.springer.com/series/4622.

[20] A. G. Yepes, F. D. Freijedo, J. Doval-Gandoy, O. López, J. Malvar, and P. Fernandez-Comesaña. Effects of discretization methods on the performance of resonant controllers. *IEEE Transactions on Power Electronics*, 25(7):1692–1712, 2010. doi:10.1109/TPEL.2010.2041256.

[21] J. Ito, Y. Hagiwara, and N. Yoshie. Development of the igbt applied traction system for the series 700 shinkansen high-speed train. In *1998 International Conference on Developments in Mass Transit Systems Conf. Publ. No. 453)*, pages 25–30, 1998. doi:10.1049/cp:19980093.

[22] M. Brenna, F. Foiadelli, D. Zaninelli, and D. Barlini. Application prospective of silicon carbide (sic) in railway vehicles. In *2014 AEIT Annual Conference - From Research to Industry: The Need for a More Effective Technology Transfer (AEIT)*, pages 1–6, 2014. doi:10.1109/AEIT.2014.7002062.

[23] P. Qashqai, A. Sheikholeslami, H. Vahedi, and K. Al-Haddad. A review on multilevel converter topologies for electric transportation applications. Institute of Electrical and Electronics Engineers Inc., 12 2015. doi:10.1109/VPPC.2015.7352882.

[24] L. G. Franquelo, J. Rodriguez, J. I. Leon, S. Kouro, R. Portillo, and M. A.M. Prats. The age of multilevel converters arrives. *IEEE Industrial Electronics Magazine*, 2:28–39, 6 2008. doi:10.1109/MIE.2008.923519.

[25] L.A.M. Barros, M. Tanta, A. P. Martins, J. L. Afonso, and J. G. Pinto. Opportunities and challenges of power electronics systems in future railway electrification. pages 530–537. Institute of Electrical and Electronics Engineers Inc., 7 2020. doi:10.1109/CPE-POWERENG48600.2020.9161695.

[26] A. Dekka, B. Wu, R. L. Fuentes, M. Perez, and N. R. Zargari. Evolution of topologies, modeling, control schemes, and applications of modular multilevel converters. *IEEE Journal of Emerging and Selected Topics in Power Electronics*, 5(4):1631–1656, 2017. doi:10.1109/JESTPE.2017.2742938.

[27] D. Ronanki and S. S. Williamson. Modular multilevel converters for transportation electrification: Challenges and opportunities. *IEEE Transactions on Transportation Electrification*, 4:399–407, 6 2018. doi:10.1109/TTE.2018.2792330.

[28] M. Tanta, L. A.M. Barros, J. G. Pinto, A. P. Martins, and J. L. Afonso. Modular multilevel converter in electrified railway systems: Applications of rail static frequency converters and rail power conditioners. pages 55–60. Institute of Electrical and Electronics Engineers Inc., 7 2020. doi:10.1109/YEF-ECE49388.2020.9171814.

[29] J. Feng, W. Q. Chu, Z. Zhang, and Z. Q. Zhu. Power electronic transformer-based railway traction systems: Challenges and opportunities. *IEEE Journal of Emerging and Selected Topics in Power Electronics*, 5:1237–1253, 9 2017. doi:10.1109/JESTPE.2017.2685464.

[30] P. Drabek, Zdeněk Peroutka, Martin Pittermann, and Marek Cedl. New configuration of traction converter with medium-frequency transformer using matrix converters. *IEEE Transactions on Industrial Electronics*, 58(11):5041–5048, 2011. doi:10.1109/TIE.2011.2138114.

[31] P.W. Wheeler, J. Rodriguez, J.C. Clare, L. Empringham, and A. Weinstein. Matrix converters: a technology review. *IEEE Transactions on Industrial Electronics*, 49(2):276–288, 2002. doi:10.1109/41.993260.

[32] M. Brena, F. Foiadelli, M. Roscia, and D. Zaninelli. Harmonic analysis of a high speed train with interlaced four quadrant converters. *IEEE Power and Energy Society General Meeting - Conversion and Delivery of Electrical Energy in the 21st Century*, 2008. https://doi.org/10.1109/10.1109/PES.2008.4596049.

[33] A. González-Gil, R. Palacin, and P. Batty. Sustainable urban rail systems: Strategies and technologies for optimal management of regenerative braking energy. *Energy Conversion and Management*, 75:374–388, 2013. doi:10.1016/j.enconman.2013.06.039.

[34] T. Kulworawanichpong. *Optimising AC Electrical Railway Power Flows with Power Electronic Control*. PhD thesis, Uni. of Birmingham, 2003.

[35] B. Bahrani and A. Rufer. Optimization-based voltage support in traction networks using active line-side converters. *IEEE Transactions on Power Electronics*, 28:673–685, 2013. doi:10.1109/TPEL.2012.2205163.

[36] T. Kulworawanichpong and C. J. Goodman. Optimal area control of ac railway systems via pwm traction drives. *IEE Proceedings: Electric Power Applications*, 152:33–40, 1 2005. doi:10.1049/ip-epa:20040979.

[37] V. A. Morais, J. L. Afonso, A. S. Carvalho, and A. P. Martins. New reactive power compensation strategies for railway infrastructure capacity increasing. *Energies*, 13, 9 2020. doi:10.3390/en13174379.

[38] CENELEC EN 50388-1:2017 - railway applications - fixed installations and rolling stock - technical criteria for the coordination between traction power supply and rolling stock to achieve interoperability - part 1: general, 2017.

[39] J. Xu, H. Qian, Y. Hu, S. Bian, and S. Xie. Overview of sogi-based single-phase phase-locked loops for grid synchronization under complex grid conditions. *IEEE Access*, 9:39275–39291, 2021. doi:10.1109/ACCESS.2021.3063774.

[40] F. Xiao, L. Dong, L. Li, and X. Liao. A frequency-fixed sogi-based pll for single-phase grid-connected converters. *IEEE Transactions on Power Electronics*, 32(3):1713–1719, 2017. doi:10.1109/TPEL.2016.2606623.

[41] H. Akagi, Y. Kanazawa, and A. Nabae. Instantaneous reactive power compensators comprising switching devices without energy storage components. *IEEE Transactions on Industry Applications*, 20, 1984.